ELECTROSLAG REMELTING OF A LOW ALLOY STEEL

A STUDY OF THE PHYSICAL AND CHEMICAL PROCESSES INVOLVED IN THE ELECTROSLAG REMELTING OF A LOW ALLOY STEEL

By

DONALD ALAN WHITTAKER, M.Sc.

A Thesis

Submitted to the Faculty of Graduate Studies

in Partial Fulfilment of the Requirements

for the Degree

Doctor of Philosophy

McMaster University

August 1967

DOCTOR OF PHILOSOPHY (1967) McMASTER UNIVERSITY
(Metallurgical Engineering) Hamilton, Ontario.

TITLE: A Study of the Physical and Chemical Processes Involved in the Electroslag Remelting of a Low Alloy Steel.

AUTHOR: Donald Alan Whittaker, B.Sc. (University of Alberta)

M.Sc. (University of Alberta).

SUPERVISOR: Dr. G. R. Purdy

NUMBER OF PAGES: ix, 114

SCOPE AND CONTENTS:

Low alloy steel electrodes have been electroslag remelted using alternating and direct current power sources. Changes in electrical contact between the furnace mould wall and mould base provided an improved understanding of the thermal and chemical processes characteristic of the remelting technique. An ion regeneration process has been postulated to account for current flow within the slag phase. Observed changes in furnace heating effects, electrode droplet sizes and in slag and metal compositions have been related to overtensions impressed on the slag/electrode and slag/ingot boundaries. The desulfurization reaction has been studied in detail.

Acknowledgements

The author wishes to express his appreciation to Dr. G. R. Purdy of McMaster University for his direction and help throughout the program and to Dr. R. G. Ward, now at the Broken Hill Proprietary Co. Ltd., Melbourne, Australia, for his advice during the initial stages of the program.

This study was sponsored by the Atlas Steels Company of Welland, Ontario. The author is indebted to that company for direct financial support. Appreciation is also extended to Dr. R. H. Read and Mr. D. J. Knight of the Atlas Steels Company for initial suggestion of the topic and for continued interest in the program.

TABLE OF CONTENTS

LIST OF TABLES*

---

* All tables have been placed at the end of the thesis.

Unless otherwise stated, all experimental results refer to melts produced using the following electroslag furnace operating conditions: 23 volts, 530 amps, 200 grams slag charge, 1 3/16" diameter electrodes and a mould wall electrically isolated from the mould base.

LIST OF ILLUSTRATIONS*

17. Photographs showing the improvement in ingot surface finish with increasing power input.

18. Photographs showing the improvement in ingot macrostructure with increasing power input.

19. Variation in sulfur content with length of ingot melted.

20. Effect of power input and electrode polarity on silicon transport.

21. Effect of power input and electrode polarity on phosphorus transport.

22. Variations in thermal characteristics for electrically isolated and conducting mould wall systems.

23. Effect of electrode polarity and mould wall electrical contact on percent desulfurization.

24. Change in rate of electrode burnoff and droplet weight with increasing electrode diameter.

25. Changes in furnace thermal characteristics with increasing electrode diameter.

26. Change in rate of electrode burnoff and droplet weight with increasing slag volume.

27. Changes in furnace thermal characteristics with increasing slag volume.

28. Percent desulfurization versus length of ingot melted using two different slags.

29. Percent desulfurization versus length of ingot melted using two different slags.

---

* All illustrations have been placed at the end of the thesis.

Unless otherwise stated, all experimental results refer to melts produced using the following electroslag furnace operating conditions: 23 volts,

530 amps, 200 grams slag charge, 1 3/16" diameter electrodes and a mould wall electrically isolated from the mould base.

1. Introduction

Present metallurgical technology demands that ferrous materials meet stringent product specifications. Steels for specialized applications must possess mechanical and physical properties of the highest order, consistent with their composition.

Recognizing that finished metal quality is strongly dependent on the structure, degree of chemical homogeniety, and inclusion content of the ingot, steel manufacturers are constantly searching for new melting and casting techniques. New methods introduced into large scale production systems include ladle and stream degassing, vacuum induction melting and consumable electrode vacuum arc melting. One of the more recent innovations is the electroslag remelting (ESR) process, involving a furnace similar to that used for vacuum arc remelting (VAR) but employing an active slag medium rather than an evacuated chamber in which to melt the consumable electrode.

The earliest form of ESR process was developed in the United States during the 1930's, requiring a direct current to remelt tubular consumable electrodes made from carbon steel sheet[1, 2]. Granular metals were added to the melt for the production of highly alloyed ingots. That technique, called the Hopkins Process, was abandoned prior to 1950. The general concept appeared in the USSR during the late 1950's, with the development of a furnace using alternating current to remelt solid consumable electrodes of the desired chemical analyses. No alloying elements were added during the remelting. This form is now of much interest in the USSR[3, 4, 5, 6], the United Kingdom [7, 8, 9, 10], France[11, 12, 13] and Japan[13]. Renewed interest is now being shown in the United States concerning both the alternating[14] and direct

current processes[15, 16, 17, 18, 19], (the latter modified by its original inventor to operate in a manner similar to the alternating current system).

Both methods consistently produce improved steels, as assessed from data published for materials covering a wide range of chemical analyses, from low alloy bearing steels to high alloy stainless steels [3, 4, 6, 9, 12, 13, 15, 20, 21, 22]. To date no extensive comparison of the two current modes has been attempted and particularly in the case of the direct current system, few data of a fundamental nature have been published. The present study was initiated to compare the two furnace operating modes and to evaluate the physical and chemical processes involved in both techniques.

2. Discussion of the Process

2.1 Principle Features of the ESR Furnace

Figure 1 is a line drawing of a typical ESR furnace operated with either direct or single-phase alternating current. In addition to the power supply, the system consists of a consumable electrode, a molten slag bath and an ingot in a water-cooled mould.

The consumable electrode may be remelted in rolled, forged or continuous-cast form[4,5]. Prior electrode scale removal by grinding and/or pickling is recommended to minimise the ingot oxygen content[23, 24]. Radiographic studies of furnace working zones have revealed the electrode tip is consumed by formation and detachment of molten metal droplets[25]. The required heat is believed generated primarily by the resistance to electric current flow within the slag bath[4, 6, 17]. With the growth to detachment of each molten metal droplet the current path between the electrode tip and the molten ingot pool is shortened, resulting in an increased current and decreased voltage. From those effects droplet size estimates are obtainable either by recording oscilloscope traces of current and voltage or by simply observing ammeter and voltmeter fluctuations[4, 7, 26, 27].

The slags are normally based on calcium fluoride with alumina and/or lime additions[5, 27, 28, 29]. Other oxide additions suggested are BaO[4], MgO[8], ZrO_2[4], TiO_2[4], FeO[4], Fe_2O_3[9], Cr_2O_3[4] and SiO_2[9], but these appear to be rarely used.

During the heat initiation period the melting process is extremely unstable and initial operation of the furnace with a relatively cold slag

results in the solidification of a thick slag layer along the mould wall. The layer decreases in thickness as the melting process becomes more stable and the furnace working zone becomes hotter[30]. Many furnace operators initiate ESR heats with explosive "igniter fluxes" to help minimize the slag build-up and the severe surface corrugations obtained at the ingot base[3, 30, 31, 32]. Those fluxes are mixtures of magnesium or aluminum powders with the normal slags. Heats may also be initiated by striking an air-arc between the electrode and base plate. Molten flux is subsequently poured into the mould from a separate slag-melting furnace[10]. After the transient initial period, constant rates of electrode consumption are maintained by automatic regulation of the current or voltage[7, 5, 18].

Both the electrodes and moulds may be round, square or rectangular in shape[4, 5, 14, 19]. The moulds may also be water-jacketed or spray cooled[4, 5] and are generally constructed from copper sheet, although occasionally steel is used[4, 5, 32, 33].

Multiple electrodes can be used with alternating or direct current power sources. In these systems, three electrodes are remelted into one mould or one electrode into each of three moulds[1, 2, 11]. In the direct current case, each electrode is separately powered. In the alternating current case, one electrode is connected to each leg of a 3-phase current supply. The multiple mould alternating current installation has severe drawbacks, since power fluctuations within one furnace will interfere with melting conditions in the remaining two furnaces[5]. Furnaces melting single electrodes into round moulds and powered by either direct or single phase alternating current were originally limited to ingots weighing less than two tons[4, 5]. More recent furnace designs are capable of melting ingots of

at least ten tons[34]. Multiple-electrode single-mould furnaces with ingot capacities of ten tons or larger are recommended for the manufacture of rectangular ingots[4].

Coarse ingot macrostructures are generally obtained with all power sources and mould designs. To obtain fine grained ingots, solenoids may be placed around the mould[4, 35], or the mould may be rotated[18].

The designs and applications of ESR furnaces are in many respects similar to those for vacuum arc remelting furnaces. Comparisons for the ESR and VAR techniques are therefore given in the literature[4, 6, 17, 20, 36, 37, 38]. (Most of the ESR published data concerns only the alternating-current technique). The superficial similarity between the systems is somewhat misleading, since as the present study emphasizes, the ESR furnace is more profitably treated as an electrochemical system. The VAR furnace is associated with processes primarily observed in the field of plasma physics.

2.2 Furnace Operation and Thermal Characteristics

Three slag-metal reaction interfaces may be defined within the ESR furnace. Each interface is in turn associated with a thermal zone and is subject to a heat balance, as follows:

(a) The electrode tip and upper slag zone:

Resistance to current flow within the electrode and slag results in the generation of heat to cause melting of the electrode tip. Heat is lost from this zone by convection and conduction through the slag to the mould wall, by conduction through the bulk electrode and by radiation to the mould atmosphere from the electrode and slag surfaces. Heat is also lost from the zone as molten droplets are detached and fall away from the

electrode tip. A further (perhaps negligible) term in the heat balance will result from enthalpies associated with electrodic reactions.

(b) The bulk slag zone:

Heat is generated by current passage through the bulk slag and is primarily lost by convection and conduction to the electrode, ingot and mould wall. Depending on the relative metal droplet and bulk slag temperatures, heat may also be gained or lost within this zone during droplet fall.

(c) The ingot pool and lower slag zone:

Heat is again generated by resistance to current passage through the lower slag layers, the adjacent ingot pool and the solidified ingot metal. The fall of molten droplets into the ingot pool may also provide heat to this zone. Heat is lost by convection and conduction to the mould through both the lower slag layers and the ingot metal.

From the above comments it is apparent that thermal conditions affecting slag-metal reactions within the ESR furnace are extremely complex and that analysis requires an accurate knowledge of slag-metal interface temperatures at the electrode tip, falling droplet and ingotpool surfaces, as well as heat transport coefficients for all phases present. To date however, the bulk slag temperatures obtained in commercial practice are not accurately known, since the slag temperatures of ∿1700° - 2000°C are too high for standard tip thermocouples and common thermocouple sheaths are consumed by the reactive slags before accurate temperatures can be recorded[9, 21, 39]. Thermal conditions within the ESR furnace are therefore open to speculation based on changes observed in molten metal droplet sizes, electrode burnoff rates and molten ingot pool depths resulting from variations in furnace operating parameters.

AC furnace practice indicates that an increase in current or voltage must result in a higher temperature within all three thermal zones since rates of electrode burnoff are increased, metal droplet sizes are decreased and slag skin thicknesses decreased[4, 7, 40, 41], the latter providing an improved ingot surface finish. Such changes are all beneficial to commercial practise. However the hotter melts also result in deeper ingot pools[4, 40, 41], which are detrimental to ingot quality because they promote radial crystal growth.

The addition of Al_2O_3 to a CaF_2 - based slag results in a faster rate of electrode burnoff, corresponding to an increase in slag resistivity [4, 27]. Larger slag volumes are claimed to provide slower rates of burnoff, shallower ingot pools and poorer ingot surfaces[4, 40]. The added slag is thought to lower the overall temperature of the system.

Operating data from an AC laboratory system indicates electrode diameter has no effect on burnoff rate or droplet frequency[7]. However in commercial AC furnace practise, increasing electrode diameters have (for unknown reasons) been associated with decreased ingot pool depths at low power input and increased ingot pool depths at high power input. Such differences in effect between laboratory and commercial furnaces are not unexpected. Thermal conditions are more critical in the laboratory systems primarily because of the greater radial heat losses experienced when using a smaller mould diameter. The fact that such differences exist, points out the danger in applying laboratory model results to predict specific operating characteristics for larger scale furnaces. At best, the model processes provide only general indications concerning thermal and chemical effects within each of the three ESR furnace zones concerned.

As the present study will show, a useful technique for studying both thermal and chemical effects is that of varying the electrical contact between the mould wall and the mould base. Commercial furnaces use water-cooled moulds with the mould base and mould wall electrically integral. In such moulds a significant portion of the current may bypass the slag-ingotinterface by flowing directly from the mould wall through the slag to the electrode tip. If the mould wall is electrically isolated from the mould base a greater portion of the current is forced to cross the slag-ingot pool interface. By changing both the DC electrode polarity and the mould wall contact, the heating effects at the upper and lower slag-metal interfaces may then be markedly changed.

2.3 Current Conduction in the ESR System

In the earliest form of ESR process (i.e., the Hopkins technique), current flow was believed to occur by means of an electric discharge between the electrode tip and molten ingot surface[1, 2, 15], in a manner similar to that obtained in submerged arc welding. More recent investigations, and particularly those concerning the X-ray photography of the ESR process[25], suggest that an electric arc does not occur during the stable remelting period. It would appear that a detailed study of the problem has not been attempted. The true nature of the current flow within the slag phase therefore remains unknown. The literature states only that for both the AC and DC processes, the slag acts as an ionized and electrically conductive medium[6, 7, 17, 18, 20].

For fused salt systems a relationship between ion charge, ion radius and ionic transport number has been proposed[42, 43] wherein:

$$t+ = \frac{Z+r-}{(Z+\ r-)+(Z-r+)}$$

and $$t- = \frac{Z-r+}{(Z+r-)+(Z-r+)}$$

for which t+, t- = cationic and anionic transport numbers respectively

r+, r- = ionic radii

Z+, Z- = ionic charges

The relation has been found to hold for limited experimental data. Because fused salt anions are normally much larger than their corresponding cations[44], the equations indicate that multiply-charged cations should be the most efficient current carrying species.

On that basis the calcium ion should be the predominate conduction species, since most ESR slags contain calcium fluoride as their primary constituent. To contribute to the overall cell current however, the ions must be discharged at the electrodes. If, under conventional ESR operating voltages, Ca^{2+} and F^- ions are assumed to be relatively inert, then Fe^{2+} and Fe^{3+} ions might be considered to be the major contributors to cell current. The electroslag process would then be analogous to the polarographic methods for quantitative analyses, wherein an inert supporting electrolyte is added in excess and dischargeable ions are transported by diffusion to the electrodes, giving rise to detectable currents at characteristic discharge voltages[45].

Calcium deposition at iron cathodes has been tentatively identified in the low current electrolysis of FeO_x - CaO semi-conducting slags. The discharged calcium, which is insoluble in steel, is thought to be evaporated at deposition temperatures over 1440°C[46]. The resulting calcium vapors would

be expected to oxidize immediately and either condense back into the slag phase or onto the water-cooled copper mould wall. To maintain charge neutrality within the slag, fluorine gas should be liberated at the anode whenever an appreciable quantity of calcium is discharged at the cathode.

A second possibility could be the dissolution of discharged calcium into the slag as a neutral species, or the physical precipitation of the calcium within the slag as a colloidal suspension. In either case the uncharged calcium must be transported by simple mass transport (i.e., transport independent of the applied field) back to the anode to be reionized, unless the colloidal calcium possesses a net negative charge.

Electronic conduction might also be proposed in ESR slags. As current densities increase at the cathode, the local electrodic field gradient rapidly rises (this effect is discussed in a later section dealing with electrodic characteristics and capillarity) to approach the gradient required for field emission. Electrons from the metal fermi surface might then easily tunnel into the slag. At the melting point of iron, thermionic emission should be negligible. Within the slag phase an electron hopping mechanism can be envisaged, with multiply charged positive ions presenting the most likely ionized sites for the transient excess electrons. The mechanism is identical to that postulated for the conduction of current in semi-conducting FeO slags[46, 47].

2.4 Metal Refinement

One slag-metal reaction interface is found within each of the three thermal zones previously discussed, i.e., the slag-electrode, slag-falling droplet and slag-ingot pool interfaces respectively. The solidification front at the liquid metal pool-solid ingot interface could also provide a site for the removal of inclusions and dissolved gases within the lower

thermal zone. Since the ESR process is considered to be a particularly efficient technique for the removal of sulfide and oxide inclusions[3, 4, 5, 6], it is of interest to analyze the reactions proceeding at each of those sites in terms of the probable desulfurization and deoxidation processes obtainable.

Unlike silicate and aluminate constituents, sulfur is soluble at all temperatures above the bulk steel solidification range. The high sulfur solubility precludes desulfurization by flotation of solid metal sulfides out of ingot pools or by physical entrainment of sulfides within slags during droplet formation and fall periods.

Desulfurization is considered to be an ionic process[48, 49, 50] involving the cathodic reaction $[S] + 2e = (S^{2-})$*. The latter is balanced both in the presence[51, 52] or absence[50, 53] of an externally applied electric current by some anodic reaction $[M] = (M^{2+}) + 2e$. A "chemical" desulfurization reaction is obtained when the two partial reactions occur on the same slag-metal interface; e.g., on the boundary between the falling metal droplet and the slag phase. An "electrochemical" desulfurization reaction is obtained when the partial anodic and cathodic reactions occur at two different interfaces; i.e. the electrode-slag and ingot-slag interfaces respectively when the ESR process is operated with a DC positive electrode polarity.

ESR tests have indicated desulfurization increases in order of melting with DC negative, DC positive and AC electrode polarities[4]. On the basis of the direct current results, it has been suggested that the

---

* [S] denotes sulfur atoms in the metal phase.

(S^{2-}) denotes sulfur ions in the slag phase.

$\{S_2\}$ denotes sulfur molecules in the gaseous phase.

desulfurization reaction is primarily electrochemical in nature and that the slag-molten pool interface is a better cathodic reaction site than the slag-electrode interface (presumably because of the longer residence time within the ingot pool, and despite the larger slag-metal contact area offered to the droplets at the electrode tip)[4]. In the case of the alternating current system, improved desulfurization characteristics have been noted, and attributed to "electrocapillary vibration" at the slag-ingot pool interface[4, 21]. (This effect will be discussed in detail in section 2.5).

Model studies at the laboratories of the British Iron and Steel Research Association have attempted to simulate ESR refining conditions by studying the formation and fall of aqueous zinc chloride droplets within liquid columns containing hexane-methyl red solutions[54]. The test work has indicated the methyl red is extracted by the aqueous zinc chloride phase at rates up to two times greater during the droplet fall periods than during the droplet formation periods. The transfer is considered negligible when the droplets are within the residence zone at the base of the column. The results are of limited value in simulating desulfurization processes because they are analogous only to the "chemical" desulfurization reactions provided between falling metal droplets and ESR slags. For an electrochemically controlled desulfurization process the most important variables are those associated with the interactions of electrode polarity, current density and residence time at the slag/electrode and slag/ingot pool interfaces.

Studies based on very closely controlled slag-metal reactions have identified the anodic and cathodic "chemical" processes associated with

desulfurization at static slag-metal boundaries[53]. Those studies have shown that the partial processes are electrically balanced in cases where no current is applied. For a number of reasons it is unlikely that balanced ionic reactions will be identified in a normal ESR process. In the high current density ESR system many electrode reactions are forced to take place simultaneously and at different rates, presenting a formidable problem of detection for each reactant and reaction rate. Physical adsorption of inclusions by slags will also complicate any attempt to determine a material balance; i.e., in the case of alumino-silicate inclusion adsorption, chemical analyses for aluminium, silicon and oxygen will bear little relation to the ionic electrochemical processes affecting those elements.

Low current slag-metal electrolysis experiments have demonstrated that cyclic parasitic processes also occur when variable valence elements are present in the slag[48, 52]. Bivalent metal ions are brought to the slag-atmosphere interface by convective and diffusive processes and there oxidized to the trivalent state by the reaction

$$2(M^{2+}) + 1/2\ \{O_2\} = 2(M^{3+}) + (O^{2-}).$$

A similar movement of both ions to the slag-ingot pool zone will result in the reduction reaction

$$2(M^{3+}) + (O^{2-}) = 2(M^{2+}) + [O].$$

The latter reaction is slow, and, when rapid oxidation of the slag occurs, a simultaneous reduction reaction is thought to result:

$$2(M^{3+}) + [M] = 3(M^{2+}).$$

Such parasitic reactions are possible with any variable valence element, (e.g. iron, manganese or chromium). The reactions tend to "pump" oxygen into both the slag and the metal and to build-up metal oxides within the

slag. Current efficiencies are then upset so that it is impossible to calculate balanced transport equations.

Metal ions completely discharged at the cathode may also remain in the molten electrolyte in the form of uncharged metal (in saturated solution) or as metallic clouds[45]. In either form the metal can then diffuse to the slag/atmosphere surface and be oxidized, or react with the anode or anodic discharge products to again produce an ionized constituent within the electrolyte. These effects again upset material balance calculations.

Slag-metal sulfur equilibria describing chemical desulfurization in open hearth and electric arc furnaces, are often expressed in terms of the displacement reaction:[48, 49]

$$[S] + (O^{2-}) = (S^{2-}) + [O].$$

The sulfur distribution ratio can then be written as:

$$\frac{(wt\%S)}{[wt\%S]} = \text{Const.} \frac{(N_O{}^{2-})}{[wt\%O]}$$

where, Henrian behavior is assumed for all components and

$N_O{}^{2-}$ = the number of gram ions of oxygen in 100 grams of slag after the oxygen requirements for the formation of complex ions such as $AlO_3{}^{3-}$ and $SiO_4{}^{4-}$ have been satisfied.

According to the latter equation desulfurization can be improved by increasing the "free' oxygen ion content of the slag and by decreasing the oxygen activity in the metal. Desulfurizing agents such as CaO, MgO and BaO have therefore been recommended[4] since those oxides tend to increase the concentration of "free" oxygen ions in CaF_2 based slags. Minor additions of known desulfurizing agents such as CaC_2 are also suggested[4], since they provide reducing characteristics to the slag and lower the oxygen potential within the system.

Based on data from commercial heats, it is claimed that ESR slags become saturated with iron and silicon oxides and with oxygen from the air[4], with the result that the slags lose their desulfurizing power. Argon mould atmospheres should then provide the desired lower oxygen potential, stop air-slag reactions and also decrease the proportion of metal oxides provided to the slag by scale formation on the hot electrode surfaces above the slag phase. From laboratory studies however, it has been suggested that as little as 25 percent of the sulfur removed from the metal may be retained in the slag, the balance escaping to the atmosphere[9]. Sulfur is thought to be evolved from the slag in the form of SO_2 or as volatile fluorides, with SF_6 considered the most likely fluoride form[9, 29, 55]. If SO_2 is evolved, the use of an argon atmosphere should decrease desulfurization, whereas an air atmosphere would make slag sulfur-saturation impossible.

Deoxidation can occur in a manner similar to desulfurization, according to the cathodic reaction $[O] + 2e = (O^{2-})$. However it is apparent that oxygen transport within the ESR system is a complex process involving both ionic and physical (solid inclusion) transport mechanisms. When melting non-deoxidized steels containing oxygen in the form of dissolved gas, increasing deoxidation is obtained in order of melting with DC negative, AC and DC positive electrode polarities[4]. The results would appear reasonable since the DC positive electrode mode places the cathodic deoxidation site at the slag-ingot pool interface and in the proper position to counteract those cyclic processes which tend to transfer oxygen into the ingot.

When melting doxidized steels in which the oxygen is present

primarily within oxide inclusions, deoxidation is claimed to increase in order of melting with DC negative, DC positive and AC electrode polarities[4]. The direct current results are interpreted to mean the slag-molten pool interface is a better cathodic reaction site. As in the previous case cited for the desulfurization process, the improved AC deoxidation characteristics are again attributed to "electrocapillary vibration" at the slag-ingot pool interface.

It has been suggested that the liquid metal pool-solid ingot interface is a site for the rejection of dissolved gases and oxide inclusions[4, 56]. It is tempting to consider the refining at that site as analogous to those processes obtained with zone refining techniques. However, the ESR process is associated with marked dendritic freezing and it is more probable that microsegregation rather than zone refining results from the solidification process. In that respect furnace operating procedures must be carefully controlled to provide maximum uniformity of inclusion and porosity dispersal. Axial crystal growth is desirable in order to avoid macrosegregation at ingot centres. Stable electrode melting is also required, in order to minimize temperature fluctuations and exogenous (slag) inclusion entrapment at ingot peripheries.

Inclusion removal from within the molten pool has been attributed to a flotation mechanism, in accordance with Stoke's Law[4, 56]. However that equation is strictly applicable to the removal of large inclusions under quiescent melt conditions. It would therefore seem likely that refining within the molten pool zone should be properly attributed to the highly turbulent conditions existing within the pool. Such conditions tend to "wash" the slag/metal interface with metal obtained from the lower pool

regions.

Model studies have considered inclusion removal during the passage of molten steel droplets in small boats through an ESR slag at 1600°C [57]. The results have indicated that: (i) inclusion concentrations decrease exponentially with the amount of slag traversed, (ii) larger inclusions are most rapidly removed and (iii) fewer inclusions are removed as the droplet size is increased. Both those studies and the work concerning the extraction of methyl red from hexane solutions by aqueous zinc chloride droplets, suggest that inclusions and/or reactants are distributed uniformly within the moving droplets but brought to the droplet surface by turbulence for subsequent absorption into the slag phase. Both studies consider a droplet traverse zone of up to 50 cm. length. Distances of that magnitude provide little help in determining the relative amounts of refining obtained during the droplet fall times, since commercial ESR furnaces provide fall spaces of only 1 to 4 cm. length[40].

In summary, it is expected that soluble impurities will be extracted primarily at electrochemical sites. Insoluble impurities may be extracted primarily by physical entrainment within the slag phase. The actual proportions of impurities removed by ionic transport and by inclusion entrainment, and the relative proportions removed at each of the three slag/metal interfaces, remains to be determined.

Changing both the electrode polarity and the electrical contact between the ESR mould wall and mould base, as suggested previously for the study of thermal characteristics, should markedly effect slag-metal reactions within the lower electrochemical zone. The technique offers an unique opportunity to examine the chemical and electrochemical desulfurization

processes and the effect of current magnitude and electrode polarity on sulfur transport.

2.5 Electrodic Characteristics and Capillarity

Electrode processes are currently the subject of intensive study, although most of the published work concerns only reactions in aqueous media. It is informative however, to consider the application of aqueous solution concepts to liquid electrode - fused salt systems characteristic of the ESR process.

Under equilibrium conditions, electrical potential gradients are obtained across metal-electrolyte interfaces. The gradients are directly attributable to the chemical potential differences existing between the ions and atoms taking part in the electrode process[58]. The relative magnitudes of the equilibrium electrode potentials are determined by reference to standard electrode potentials (e.g., the hydrogen standard electrode). The actual gradients are dependent on the prevailing boundary structures.

In metal electrode-aqueous electrolyte systems, boundary structures are reasonably well characterized. Most theories agree interfacial double layers are obtained[59], each consisting of a compact layer of one ion thickness immediately attached to the electrode surface (i.e., the Helmholtz layer), associated with a linear fall of electrical potential and an adjacent diffuse layer of many ions thickness extending into the bulk electrolyte (i.e., the Gouy layer), associated with an exponential fall of potential.

The most reasonable interpretation of the double layer structure considers the Helmoltz layer to consist mainly of adsorbed water molecules,

and competatively adsorbed surface active ions or surfactants[59]. Anions are more likely to be specifically adsorbed than cations. The latter are usually smaller ions with stable primary hydration shells (i.e., ions associated during transport with a definite number of water molecules). Because of their hydration, the cations tend to remain within the Gouy layer.

An electric charge is associated with the adsorption of ions at the interface. As a consequence, an equal and opposite "image" charge is obtained on the electrode. Both the electrical capacitance of the double layer, and the presence of a surfactant within the Helmholtz layer, can be determined by capillary electrometer experiments, wherein the forced discharge of the double layer is observed in terms of an interfacial tension effect[58]. In the absence of specific ion adsorption, the tension is greatest when the net coulombic repulsion at the interface is minimized. An electrocapillary maximum is therefore observed at the zero charge potential. Altered zero charge potentials and electrocapillary curve slopes are noted when surfactants are present in the electrolyte.

Studies of molten metal-fused salt systems have also demonstrated the presence of double layers and electrocapillary effects. However no simple relation can be derived to directly associate the phenomena observed in aqueous and molten salt systems. In aqueous electrolytes, the two-part Helmholtz-Gouy structures, are primarily determined by hydration effects which do not occur in fused salts. It has been suggested that excess charges are adsorbed several ion layers deep at fused salt interfaces[60], thus providing only one type of boundary layer structure on the electrolyte side of the interface.

For the ESR system (in analogy with the capillary electrometer

experiments discussed above) it is suggested that the impression of an alternating potential on a slag/metal system should promote a rapid expansion and contraction of the phase interfaces. The postulated boundary movement has been termed "electrocapillary vibration" and is considered a mechanism which might account for the improved desulfurization and deoxidation characteristics noted with alternating current ESR systems[4, 21]. The resulting convection and the increase in slag/metal boundary area are expected to provide a greater opportunity for both inclusion absorbtion and chemical reaction.

There is limited evidence to suggest electrocapillary vibration is not a dominant feature in the ESR process. Radiographic examination of the slag/ingot pool interface has detected wave-like oscillations which are damped when the flow of molten droplets ceases. No observable vibrations are detected however, when AC current is applied using a non-consumable electrode[25].

Little has been done to relate studies of double layer structures to electrode reactions. It is usually assumed that double layer structures are unaffected by kinetic processes, although the Guoy layer obtained with aqueous electrolytes may contribute to reaction rate control by inhibiting diffusion of reactants to the electrode. Such contributions will be minimized in very strong electrolytes and in fused salt systems.

To produce a reaction rate (or a type of reaction) differing from that observed under equilibrium conditions, the equilibrium potential difference across the double layer must be altered by applying an external potential to the system. The difference between the equilibrium electrode potential, and the applied potential causing the required reaction, is

called the overtension (overpotential or overvoltage). The overtensions required to promote reactions may be appreciable, and due to one or more phenomena commonly classified according to specific causes[45].

Reaction overtensions are encountered when the primary reacting substance must first be formed by a slow chemical reaction. The intermediate reaction results in a loss of primary reactant concentration and an overtension is required to maintain a constant current. Diffusion or mass transfer overtensions are encountered when the rate of reactant diffusion from the bulk solution to the electrode ultimately controls the reaction rate. Rapid stirring speeds up such reactions by decreasing the thickness of the diffusion layer, which in aqueous solutions may be approximately 10^{-3} cm. in width. Crystallization overtensions due to surface diffusion on solid electrodes may also be important, particularly at low current densities and low overtension values. Experiments with the gallium-gallium chloride system have shown crystallization overtensions are negligable at liquid metal electrodes and at high current density-solid metal electrodes (for the case of activated surfaces)[60].

Normally the most important overtension is that required for charge transfer through the double layer[45, 61]. At any given potential, both a forward reaction ($M \rightarrow M^+ + e$, at the anodic electrode) and reverse reaction ($M^+ + e \rightarrow M$) will occur at the same time and location. The rates for the two processes are proportional to the observed anodic and cathodic partial current densities, i+ and i- . At the equilibrium potential the two currents are equal. If a transfer overtension is applied across the double layer, the activation energy required for the forward charge-transfer reaction may be decreased, and the activation energy for the reverse

reaction correspondingly increased. A net current will then be developed. If the applied overtension is sufficiently large the reverse reaction will become negligible. Since the effect of the overtension on the forward and reverse reaction is not necessarily symmetrical, a transfer coefficient or symmetry factor, β, is obtained in the corresponding rate equations. Values of 0.5, expressing symmetrical overtension effects, are observed in many metal-electrolyte systems but other β values have been reported[58].

The intensity of each anodic and cathodic partial current is usually expressed in terms of a Tafel equation, $\eta = a + b \log i$, where a and b are constants, η is the overtension and i the operative (partial) current density. Overtension - log current density plots provide lines of constant slope over the range of strict Tafel behaviour. Depending on β values and other effects (eg., slow one-electron transfer steps; adsorption of gaseous films on anodes), non-symmetrical anodic and cathodic Tafel lines may be observed. At high current densities, "limiting currents" are also approached, wherein non-Tafel behaviour is exhibited by rapidly increasing overtensions.

When plating copper on to copper electrodes from aqueous $CuSO_4$ solutions, linear Tafel relations are obtained for both the anodic and cathodic reactions at currents up to 2.5 milliamps/cm^2. At any particular current density however, the cathodic overtensions are much larger than the anodic overtensions. The lack of symmetry is attributed to a slow one-electron transfer step at the cathode:[60]

$$Cu^{++} + e \xrightarrow{\text{slow}} Cu^{+}$$

$$Cu^{+} + e \xrightarrow{\text{fast}} Cu$$

The particular one-electron step is probably unique to the aqueous solution since it requires a partly hydrated ion to be transferred from the double layer and adsorbed on a lattice site from which it must be desolvated.

Similar one-electron transfer reactions, obeying symmetrical Tafel relations, have been noted for the deposition of iron on iron from sulfate solutions and silver on silver from $Ag\ ClO_4$ [60]. Such results are dependent on operating conditions however. At low current densities the rate of silver deposition on a thermally etched (non-activated) silver electrode is believed to be dependent on a surface diffusion mechanism. At moderate current densities (0.5 amps/cm^2), growth points become more frequent and charge transfer is the rate controlling step. At higher current densities (> 3 amps/cm^2), transfer control is maintained but limiting currents are approached and marked deviations from Tafel behaviour occur. The latter effects have been theoretically attributed to changes in the (β) symmetry factors with increasing current.

In the fused salt electrolysis of alumina[62], strict Tafel behaviour is observed with two-electron charge transfer controlling the rate of reaction at overtensions and current densities up to approximately 0.4 volts and 0.5 amp/cm^2 respectively. At higher current densities the anodic and cathodic processes become non-symmetrical and marked deviations from Tafel behaviour occur. Anode current densities greater than 0.5 amps/cm^2 are associated with very high overpotentials of 1.5 to 4 volts. The major factor contributing to the large overtension is believed to be the change from a charge transfer to a mass transfer polarization effect. Oxygen containing anions are involved in the anode process and it is suggested chemisorption of a C_xO complex is obtained at the anodic interface[62].

In summary it may be noted there is little information available concerning the electrolysis of molten salt systems and indeed concerning any electrolytic system employing current densities approaching those used in ESR processes. It may be inferred from the available literature however, that mass transfer will be important in ESR systems. Large overtensions and non-Tafel behaviour might be expected. Similarly, non-symmetrical anodic and cathodic overtension-current density relations are distinct possibilities.

Interesting experimental work of a chemical (rather than an electrochemical) nature has been reported for iron-slag systems in which surface active elements markedly influence interfacial tensions[63]. Sulfur and oxygen are observed to be surface active in molten iron droplets held under inert atmospheres. The metal surface films are believed to consist of $Fe^{2+}\!\!-\!\!O^{2-}$ and $Fe^{2+}\!\!-\!\!S^{2-}$ ionic double layers with the anions dispersed within the films to provide structures similar to those in bulk solid FeO (111) and FeS (010) planes.

When sulfur-free and 1% sulfur-bearing $CaO - Al_2O_3 - SiO_2$ slags are placed in contact with desulfurized iron droplets (3%C/0.005%S), interfacial tensions in the order of 800 dynes/cm are obtained. When the same sulfur-free slags are placed in contact with 3%C/0.7%S droplets the interfacial tensions are reduced by a factor of 160 (to an estimated 5 dynes/cm tension) during the initial desulfurization period. As the desulfurization of the metal proceeds to a level of 0.01% sulfur, the interfacial tensions again rise to 800 dynes/cm. It is concluded that the initial drastic decrease in tension is due to the diffusion of $Fe^{2+}\!\!-\!\!S^{2-}$ couples through the slag/metal interface[63]. These data, although based

strictly on a chemical desulfurization process, may be applicable to the understanding of polarity effects on droplet size changes in ESR processes.

Electroslag welding trials with 3 mm diameter wires have shown that for a given rate of electrode burnoff, metal droplet frequencies increase and droplet sizes decrease in order of melting with AC, DC negative and DC positive electrode polarities[4]. Various authors have suggested those droplet variations should also occur in the ESR process and that they are due to "pinch effects" analogous to those observed in metal arc welding processes[4, 26, 27].

In metal arc systems each element of arc current produces a magnetic field attracting the adjacent element with a force directly proportional to the square of the elemental current and inversely proportional to the distance between two such elements. The forces are appreciable at points where currents are constricted, and result in regions of high pressure adjacent to consumable electrode surfaces[64, 65, 66, 67]. The largest metal droplets are obtained when arc welding with cathodic electrodes, one rationale being that the arc termination wanders over the cathode surface to provide a larger molten zone, while the anode arc termination is static[64, 67, 68]. The bulk of the electrode current then flows through each of the large cathodic drops, providing a high pressure region below the droplet to oppose its detachment. When the electrode is anodic, most of the current flows through the electrode surface above the droplet, resulting in an added drop detachment or "pinch" force. As the anodic current densities are increased, transition points are reached when the "pinch effects" are sufficient to promote detachment of fine metal droplets in the form of molten "sprays" [64, 69, 70, 71, 72].

For those arc welding systems in which strong pinch effects are noted, electrode diameters of 1/16 to 3/16 inches and current densities of ~35,000 amps/square inch are used[64, 71]. In the present ESR study, a 1 3/16 inch diameter electrode is employed at a current density of 475 amps/square inch. Similarly, commercial ESR furnaces operating with 5 1/2 inch diameter electrodes use currents in the order of 250 amps/square inch[27]. These marked differences in arc welding and ESR current densities suggest pinch effects should be much weaker within the ESR systems. To date in fact, no experimental work has confirmed the presence of pinch forces at ESR electrode tips. One study, which tends to discredit the suggestion of strong pinch forces[25], has indicated that when two mild steel electrodes are placed in the same bath and current is applied to only one electrode, their electrode droplet sizes become equal.

In the absence of strong pinch forces, slag/metal interfacial tensions must be important in determining droplet size. In that respect it is noted from the ESR literature that droplet transfer frequency increases regularly with melt time when using an alternating current. The change in frequency has been attributed to either an increase in furnace temperature as the melt proceeds, or to a progressive change in slag composition[26]. Both effects promote variations in slag/metal interfacial tension. By analogy with the data previously cited, electrochemical deoxidation and desulfurization effects may account for the observed changes in droplet size with electrode polarity and melt time. Possible correlations between droplet size and electrochemical effects at slag/metal interfaces therefore require investigation.

2.6 Desulfurization and Transport Theory

The major ionic reactions obtained within the ESR system, will be those involving discharge of the predominant current carrying species at the anodic and cathodic slag/metal interfaces. The transport of sulfur across either boundary, will be influenced in part by the prevailing difference in chemical potential promoting desulfurization of the metal phase, regardless of the electrode polarity, and in part by the electrical potential difference associated with the predominant electrode reactions. The latter portion of the desulfurizing reaction may be regarded as a parasitic process, assisted by the prevailing overtension for current transport at the cathode and discouraged by the corresponding overtension at the anode.

Irrespective of the driving force, desulfurization may be mass or charge transfer controlled, in a manner analogous to any molten electrolyte-liquid metal transport process in which no intermediate reaction stages are involved. The results in the present study support the postulate of previous investigators[4], by showing that desulfurization within the ESR furnace is primarily dependent on processes occurring at the slag/ingot pool interface. An analysis of the desulfurization process is therefore required, to facilitate discrimination between reactions proceeding at that interface under mass transfer or charge transfer control.

Slag-metal transport processes normally require five separate steps. For the specific case of desulfurization these may be listed as follows:

1. Movement of sulfur by convection and diffusion from within the bulk metal phase to the static metal layer adjacent the metal-electrolyte boundary.

2. Diffusion of sulfur atoms across the static metal layer.

3. Transfer of electrical charge according to the reaction $S + 2e = S^{2-}$.

4. Diffusion of S^{2-} ions across the static slag layer adjacent to the metal/electrolyte boundary.

5. Movement of S^{2-} ions into the bulk slag phase by convection and diffusion.

In the ESR system, steps 1 and 5 are probably rapid, because of the high temperatures attained, the turbulent motion provided by the falling droplets and the continuous creation of new slag-metal interfaces. Steps 2, 3 and 4 must be considered in detail, however, to determine the rate controlling mechanism.

Any solute, such as sulfur, will be partitioned between two mutually immiscible slag and metal phases to the limit of an identical electro-chemical potential within each phase. The equilibrium sulfur distribution can be expressed in terms of a distribution coefficient, written as

$$K = \frac{\text{mole fraction sulfur in slag}}{\text{mole fraction sulfur in metal}} = \frac{N^{II}}{N^{I}}$$

The value of the distribution coefficient is postulated to remain approximately constant for a given operating condition but will vary with the initial slag and metal compositions, with the magnitude of the relevant overtension and with furnace temperature.

The altered sulfur capacity of slags under applied currents is well documented[51, 52]. It is instructive to estimate the dependence of the distribution coefficient on boundary overtension. At equilibrium, the

electrical potential difference across the interface will be balanced by a chemical potential difference, and the distribution coefficient may be written in terms of this chemical potential difference as

$$K = \frac{N^{II}}{N^{I}} = \frac{\gamma_o^{I}}{\gamma_o^{II}} \; e^{\frac{\mu^{II} - \mu^{I}}{RT}}$$

assuming that sulfur obeys Henry's law in the metal (I) and slag (II) phases. (γ_o^{I} and γ_o^{II} are the appropriate Henry's law coefficients).

If, in the absence of experimental information, it is assumed that an applied current displaces the boundary charge difference symmetrically from its equilibrium value for both the anodic and cathodic electrode polarities, then the chemical potential difference will also be displaced symmetrically from its equilibrium value, and the distribution coefficient K will be affected in a non-symmetric manner. (i.e., an increased slag-to-metal chemical potential difference ($\mu^{II} - \mu^{I}$) will tend to raise the distribution coefficient more than an equivalent decrease in chemical potential difference will lower it, because of the exponential nature of the above relationship).

If diffusion is considered the rate determining process for metal desulfurization, then local equilibrium conditions should be established at the interface, and under that hypothesis the interfacial sulfur concentrations will be given at any instant by

$$C_i^{II} = K' \, C_i^{I}$$

(The interfacial concentrations are designated by the subscript i, and the bulk phase concentrations by the subscript b. The concentration, C, is in units of moles/unit volume).

Consider a slag/ingot pool interface of area A cm^2, a cylindrical metal pool with convective transport depth L^I cm, and a slag pool with convective transport depth L^{II} cm. There are two static diffusion transport layers, of width Δ^I cm << L^I cm and Δ^{II} cm << L^{II} cm on the metal and slag sides of the interface respectively. The sulfur diffusivity in the metal boundary layer is D^I cm^2/sec and that in the slag layer is D^{II} cm^2/sec.

Referring to the idealized concentration - distance profiles given in Figure 2, the amount of sulfur carried by diffusion across a unit area of slag/metal interface is

$$J_s = -D^I \frac{C_i^I - C_b^I}{\Delta^I} = - D^{II} \frac{K'C_i^I - C_b^{II}}{\Delta^{II}}$$

During an ESR melt, molten electrode droplets of sulfur content C_e supply sulfur to the ingot pool at a constant rate, J_e moles/second. The flux J_s is transported into the slag. The flux J_i is transported across the solid-liquid interface and is trapped within the ingot. As discussed previously, the dendritic freezing process is expected to minimize refinement at the liquid/solid ingot interface. The fluxes are related by mass balances:

$$J_e = J_s + J_i + L^I \frac{\partial C_b^I}{\partial t} ,$$

with $J_i = v C_b^I$,

and $J_s = v (C_e - C_b^I) - L^I \frac{\partial C_b^I}{\partial t} = L^{II} \frac{\partial C_b^{II}}{\partial t}$,

where v = the (steady) solidification rate of the ingot.

The only constant flux is J_e. As described pictorially in the sequence of figures 2a, 2b and 2c, the boundary conditions for the diffusion process,

and the bulk concentrations in the ingot, ingot pool and slag are all time dependent, until the sulfur content of the bulk slag reaches a limiting value $K'C_e$. Prior to that time, the sulfur content of the ingot will be a steadily increasing function of the length of ingot melted. The sulfur profile in the solidified ingot may be obtained by numerical integration of the above equations, provided that sufficient kinetic and equilibrium data are available.

The above treatment implicitly assumes that no sulfur is lost from the slag to the mould atmosphere. If, as suggested by some studies[4], a large fraction of sulfur is removed from the slag, then a further term must be added to the mass balances, and the sulfur content of the slag may approach a steady limiting value $C_b^{II} < K'C_e$.

It should be noted that the assumption of local equilibrium is an approximation which assumes that the interfacial reaction occurs as quickly as material can be transported to and from the interface. The reaction, however, requires a small driving force, which may be approximated as $a^I - a^{II} e^{-\frac{nF\Delta\phi}{RT}}$ (where $\Delta\phi$ is the boundary overtension). This implies that a (negligibly) small departure from local equilibrium must always exist.

Finally, it may be remarked that reversal of a DC electrode polarity will, on the above model, result in different rates of desulfurization, primarily through a change in the distribution coefficient. The effect of a field on the diffusion coefficient D^{II} must also be considered.

If the rate determining process in desulfurization involves the transfer of electrons to form S^{2-} ions, then (for chemical or electrochemical processes) diffusion within both interfacial boundary layers must be relatively fast, and no appreciable concentration gradients should exist

at the interface. This situation is shown pictorially in Figures 3a, b and c, for different stages in the desulfurization process. The mass balances obtained above, also apply to this case.

For the reaction controlled process, the concentration difference at the interface ($C_b^{II} - C_b^{I}$) is a direct measure of the initially large, time-dependent, chemical potential difference between the two phases. Under these conditions, a major portion of the overtension is imposed on the single desulfurization step. The corresponding free energy-reaction coordinate diagrams are as shown in Figures 4b and 4c, and are to be compared with the diagram for the diffusion controlled process, 4a. The cathodically imposed overtension will facilitate desulfurization through a reduction of the height of the forward free energy barrier by an amount $\beta n F \Delta\phi$, where β is a symmetry factor[58], and $\Delta\phi$ is that part of the overtension which acts through the charge transfer reaction. A corresponding anodic overtension, $(1 - \beta)nF\Delta\phi$, will hinder the reverse transfer of sulfur by raising the height of the barrier.

Using absolute rate theory[73], the equilibrium constant for the formation of an activated complex (+) may be written

$$K^+ = \frac{a^+}{a^I} = \frac{N^+\gamma^+}{N^I\gamma^I} \quad ,$$

and the rate of the forward reaction written as

$$\nu N^+ = \frac{N^I\gamma^I K^+}{\gamma^+} \quad ,$$

where ν is a frequency factor and all activity coefficients (γ), activities (a) and mole fractions (N) refer to sulfur in solution.

Since $\Delta F^+ = - RT \ln K^+$,

or $K^+ = e^{- \Delta F^+/RT}$,

the rate of the forward reaction at the zero charge potential is then

$$\vec{J} = \sqrt{N^+} = N^I \left[\sqrt{e}^{- \Delta F^+/RT} \frac{\gamma^I}{\gamma^+}\right]$$

Similarly, for the reverse reaction,

$$\overleftarrow{J} = N^{II} \left[\sqrt{e}^{- (\Delta F^+ + \Delta F_R)/RT} \frac{\gamma^{II}}{\gamma^+}\right]$$

and if ΔF_R is sufficiently large,

$$J_{net} = \vec{J} - \overleftarrow{J} \simeq J^{\rightarrow} = \vec{K} N^I$$

In the case of a cathodic reaction (Figure 4b),

$$J_{cathodic} = \vec{J}_{cathodic} - \overleftarrow{J}_{cathodic}$$

$$= N^I \left[\sqrt{e}^{- (\Delta F^+ - \beta n F \Delta\phi)/RT} \frac{\gamma^I}{\gamma^+}\right]$$

$$- N^{II} \left[\sqrt{e}^{- (\Delta F^+ + \Delta F_R + (1-\beta)\, nF\Delta\phi)/RT} \frac{\gamma^{II}}{\gamma^+}\right]$$

Assuming the reverse reaction (second term) is neglibible then

$$J_{cathodic} = \vec{K} N^I e^{+ \beta n F \Delta\phi/RT}$$

If an anodic overtension occurs at the slag-ingot interface (Figure 4c),

$$J_{anodic} = \vec{J}_{anodic} - \overleftarrow{J}_{anodic}$$

$$= N^I \left[\sqrt{e}^{-(\Delta F^+ + \beta n F \Delta\phi)/RT} \frac{\gamma^I}{\gamma^+}\right]$$

$$- N^{II} \left[\sqrt{e}^{-(\Delta F^+ + \Delta F_R - (1-\beta)\, nF\Delta\phi)/RT} \frac{\gamma^{II}}{\gamma^+}\right.$$

where the second term may not be negligible.

$$\text{Then } J_{\text{anodic}} = \frac{\sqrt{e^{-(\Delta F^{+} + \beta nF\Delta\phi)/RT}}}{\gamma^{+}} \left[a^{I} - a^{II}\, e^{-(\Delta F_{R} - nF\Delta\phi)/RT}\right]$$

The caluclated value for J_{anodic} could then tend to a zero rate of desulfurization.

These equations suggest that the increase in reaction rate obtained with a (DC) cathodic overtension will be much greater than the reduction in rate to be expected under anodic polarization conditions. Further, the overall effect of an alternating potential with the same r.m.s. value as the steady DC potential, may be to raise the rate of desulfurization above that obtained with either DC mode. This conclusion rests on the exponential relationship between reaction rate and overpotential.

A similar case can be made for increased desulfurization rates with AC operation when considering the local equilibrium diffusion control model discussed previously (again without reference to electrocapillary vibration). Here a difficulty arises from the fact that the frequency of the voltage alternation is much less than the mean time spent by a diffusing atom or ion in the boundary layers (approximately $\frac{\Delta^2 cm^2}{D\ cm^2/sec} = \frac{(.01)^2}{10^{-4}} = 1$ second). It seems reasonable to assume the system would obey a time-averaged distribution coefficient, which, again because of the exponential relationship between K and $\Delta\phi$, could be much greater than that of the mean for the two DC modes under equivalent current and voltage conditions.

A possible method for distinguishing between diffusion and reaction control is suggested by the equation for initial (cathodic) pool desulfurization under reaction control conditions. Assuming the initial chemical

potential difference between the bulk slag and metal phase is large, and that the value for $\Delta\phi$ does not change appreciably as melting continues, the equation then implies that for reaction control the desulfurization rate will depend directly on the sulfur content of the metal pool.

$$\text{i.e.,} \qquad J_{\text{cathodic}} = \vec{K}\, N^{I}\, e^{-\beta n F \Delta\phi / RT}$$

If pure interfacial charge-transfer (reaction) control is assumed, the level of sulfur in the ingot should be approximately constant with length deposited, until the slag approaches saturation, at which point the ingot sulfur content should rapidly increase.

For diffusion control, the sulfur content of the ingot will be a steadily increasing function of length melted.

Finally, it should be remarked that the two rate-determining steps considered here are extremes, and that intermediate cases can be discussed.

3. Experimental Apparatus and Procedure

3.1 Selection of Variables to be Studied

There are at least nine major variables affecting ESR furnace operation. These are:

1. Power input mode: AC, DC negative or DC positive electrode polarity.
2. Current
3. Voltage
4. Mould wall electrical contact: mould wall electrically isolated or integral with the base plate.
5. Mould cooling-water temperature.
6. Electrode composition.
7. Electrode diameter.
8. Slag composition.
9. Slag volume.

Although electrode and slag analyses are important variables, many of the thermal and chemical phenomena can be studied with the use of only a single composition for each of those materials. The electrode material chosen was therefore a simple low alloy constructional steel with a high sulfur content, marketed by the Atlas Steels Company in the hot rolled and surface ground condition as Atlas Superior Shafting, with nominal analysis of .40C - 1.10 Mn - 0.020 P - .080 S - .20 Si.

A slag advocated by the British Iron and Steel Research Association [8, 22], of composition 70% CaF_2 - 20% Al_2O_3 - 10% CaO, was chosen for most

of the experimental heats. To investigate the effects of slag basicity on desulfurization, three other slag compositions were also used. i.e., pure CaF_2, 70% CaF_2 - 30% Al_2O_3 and 60% CaF_2 - 20% Al_2O_3 - 20% CaO slags.

The flow of hot tap water to the mould wall was regulated to provide a near-boiling or gently-boiling condition within the mould jacket. A jacket containing vigorously boiling water would have provided the ideal constant temperature coolant but with a rapid boil it was found difficult to eliminate mould wall buckling at local hot spots.

During the initial stages of the program, a wide range of electrode diameters and slag volumes were used to determine their effects on furnace thermal characteristics. Optimum values for both parameters were chosen and held constant for the remaining program.

The effects of amperage, voltage, electrode polarity and mould wall electrical contact were studied in detail. The effects of those parameters were assessed in terms of furnace thermal characteristics and changes in both slag and metal chemistries. Particular emphasis was placed on the associated desulfurization reactions.

3.2 Laboratory Furnace Construction

The mould system, and a metal tray to catch the run-off water from the open-topped mould jacket, were suspended from a steel table as shown in Figures 5 and 6. The upper furnace shell consisted of a heavy-walled steel ring supporting the electrode drive assembly taken from a laboratory vacuum arc furnace supplied by Edwards High Vacuum Limited. Entries were cut into the support ring for use as slag addition and fume exhaust ports. A small AC motor and gear reduction system was coupled to the electrode drive

assembly as shown in Figure 7.

Two mould designs were used, one as shown in Figure 8 with the mould base electrically isolated from the mould wall, and the other as shown in Figure 9 with the mould base electrically integral with the mould wall. Both designs used a "heat initiation pad" of the same analysis as the electrode to prevent destruction of the copper base plate during the initial air-arc, and to prevent contamination of the ingot with copper arc-spatter. Early trials with initiation pads machined to a close fit within the mould wall resulted in occasional arcing between the pad and wall. To eliminate eventual arc-penetration of the wall, the pads were machined to a smaller diameter and the annular space electrically insulated by packing with dry magnesite mould ramming mix . Moulds of both designs were clamped rigidly between the furnace table and the bottom plate of the mould suspension system. A polythene sheet was placed around the mould suspension system to direct the coolant water into the collection tray as it overflowed from the open water jacket.

The mechanical part of the electrode drive system consisted of a 1.2 amp 6000 rpm non-reversing universal motor, a speed reducer with a 400/1 gear reduction and a rubber-faced friction wheel, all mounted on a hinged aluminum plate. The remelting process was initiated by manual control but when stable melting was attained the automatic feed system was engaged by raising the aluminum plate to contact the hand-cranked electrode drive with the electronically regulated friction drive. The electronic part of the control system is shown schematically in Figure 10. 110 volt AC power was supplied from an isolation transformer to the electrode drive motor. A silicon controlled rectifier acted as an open circuit "gate" to prevent

a flow of current to the motor. The potentiometer resistance was chosen such that sufficient DC voltage to open the "gate" would be obtained from the electroslag furnace circuit when a pre-determined voltage was exceeded by that system.

To operate the furnace in the DC mode, current was supplied from a Lincoln Manufacturing Company "Shield Arc SAE 600 Welder", a motor-generator set producing a rated output of 600 amps and 40 volts at a 60 percent duty cycle. The machine provided a "drooping" volt-amp external characteristic with a wide range of continuous amperage and voltage control, as shown in Figure 11. Power for the AC furnace mode was supplied from a Westinghouse TCH-650 Industrial Welder, consisting of a transformer - reactor system providing a rated output of 650 amps and 40 volts at a 60 percent duty cycle. The machine had an external characteristic and continuous volt-ampere control range similar to that for the DC power supply.

The applied voltages were measured at the output terminals on both welding machines. The ammeters and voltmeters used in this program provided values of $\pm$ 3 percent accuracy.

3.3 Methods of Chemical Analysis

All ingot and slag analyses were based on ASTM standard procedures adapted for use by the Atlas Steels Company. The methods used for analyzing the electrode and ingot materials are outlined briefly in Table I. The slag analysis methods are given in Table II.

To determine the type of gaseous sulfur compound evolved during the ESR process a sample of the mould atmosphere was drawn through a U-tube immersed in a cold trap containing 2-Butyl Methane, maintaining a temper-

ature of -160°C. The sampling line is schematically shown in Figure 12. After trapping the sulfur-bearing gases from a furnace heat, the U-tube was fitted to a mass spectrometer gas intake valve and the contents drawn into the spectrometer to detect the sulfur compounds present.

Quantitative analysis of the mould atmosphere for SO_2 gas was accomplished using the titration apparatus from a Leco Model #517 Combustion/Iodate Titration system. The analysis train is schematically shown in Figure 13. The mould atmosphere was continuously drawn from the mould area into the analysis apparatus. If the SO_2 was evolved in excess of that conveniently handled by the titre in one burrette a constant gas flow was maintained through the by-pass portion of the sampling train while the Leco burrette and reaction chamber was readied for a repeat titration. The mould gases were then alternately sampled for 1 to 2 minutes and by-passed for 1 to 2 minutes throughout the 15 to 20 minute duration of a normal heat.

3.4 Slag Preparation

The CaF_2, Al_2O_3 and CaO slag components were purchased from a chemical distributor in the form of analytical grade powders. To avoid moisture problems indicated by the generation of large "wormholes" in preliminary ingots, the CaO and Al_2O_3 powders were dried at 1050°C and the CaF_2 powder at 400°C for 24 hours. The fluxes were then kept in separate sealed glass containers until immediately before use, when they were weighed and mixed in the desired proportions.

3.5 Sulfur Printing

To determine molten ingot pool shapes 3 grams of granular ferrous sulfide (FeS) were added to the liquid slag when approximately 3 1/4 inches of ingot had solidified. Upon completion of the heat, the ingot was slit longitudinally and one half-section surface ground to receive a sulfur print according to ASTM standard techniques.

3.6 Droplet Fall Space Measurements

Care was taken to select a large number of electrode tip shapes for each measurement since the size of the droplet remaining on the tip affects the fall space measurement.

Slag cap weights were determined at the end of each melt. Using a slag density value of 3.3 grams/cc, the corresponding slag cap volumes were calculated. The equivalent volume of water was then placed in a beaker of 2 inch inside diameter (i.e. the same diameter as the water cooled copper mould) and the electrode tip immersed in the water to the height attained by the slag during the remelting process. The fall space from the shoulder and tip of each electrode, to the bottom of the beaker was then measured.

The features of each electrode tip were outlined on the ground glass screen of a photographic enlarger. The outlines were then traced, and combined with the measured heights of slag cap, to provide line drawing impressions of the appropriate fall spaces obtained during each laboratory melt.

3.7 Furnace Operating Technique

As anticipated from comments in the literature [7, 30, 32, 74], severe heat initiation problems were encountered and a large number of heats were attempted before a satisfactory operating technique was established. The procedures finally adopted for both the AC and DC processes were as follows:

Required ESR currents were obtained by manual control of the output available from the AC or DC power source. The voltage was controlled at pre-determined values by means of the electronic system regulating the electrode travel. With power applied, an electrode was manually driven down to strike and sustain a metal arc against the heat initiation pad at the base of the mould. The slag constituents were then slowly added to the mould with the power maintained at approximately 350 amps and 30 volts. When the arc ceased and all of the slag had become molten, the automatic electrode feed was engaged to provide the required furnace voltage and the current finally adjusted to the input value desired.

The electrode burnoff rate was determined by noting the time to feed a given length of electrode into the mould, correcting that value for the corresponding increase in ingot height and calculating the total weight of electrode consumed in a unit time. By observing the voltmeter variation of 3 to 5 volts as each droplet formed and detached from the electrode, the droplet frequency was obtained and the droplet size then calculated from the electrode burnoff rate.

When melting an electrode section 1 3/16" dia. x 14" long into a mould 2" dia. x 9" long, an ingot weighing approximately 5 1/2 lbs. and 6" in height was obtained. At least the bottom 1 1/2" of each ingot was discarded as non-representative of uniform operating conditions.

4. Experimental Results

Preliminary furnace trials established a general operating technique and indicated acceptable operating conditions could be obtained with a 1 3/16" diameter electrode, a 200 gram weight of slag and a mould wall electrically isolated from the mould base.

Using those parameters, the extremes in amperage and voltage outlining the stable melt range were determined. The stable melt range obtained with a DC positive electrode polarity is shown in Figure 11. Very similar ranges were observed with AC and DC negative electrode polarities.*

Under constant current conditions, the minimum operating voltage was defined by a "short circuit" when the electrode tip contacted the ingot pool. The maximum operating voltage was defined by the occurrence of an air-arc between the electrode tip and slag surface. Under constant voltage operating conditions, the fall space was relatively insensitive to changes in current. The lower operating limit for current input was bounded by a poorly defined region where the furnace was too cold to maintain a reasonable electrode melt rate. Because heat was similarly generated within the power supply equipment, the upper current limit was defined by the safe operating range available from the power source and not by operating conditions within the furnace.

Using all three electrode polarities, and an electrically isolated

---

* Unless otherwise stated, all experimental results provided in tabular or graphical form refer to melts produced using the following furnace operating conditions: 23 volts, 530 amps, 200 grams slag charge, 1 3/16" diameter electrode and a mould wall electrically isolated from the mould base.

mould wall configuration, heats were made at various amperage and voltage values covering a wide power input range within the stable melting zones. The initial electrode analyses used for those melts, and for all melts throughout the program, are shown in Table III. Typical thermal effects are presented in Tables IV to VII and in Figures 14 to 18 inclusive, in terms of electrode burnoff rates, electrode droplet sizes, fall spaces, molten ingot pool shapes, ingot surface appearances and macrostructures. Chemical effects are presented in Tables IV to VII, and in Figures 19 to 21, in terms of percentage electrode desulfurization, final cap slag analyses and changes in chemical analyses at 3 inches above the base of each ingot.

Those melts indicated that, in general, furnace thermal characteristics were improved with increasing power input. It was also obvious that rates of electrode burnoff, ingot pool depths and electrode droplet sizes were particularly sensitive to changes in electrode polarity. To provide further information concerning those effects, melts were then made comparing electrically isolated and conducting mould wall systems. Thermal conditions obtained with the changes in mould wall electrical contact are given in Table VII and Figure 22. The chemical results, again concerning only desulfurization characteristics, are given in Table VII and Figure 23.

The above results indicated the DC negative electrode polarity provided both the slowest melt rate and the poorest desulfurization characteristics, and also severely oxidized the ingot metal. The DC positive and AC electrode polarity heats exhibited differing thermal effects but provided very similar chemical characteristics. A decision was therefore made to further investigate the effects of furnace operating

parameters, using only the DC positive electrode and electrically isolated mould wall system.

Furnace thermal characteristics corresponding to changes in electrode diameter, are given in Figures 24 and 25. Thermal conditions associated with changes in slag volume are given in Figures 26 and 27. The data imply that furnace operating characteristics can be optimized with the proper choice of electrode diameter and slag volume.

DC positive polarity heats were also made using three other slag analyses to evaluate the changes in desulfurization possible with varied slag composition. Those results are shown in Figures 28 and 29. The data indicate desulfurization is markedly improved by the addition of a basic metal oxide (i.e., calcium oxide) to the slag phase. As shown in Table VIII, however, metal oxidation problems are increased as the slag basicity is increased.

To determine the proportion of sulfur evolved from the slag, the atmosphere from a DC positive polarity heat was sampled using the cold trap apparatus described previously. Analysis by mass spectrometry detected only the presence of SO_2 gas, with the possibility that a very minor proportion of H_2S could be formed. The mould gases from two DC positive electrode polarity heats were then analyzed using the iodate titration technique. It may be noted that this method determines the total sulfur present in the form of both H_2S and SO_2 gases. The calculated sulfur balances for the corresponding ingots, slags and mould atmospheres are given in Table IX. Because the sulfur content of the atmosphere was observed to be small, and in fact less than the error in closure for the sulfur balance, no further gas sampling tests were attempted. Argon

atmospheres were provided within the mould however, to check the postulate that a negligible reaction occurred between the sulfur in the slag phase and oxygen in the atmosphere. A typical test result is shown in Table X. The data indicates desulfurization was actually improved, and ingot oxidation lessened, by excluding oxygen from the slag surface.

To complete the experimental program, the conduction characteristics of calcium fluoride slag were briefly observed. A 100 gram lot of pure CaF_2 powder was melted in a graphite crucible under an argon atmosphere. Using graphite, molybdenum and mild steel electrode pairs, currents in the order of 10 amperes (at 5 volts) could be carried between electrode surfaces 0.5 cm square and 1 cm apart.

In addition to the very high conduction characteristics, it was noted that a gas (presumably fluorine) was liberated at the anode, regardless of the anode composition. Colloidal calcium (as subsequently proven by the microprobe analysis of a slag sample) also collected on the melt surface at the anode.

A 3.5 gram ball bearing melted under a second 100 gram slag of pure CaF_2, suffered no weight loss after 30 minutes in the molten state. This suggests that iron ions have a negligible solubility in pure, molten, calcium fluoride.

5. Discussion

5.1 Current Conduction Mechanisms

It has often been stated that ionic transport may be responsible for current flow in ESR slags[6, 7, 17, 18, 20]. Calcium fluoride is readily electrolyzed with a high current efficiency and shows no tendency to form complex ions[48]. Simple electrolysis of that material, however, cannot account for the integrated current flowing through an ESR heat. A 200 gram slag, for example, would be completely discharged by the passage of approximately 10^6 coulombs, a total charge that was approached in most of the DC laboratory heats listed in this program. However slag losses were never greater than 2 percent of the charged slag weight.

It is therefore useful to examine conduction mechanisms which might account for the high currents passed without involving excessive loss of slag constituents. Possible mechanisms considered here concern the plating of iron from solution, electronic conduction within the slag phase and cyclic or regenerative reformation of calcium fluoride after ionic discharge of calcium and fluorine.

If iron (Fe^{2+}) ions were to "polarographically" carry the required currents, slag contents of at least 20 weight percent iron would be necessary, as shown by the following calculation:

The flux of iron ions required to carry a 500 ampere current is

$$J_{Fe^{2+}} = \frac{500 \text{ coulombs/sec}}{96{,}500 \text{ coulombs/gm mol wt}} \times \frac{55.85 \text{ gms } Fe^{2+}/\text{gm mol wt}}{2}$$

$$= 0.145 \text{ gms/sec.}$$

Considering a diffusivity of 10^{-4} cm^2/sec for the diffusion[49] of iron ions across a static slag/ingot boundary layer of 0.01 cm thickness and 20 cm^2 area, the concentration of iron in the bulk slag to carry the 500 ampere current is obtained from

$$J_{Fe^{2+}} = \frac{DA\,(C_{bulk} - C_{interface})}{\Delta x}$$

$$0.145\ gms/sec = \frac{20\ cm^2 \times 10^{-4}\ cm^2/sec\ (C_{bulk} - 0)\ gm/cm^3}{0.01\ cm}$$

$$C_{bulk} = 0.725\ gms/cm^3$$

For a slag of approximate density 3.3 gms/cm^3, the bulk slag concentration of iron must be $C_{bulk} = \frac{0.725}{3.3} \times 100 = 22$ weight percent.

The data given in Tables IV through VII indicate the laboratory ESR heats rarely contained more than 3 percent iron by weight. Microscopic examination and electron microprobe analysis suggested those iron contents were obtained in the form of tiny globules, in sizes 5 microns to 2 mm. diameter. The globules are probably secondary droplets injected into the slag phase during the period when primary ESR droplets are removed from the electrode tip[4]. A similar phenomenon has been well documented by cine-photography of the drop detachment period in inert-gas shielded arc-welding experiments[70].

As previously mentioned in Chapter 4, the iron solubility in pure calcium fluoride slag at 1700°C was found to be extremely small. Similarly, 10 ampere currents were carried through pure calcium fluoride slags held in graphite crucibles, when using identical carbon and molybdenum electrode pairs. Those results offer conclusive evidence that current

is not carried within the slag phase by the polarographic transport of iron ions.

Electrons might enter or leave the slag phase by tunnelling through the appropriate slag/electrode boundaries. Electronic conduction within the bulk slag, would require that electrons hop from Ca^{2+} to Ca^{+} ions, or from Fe^{2+} to Fe^{+} ions. In the present case the iron solute is considered too dilute to transport the necessary current. Considering the high ESR furnace operating temperatures, the possibility of non-stoichiometric semiconductor behavior by calcium fluoride slag cannot be neglected. However that mechanism is also believed unlikely, in view of the low current density experiments, in which all of the current may be accounted for by calcium and fluorine ion discharge[48].

A more probable conduction mechanism involves the cyclic discharge of calcium ions at the cathode, with neutral calcium ions returned to the anode to react with the discharged fluorine or to re-form Ca^{2+} ions. The cyclic process would require the molten ESR slag to have an appreciable solubility for calcium. This requirement is satisfied by pure liquid calcium fluoride, which is completely miscible with liquid calcium. The dissolved metal species is most probably neutral Ca^{o}.[75] Below the melting point of CaF_2, the solubility for Ca is negligibly small.

The present observations of high current CaF_2 electrolysis strongly suggest that excess calcium is indeed present during electrolysis, and that the dissolved calcium may be precipitated at any cold surface. This, in turn, implies that under the conditions employed in this investigation, the electrolyte was hypermonotectoid (i.e. contained >20 mol % Ca^{o}) since the initial surface precipitate proved, on cooling, to be calcium metal. (The

preferential collection of colloidal metal at the anode is presumably related to unbalanced double layer charges[58] leading to a net negative charge on the metal particles).

In the ESR process, rapid convective transport in the slag phase will sweep calcium into contact with fluorine evolved at the anode, and into contact with the anodic diffusion layer, where it may diffuse to the anode and be re-ionized.

It must be emphasized that some form of regenerative process must operate in the absence of an electronic mechanism. On the basis of presently available evidence, a major electronic contribution is considered unlikely.

5.2 ESR Thermal Characteristics

5.2.1 Direct Current Furnace Parameters

The effects of a given furnace operating parameter on the observed rates of electrode burnoff, molten ingot pool depths and slag skin thicknesses, are of very practical significance for the efficient operation of an industrial ESR furnace. Fast rates of electrode burnoff are desired to maintain high rates of ingot production. The thinnest possible slag skins are also required to minimize slag entrapment and to reduce the amount of ingot preparation required before hot working. Shallow molten pools are desirable because they promote axial crystal growth, in turn improving hot working characteristics and reducing macrosegregation effects.

As shown in Figures 14 and 16, all of the above mentioned thermal characteristics are improved with increasing power input, regardless of the electrode polarity. Greater kilowatt power inputs promote better heat dispersion throughout the slag phase, with the result that less slag is solidified along the mould wall. Electrode-to-ingot fall spaces are also increased,

particularly with the AC current systems. Thinner slag skins and greater fall spaces allow more rapid radial heat extraction from both the solidified ingot and molten metal pool zones. Shallower ingot pools therefore result, despite an increase in total power input.

It should be noted that ingot pools obtained in commercial furnaces actually increase in volume as the power input is increased[4, 40, 74]. The discrepancy may be attributed to the relatively greater radial heat losses obtained with thin slag skins and wide fall spaces when operating small mould systems.

From Figure 17 it may be noted that surface finish is improved with heat input. Similarly the macrostructures given in Figure 18 indicate that hotter melts provide more axial crystal growth, although as previously noted the same affect may not be observed with larger diameter moulds. It may be concluded better surface finish and axial crystal growth should be obtained with increased voltage, since fall spaces increase directly with voltage for all ESR systems regardless of the mould size. The conclusion is consistent with results oberved in commercial practice, indicating that when given rates of electrode burnoff are obtained by using high voltages rather than high amperages, smoother ingot surfaces and improved crystal growth patterns are provided[4].

The thermal effects corresponding to changes in electrode diameter are given in Figure 24 and 25. Large diameter electrodes provide greater cross-sectional areas for current flow, and therefore improve the heat distribution within the molten slag zone. Heat losses from the electrode are increased with larger electrode diameters. The fall space is also enlarged as the electrode diameter is increased. All three effects allow a more rapid heat loss from the mould, attendant with the formation of

shallower molten metal pools and reduced rates of electrode burnoff.

Under constant electrical conditions, fall spaces and rates of electrode burnoff vary little with changes in slag volume. Typical results are shown in Figures 26 and 27. A limiting slag volume is obtained when insufficient slag is available to provide a resistance path consistent with the total potential drop required across the slag-metal system. Since less heat can be dissipated to the mould wall from a shallow slag pool, the corresponding molten ingot pool receives more heat and becomes enlarged. With excessively large slag volumes, insufficient heat is available to completely melt slag layers located well above the fall space. In the extreme case, when the uppermost slag remains unmelted throughout the entire heat, an effective barrier is imposed on heat lost by radiation from both the slag and electrode surfaces. Again additional heat must be extracted through the ingot pool and larger molten metal pools result.

The above observations indicate that complex correlations must be made between a number of operating parameters in order to attain maximum thermal efficiencies in ESR furnaces. In general the results suggest that for small mould furnaces, alternating current systems should provide the best operating characteristics. The slower rates of electrode burnoff and deeper molten pool zones associated with the DC positive electrode systems, make that polarity mode less favorable. The DC negative electrode systems are decidedly inferior, because of their very low rates of electrode burnoff, and as will be discussed in a later section, because of their poor electrochemical characteristics. The results also indicate that electrode diameters and slag volumes must be optimized to provide proper thermal characteristics for each furnace design.

5.2.2 Direct Current Interfacial Heating Effects

As shown in Figure 25, a pronounced correlation between fall space and electrode diameter is observed when melting with a DC positive electrode polarity and an electrically isolated mould wall. It is evident from those results that the slag/electrode interfacial voltage drop is a function of the current density. An increased electrode tip area results in a lesser boundary current density and thus a decreased boundary overtension. The resistive slag path must then be enlarged to maintain the required voltage drop.

A second outstanding change in fall space is noted from the results shown in Figure 22, comparing the electrically isolated and conducting mould wall heats melted with a DC positive electrode polarity. Lowest cathodic current densities and boundary overtensions are obtained when remelting with an electrically conducting mould wall. As expected, that remelting mode is associated with the largest fall space.

When using a DC positive electrode and an electrically conducting mould wall configuration, the decreased electrode boundary area should be associated with a small increase in current density, and thus a small increase in boundary overtension. If the melt rate is decreased when changing from an isolated to a conducting mould wall configuration, then fall space must control the furnace thermal conditions. If the melt rate remains constant or increases with the change from an isolated to a conducting mould wall, interfacial heating at the electrode tip must control the observed thermal effects. The results given in Table VII indicate the electrode burnoff rate is increased. It is therefore concluded that slag/metal interfacial heating is obtained, and is important, in the small mould ESR

system.

Since the melt rates observed with the DC positive electrode polarity are greater than those observed with the DC negative electrode polarity, regardless of the mould configuration, it may also be concluded that the anodic slag/metal boundary is more intensely heated than the corresponding cathodic boundary. Similarly, overtensions must be greatest at the anodic boundaries.

It should be noted the fall space and rate of electrode burnoff are also expected to increase when changing from an isolated to a conducting mould wall, with the DC negative electrode polarity systems. Unfortunately the measurements were in both cases too erratic and limited in number to provide conclusive results. The electrode position for the DC negative electrically conducting mould wall heat, is therefore shown as a broken line in Figure 22.

The large overtensions obtained at the anodic boundaries might be associated with fluorine ion discharge on electrode surfaces containing adsorbed fluorine gas. Specifically adsorbed sulfur and oxygen ions will also interfere with fluorine discharge. Excessive evolution of fluorine should markedly raise the anodic overtension, in a manner similar to the "anode effect" observed with Hall cell cryolite melts. (The latter effect may be primarily dependent on the electrode material. Fluorine was rapidly evolved in bubble form when carbon electrodes were used to electrolize calcium fluoride slag. No large gas bubbles were observed when the fluorine was discharged on a molybdenum electrode. It was concluded that good nucleation sites for gaseous bubble formation were provided by the porous carbon anode).

In summary, it has been shown that a pronounced local heating effect is obtained at the anodic slag/metal boundary, as a result of a strong overtension developed at that interface. It has also been demonstrated that for small mould ESR systems, boundary heating effects will have a greater influence on furnace thermal conditions than will electrode-to-ingot fall spaces.

52.3 Thermal Characteristics for the AC Furnace

The data given in Table VII and Figure 14 indicate the melt rates obtained with the alternating current systems are much greater than those obtained with either of the direct current processes. However the current and voltage peaks obtained with the AC system are 1.41 times larger than the corresponding values supplied by the direct current systems. It may be that increased overtensions associated with those peak inputs provide greater local heating effects at the AC electrode tip, and therefore faster rates of electrode burnoff.

As shown in Figure 22, very shallow ingot pools and very thin slag skins were obtained when using the alternating current process. Those results are not consistent with the rapid rates of electrode burnoff and small fall spaces observed. To account for the shallow pools and thin skins, it is suggested that a large portion of the AC current must flow through the peripheral slag regions when using an electrically isolated mould wall. Similarly, more current should flow through the copper mould when using an electrically conducting mould wall.

Current channelling is commonly encountered with solid conductors carrying alternating currents. The phenomenon, called the "skin effect",

requires that 1/e of the total current should flow through the conductor at a skin depth δ, calculable from [76]

$$\delta = \left(\frac{2}{w \, \mu_R \, \mu_o \, \rho} \right)^{1/2}$$

where δ = skin depth in meters

w = current frequency = $2\pi f$ radians/second

μ_R = relative permeability of the medium

μ_o = permeability of free space = $4\pi \times 10^{-7}$ henries/meter

ρ = conductivity of the medium in mhos/meter.

For a mild steel conductor of the type used in this program, μ_R is approximately 1000 and ρ is 5.9×10^6 mhos/meter at room temperature[77]. The corresponding skin depth is calculated to be 0.84×10^{-3} meters.

Similar calculations indicate that 1/e of the total AC current should be concentrated within 1 mm of the ESR ingot surface at all temperatures below the magnetic change or Curie point (771°C). Since that temperature may be obtained within regions close to the ingot pool, it is suggested that appreciable current channelling may occur within the lower slag zones when using an electrically isolated mould wall. Concentration of the current flow along the peripheral slag/molten ingot boundary, should result in the provision of greater heat along the mould wall. The slag skin thickness would then be minimized. Rapid extraction of the heat generated near the mould wall, would promote the formation of a shallow molten ingot pool.

5.3 ESR Chemical Characteristics

5.3.1 The Desulfurization Process

It will be recalled that desulfurization reactions are believed to occur at three slag/metal interfaces within the working zone of the ESR furnace. The reactions may involve "chemical" or "electrochemical" processes, and may be diffusion or reaction controlled. It is also suggested in the ESR literature that sulfur may be continuously evolved from the molten slag surface, in the form of either sulfur dioxide or complex sulfur fluoride vapors (eg., SF_6). A primary object of the present investigation was thus to better define the nature of the desulfurization process, as it occurs in the ESR furnace.

53.1.1 Evolution of Sulfur To the Atmosphere

The gas analysis data obtained in this program, indicated that only SO_2 and very minor quantities of H_2S gases were evolved from the slag phase. No sulfur fluoride compounds were detected. Typical sulfur balances for those laboratory heats made with DC positive electrode polarities and electrically isolated mould walls are shown in Table IX. The data indicate only 0.05 percent of the initial electrode sulfur content was evolved to the atmosphere when remelting with a power input of 8 kilowatts. When using a 15.3 kilowatt power input, 2.5 percent of the initial sulfur in the electrode was evolved. In both cases the amounts of sulfur detected in the atmosphere were less than the errors of closure in the corresponding sulfur balances. The results indicate that SO_2 gas evolution is greater at higher temperatures. The amounts evolved, however, are much too small to be considered more than a very minor factor in the overall desulfurization

process.

5.3.1.2 Effect of Slag Basicity

The results given in Figures 28 and 29, show that desulfurization is markedly improved when "free" oxygen ions, in the form of calcium oxide slag constituents, are added to calcium fluoride-based slags. Alumina additions to the slag do not provide free oxygen ions, and therefore offer little improvement over those desulfurization characteristics available with the 100 percent CaF_2 slags. These results support the conclusions obtained from commercial AC furnace practice, i.e., that classic desulfurizing agents such as CaO, BaO and MgO should improve the amount of desulfurization attainable within an ESR furnace. The additions must be made with care however. The results in Table VIII indicate that desulfurization improvements were obtained only through sacrificial increases in ingot oxygen content. (The mechanisms controlling these detrimental oxidation reactions will be discussed in a subsequent section).

5.3.1.3 Direct Current Desulfurization

The experiments made with the two DC electrode polarity modes and with the electrically isolated and conducting mould wall configurations, were designed to determine the relative magnitudes of the chemical and electrochemical slag/metal reactions occurring within the ESR furnace. The same tests were also designed to determine the importance of each slag/metal interface as a reaction site for molten metal desulfurization.

When a DC positive electrode and an electrically conducting mould wall are used, the anodic electrode potential will oppose any form of metal

desulfurization at the slag/electrode boundary. The reduced current flow across the slag ingot boundary will also decrease the tendency for electrochemical transport of sulfur across the slag/ingot pool interface.

The results given in Figure 23 indicate that desulfurization is minimal when using a DC positive electrode and an electrically conducting mould wall. Since part of the sulfur transport can be attributed to a minor electrochemical effect at the slag/ingot boundary, it is suggested that with the given operating mode, chemical desulfurization reactions are virtually negligible at all three slag/metal interfaces.

With a DC negative electrode and an electrically conducting mould wall, both chemical and electrochemical desulfurization reactions can occur at the slag/electrode interface, but the reactions should be primarily chemical in nature at the falling droplet and slag/ingot interfaces. The results given in Figure 23 indicate the consumed electrode material was desulfurized by an amount similar to that observed with the positive electrode polarity and electrically conducting mould wall, suggesting that all of the sulfur transport can be attributed to electrochemical desulfurization at the slag/electrode interface.

When using a DC positive electrode and an electrically isolated mould wall, a strong cathodic potential is impressed on the slag/ingot interface. The results shown in Figure 23 indicate a 5-fold increase in sulfur transport was obtained, compared to the desulfurization occurring when the mould wall was electrically integral with the mould base.

It might be expected that the electrically isolated mould wall DC negative electrode configuration would yield significantly poorer desulfurization

than the conducting wall DC mode. Unfortunately the statistical variation of results in Figure 23 is sufficient to mask any trend of this kind.

In summary, comparison of the four direct current operating modes indicates a negligible amount of chemical desulfurization occurs at all three slag/metal interfaces. Regardless of the power supply used (AC, DC positive or DC negative electrode polarity) desulfurization will be electrochemical in nature. The slag/falling droplet interface can be neglected as an effective reaction site for sulfur transport. Maximum electrochemical desulfurization will be obtained when remelting with a DC positive electrode polarity and an electrically isolated mould wall.

5.3.1.4 The Rate Determining Step in the Direct Current Desulfurization Process

From the direct current data given in Figure 23, it will be noted that desulfurization decreases steadily with melt time, regardless of the electrode polarity or the mould wall configuration. An extreme case exhibiting that trend is shown in Figure 19, where the ingot sulfur content is plotted in detail, as a function of the length of ingot melted when using a DC positive electrode polarity and an electrically isolated mould wall. The sulfur contents are scattered within the first two inches of ingot length. The same section also had a very poor macrostructure and surface finish. (Similar results were obtained for every ingot melted throughout the program. The bottom 1 to 2 inches of all ingots were

therefore rejected as unrepresentative of steady remelting conditions). The remaining portion of the ingot, again referring to Figure 19, indicates a regular decrease in desulfurization with length remelted.

It will be recalled from the analysis given in Section 2.6, that diffusion-controlled desulfurization reactions should be characterized by steadily decreasing rates of desulfurization. Charge-transfer controlled reactions are expected to provide constant rates of desulfurization until the slag phase is very nearly sulfur saturated, at which point the rate of sulfur transfer is expected to abruptly decrease. The desulfurization values given in Figure 19, therefore provide a strong indication that the direct current reaction is diffusion controlled.

5.3.1.5 Desulfurization With Alternating Current

As shown in Figure 23, the AC and DC positive electrode electrically isolated mould wall configurations provide nearly identical desulfurization characteristics at the given power input. Additional data given in the same figure indicate the rate of desulfurization is surprisingly rapid when using an AC electrode polarity and an electrically conducting mould wall.

A current rectification effect is obtained when commercial AC furnaces are operated with electrically conducting mould walls[4, 78]. The resulting direct current component may have a magnitude approaching 30 percent of the rms alternating amperage, and is observed to flow in a manner requiring the electrode tip to be cathodic. It will be recalled from Section 2.6 that sulfur transport should increase exponentially with the cathodic overtension impressed on a slag/metal boundary. It is therefore suggested the high desulfurization values observed with the AC electrode

polarity and conducting mould wall configuration are a consequence of the very high overtensions obtained when the direct current component is superimposed on the half cycle cathodic currents obtained at the electrode tip.

Faster melt rates are provided with the use of AC polarity electrodes. The AC systems thus allow less time for sulfur to cross the slag/electrode and slag/ingot interfaces. Assuming diffusion control for the desulfurization reaction, the identical AC and DC positive isolated mould wall results, might be taken to indicate that electrocapillary vibration is important in the ESR process.

Because of the exponential relationship between the applied boundary overtensions and the sulfur distribution coefficient (K), higher sulfur contents may be favored within the slag phase when remelting with alternating currents. The value of the distribution coefficient will in turn determine the instantaneous chemical potential difference between the slag and metal phase, and thus affect those rates of desulfurization limited by both mass transport and charge-transfer reactions. The alternating overtensions impressed on a slag/metal boundary will have a negligible net effect on the diffusivity of a sulfur ion within the slag phase.

In summary, a reasonable explanation for the rapid AC sulfur transport thus does not necessarily require an electrocapillary vibration postulate. The improved desulfurization results may be based solely on peak AC overtension effects obtained at slag/metal boundaries. Because diffusion and reaction controlled processes could be similarly affected, the alternating current results do not provide an unique method for establishing the rate determining step in the desulfurization reaction.

5.3.2 The Deoxidation Process

Metal deoxidation can be obtained by both ionic reaction and physical entrainment of metal oxide inclusions within the slag. The data given in Table VII indicate a deoxidation effect is only obtained when using a DC positive electrode polarity and an electrically isolated mould wall. The initial electrode oxygen contents are widely varied, however, and for that reason the oxygen analyses given in the table are not directly comparable. The two DC positive polarity, isolated mould wall heats listed in Table VII, were melted with electrode oxygen contents of 0.0078 weight percent. Shown in Table XI are oxygen analyses for an ingot remelted under identical furnace conditions, but from an electrode containing only 0.0015 weight percent oxygen. In the former case the metal phase was deoxidized. In the latter case a metal oxidation effect was obtained.

The above results suggest that the deoxidation process is primarily ionic, and that an equilibrium distribution coefficient can be written for the reaction. The prevailing oxygen balance must be close to the equilibrium distribution, since the direction of oxygen transport is very sensitive to relatively small changes in electrode oxygen content. Inspection of the results indicates the equilibrium distribution should be closely attained when the ingot analyses approach a common value of 0.0030 weight percent oxygen.

As previously noted in Section 5.3.1.2, desulfurization is improved with the use of increasingly basic slags. The classic equation describing the sulfur-oxygen displacement reaction,

$$[S] + (O^{2-}) = [O] + (S^{2-})$$

will not be applicable, since it is only useful for those systems in which the transport reactions are chemical in nature, and no macroscopic currents are passed. However an increase in free oxygen ion concentration within the slag phase should be associated with an increase in metal oxygen content if an equilibrium distribution coefficient is to describe the system with some degree of validity. That effect is shown in Table VIII, where it is noted the non-equilibrium ingot oxygen contents rapidly increase with increasing slag basicity.

When argon is used as a mould atmosphere, the oxygen potential is lowered and a decrease in the amount of oxygen transferred from the slag to the metal phase is to be expected. Such results are indicated by the data given in Table X. The use of an argon atmosphere will also help minimize metal oxidation by preventing electrode scale formation.

As shown in Tables V and VII, severe oxidation of the ingot is obtained when using a DC negative electrode polarity. Those results are consistent with the expected direction for oxygen transport when a strong anodic overtension is impressed on the slag/ingot boundary. The rapid oxidation reaction, coupled with a very slow rate of electrode burnoff, completely negates the use of a DC negative electrode polarity as a practical operating mode.

5.3.3 Removal of Metallic Elements From the Metal Phase

As previously described, most of the iron contained with any ESR slag cap is in the form of secondary electrode droplets. The iron contents within each slag (shown in Tables IV to VII) are therefore consistent with the rates of electrode droplet formation obtained with the corresponding

furnace operating mode.

The manganese contents for those slags listed in Tables IV to VII, cannot be attributed solely to secondary droplet formation. A 3 weight percent iron concentration (an extreme case), will carry only 0.03 percent manganese into the slag phase. The manganese contents within each slag must therefore be attributed to oxidation effects and to electrochemical transport of manganese within the ESR furnace.

Greatest manganese losses are obtained when remelting with DC negative electrode polarities. The results are consistent with the anodic transport of manganese across the slag/ingot boundary, in accordance with the reaction $[Mn] = (Mn^{2+}) + 2e$. The same loss of manganese may be also attributable to rapid oxidation of the metal phase, with subsequent entrainment of manganese as MnO within the slag. As shown in Table VII, the manganese contents within the slags are surprisingly high when remelting with a DC positive electrode and an electrically conducting mould wall. It may be that furnace configuration causes the manganese to discharge on the mould wall, with subsequent solution of the uncharged manganese into the slag phase.

The data given in Tables IV to VII and in Figure 20, indicate silicon may be appreciably removed from the metal phase. The results are scattered, and no consistent correlation is observed between silicon transport and electrode polarity. However the ratio of oxygen to silicon present within the metal phase is so low that entrainment of silicate inclusions within the slag phase cannot be considered as the predominant process for silicon transport.

The data given in Tables IV to VII further indicate that aluminum transport is directly affected by the movement of oxygen between the slag and

the metal phases. The high ingot aluminum and oxygen contents obtained with the DC negative electrode polarity are particularly interesting, and suggest that aluminum pickup by the metal phase may be accomplished through discharge of complex aluminate ions at the slag/ingot pool interface. Such reactions may occur in a manner similar to the oxygen discharge reaction postulated for aluminum recovery from Hall cell cryolite melts;[62] i.e.,

$$2\ (AlO_3^{3-}) = [Al_2O_3] + 3[O] + 6\ e$$

A similar correlation would appear likely between oxygen and phosphorus transport, since dephosphorization is also minimized when remelting with a DC negative electrode polarity, as shown in Fig. 21. The results are consistent with the discharge of a complex phosphate anion at the slag/ingot interface. The classic equation for that reaction is written as:

$$2(PO_4^{3-}) = 2\ [P] + 5\ [O] + 3(O^{2-}).$$

5.4 Electrocapillarity and Electrode Droplet Size

Small electrode droplets should maximize the entrainment of non-metallic inclusions within ESR slags. A detailed analysis of the factors affecting the droplet size is therefore of practical value, as well as of academic interest.

The results shown in Figure 15 indicate marked differences in droplet size are obtained for the three electroslag remelting modes. In general a trend to a decreased droplet size with increasing power input is evident. Droplet sizes are largest for the AC polarity mode and smallest for the DC positive electrode operation. The same droplet size sequence has been previously noted when electroslag welding with 3 mm diameter wires.

The present investigation indicates that a pronounced droplet size transition occurs with increasing power input, when remelting with a DC negative electrode polarity. The transition is correlated with an equally marked change in droplet position on the electrode tip, and with ingot pool shape, macrostructure and surface appearance. At low power inputs the drop precesses along the electrode perimeter as remelting proceeds, resulting in a spirally deposited ingot, as shown in Figures 17 and 18. Above the transition, the droplet characteristics are normal; i.e., similar to the droplet characteristics obtained with the AC and DC positive electrode polarity melts.

As discussed in Section 2.5 the only previous attempt to relate droplet size with the remelting operation, invoked pinch forces to account for the observed changes. That concept is not considered satisfactory, primarily because the electrode current densities are too low to impose appreciable forces on the electrode tips.

In the absence of strong pinch forces, surface tension is the only variable that can result in the large effects observed. The differences in drop size are of an order that may be accounted for through changes in surface tension by factors of 3 or 4. For example, a 1 gram droplet would correspond very roughly to an interfacial tension of 500 dynes/cm, while a 5 gram drop would require an interfacial tension in the order of 1700 dynes/cm.

The gradual decrease in drop size observed in Figure 15 for the AC and DC positive electrode polarity modes, is consistent with a corresponding decrease in interfacial tension as melt temperatures and electrode melt rates are increased.

It has also been shown that large variations in interfacial tension accompany the charging of electrode-electrolyte interfaces[58]. Similarly, chemical transport of surface active elements from the metal to the slag phase have been shown to alter the instantaneous or non-equilibrium interfacial tensions by factors of 160[63]. It is therefore proposed that the drop sizes associated with each electrode polarity, and the drop size transition for the DC negative electrode polarity, are entirely due to electro-capillary effects.

The following discussion makes use of the classical electrochemist's explanation for the decreased surface tension accompanying formation of a double layer; i.e., coulombic repulsion between ions of like charge will be responsible for decreased interfacial tensions. A similar rationale discussed in Chapter 2.5 is based on the belief that changes in interfacial tension are associated with the diffusion of Fe^{2+}—S^{2-} "couples" across the slag/metal interface[63]. It would seem more reasonable to assume that the charge transfer reaction $[S] + 2e = (S^{2-})$ should provide a net excess of negative sulfur ions on the slag side of the interface, and that lateral coulombic forces between those ions should limit the rate of desulfurization and simultaneously reduce the interfacial tension.

Referring first to the DC positive operating mode, the predominant ion species in the double layer at the electrode drop must be fluorine. Multiply-charged oxygen and sulfur ions will further increase the ionic repulsion forces provided by the fluorine ions. If sulfur atoms cross the interface from the metal phase, to enter the slag layer, the lateral repulsion force will again be increased and the resultant interfacial tension will therefore bevery low.

With a DC negative electrode polarity, calcium ions will predominate within the droplet double layer, and a similarly reduced interfacial tension will be expected. However, sulfur transport from the metal to the slag phase, in this case promoted by the cathodic overtension, will result in a transient anion concentration within the slag boundary. The prevailing tension will be greater than that obtained with a DC positive electrode polarity. The metal droplets obtained with the DC negative electrode polarity should therefore be larger than those droplets obtained with the corresponding DC positive electrode polarity.

At low power inputs, it is expected that current will be concentrated within the drop tip region. When using a DC negative electrode polarity, the transient anion concentration (S^{2-}, O^{2-}) at the slag/electrode interface should locally raise the interfacial tension. The instability providing the droplet precession with a DC negative electrode, is thus a consequence of the tendency for liquid metal drops to move toward regions of reduced interfacial tension.

It may be assumed the sulfur supply to the cathodic double layer will be dependent on diffusion within the liquid metal drop. An increased current density should have little effect on the rate of arrival of sulfur at the interface. However, greater currents should reduce the transient anion concentration within the double layer simply by increasing the tendency for cations to be attracted to the electrode. If the rate of removal of anions is accelerated in that way, a decreased interfacial tension will result and the conditions for droplet precession will vanish.

In summary it may be concluded that for the small mould, direct current ESR processes, ingot macrostructures are strongly dependent on

droplet characteristics. Throughout the power input range investigated, the electrode droplet sizes are controlled by electrocapillary phenomena. Variations in electrode droplet size may be understood in some detail on that basis.

AC electrode droplet sizes are consistently larger than those associated with either DC remelting mode, with the exception of the unstable droplets obtained when using DC negative polarities at low power input. Since the formation time for an electrode double layer is much less than the frequency of alternation for the AC current, it can only be supposed that the corresponding interfacial tensions rapidly alternate between two low values bounding the tension at the electrocapillary maximum. However the formation and detachment of droplets involves viscous flow, so that it seems reasonable to propose the effective tension governing the droplet size is a time average of the interfacial tension through a complete cycle. The fact that the AC droplets appear to be smaller than those obtained under low power DC negative polarity conditions, implies that cathodic interfacial tension effects are dominant in the AC process.

6. Conclusions

1. In the absence of an electronic conduction mechanism, a regenerative ion model is required to account for the high current densities in the ESR furnace. The most probable conduction process involves the discharge of Ca^{++} ions to form neutral Ca^{o}, which is dissolved in liquid slag and returned to the anodic site by simple mass transport.

2. Small mould ESR furnaces are sensitive to radial heat loss. Optimum thermal conditions are obtained when using an alternating current and an electrically conducting mould wall. Optimum electrode diameters and slag volumes must be determined for every furnace design.

3. Large overtensions and strong local heating effects are obtained at the anodes when using direct currents. The locations of the anode sites therefore have a pronounced effect on the rates of electrode burnoff, molten ingot pool depths and slag skin thicknesses. It may be suggested that the high anodic overtensions are associated with fluorine gas adsorption on the molten anode surfaces.

4. Thermal effects obtained with alternating current systems are difficult to rationalize. It is suggested that current is concentrated within a peripheral zone at the slag/ingot interface. Boundary overtensions obtained with alternating currents, exceed those overtensions obtained at either slag/metal interface when using direct currents.

5. The following conclusions are obtained from a detailed study of the direct current desulfurization process:

(a) Maximum desulfurization is obtained when using a positive electrode polarity and an electrically isolated mould wall.

(b) Sulfur is evolved from the slag phase in the form of SO_2 and H_2S gases. However the amounts evolved from the laboratory furnace were less than 2.5 percent of the initial electrode sulfur content and were therefore considered of only minor importance in the overall desulfurization process.

(c) Desulfurization is improved with the use of flux additions providing free oxygen ions in the slag phase.

(d) Virtually all of the sulfur is transported to the slag phase by electrochemical reaction.

(e) As a consequence of conclusion 5 (d), the slag/falling droplet interface can be neglected as an effective site for desulfurization.

(f) The direct current results indicate the electrochemical desulfurization reaction is diffusion controlled.

6. The alternating current, electrically isolated mould wall configuration will provide desulfurization results equivalent to those obtained with the best direct current practice.

7. Compared to the corresponding direct current results, sulfur transport is surprisingly rapid when using an alternating current and an electrically conducting mould wall (i.e., when using an operating mode similar to that used in commercial AC furnace practice). The improved sulfur transport is attributed to a combined current rectification and peak cathodic overtension effect obtained at the AC electrode tip.

8. The ingot phase is severely oxidized when the slag/ingot interface is anodic (i.e., when using a DC negative electrode polarity). A

tendency to electrochemical deoxidation should be obtained when electroslag remelting with AC and DC positive electrode polarities.

9. Because of the electrochemical nature of the deoxidation reaction, ingot oxygen contents are sensitive to changes in slag basicity and initial electrode oxygen content. Argon atmospheres decrease the amount of metal oxidation by decreasing both the prevailing oxygen potential and the amount of electrode scale formed.

10. The laboratory results indicate silicon must be removed by an electrochemical process rather than by physical entrainment of silicate inclusions within the slag phase. A correlation exists between the deoxidation reaction and the transport of manganese, aluminum and phosphorus from the metal phase. When using a DC negative electrode polarity, dephosphorization is minimized and aluminum is transported to the metal from the slag phase. It is suggested the latter effects may be attributed to complex phosphate and aluminate ion discharge at the anodic slag/ingot boundary.

11. The test work has confirmed that electrode droplet sizes increase in order of remelting with DC positive, DC negative and AC electrode polarities. In addition, the test work indicated an abrupt droplet size transition is obtained when remelting with a DC negative electrode polarity.

12. Electrode droplet characteristics can be explained in terms of electrokinetic theory: i.e., droplet sizes are determined by interfacial tension effects and therefore vary with electrode polarity, boundary overtension and specific adsorption of anions within slag/electrode boundaries.

7. Suggestions For Future Work

Most of the thermal and chemical effects obtained in the small mould ESR process can be directly associated with boundary overtensions at slag/electrode and slag/ingot interfaces. The magnitudes of those overtensions are dependent on electrode polarities, current densities, boundary layer structures and specific ion adsorption phenomena.

It is suggested that a further understanding of the ESR process will therefore require the determination of electrocapillary curves and Tafel relations for both the anodic and cathodic processes.

In addition to those programs, future investigators might also consider attempting a detailed study of the regenerative ion process providing current conduction within the ESR furnace and methods for determining accurate temperatures within the bulk slag and at the slag/electrode and slag/ingot interfaces.

8. References

1. United States Patent 2, 191, 479: Feb. 27, 1940, Manufacture of Alloy Ingots. Robert K. Hopkins assignor to M. W. Kellogg Company.

2. Canadian Patent 407,990: Oct. 13, 1942, A method of and Apparatus For Making Consistently Uniform Semi-Finished Alloy Products. Robert K. Hopkins assignor to M. W. Kellogg Company.

3. W. Richling, Electroslag Remelting, Neue Hutte, No. 9, 565-572 (1961) BISI translation 2608, Feb. 1962.

4. B. I. Medovar et al, Electroslag Remelting, Joint Publications Research Service, U.S. Department of Commerce, #22,217, Dec. 10, 1963.

5. I. Kasik et al, The Electroslag Remelting of Steels and Alloys In the USSR, Hutn. Listy, 19, No. 5, 311-318 (1964). BISI translation 4199, May, 1965.

6. B. E. Paton et al, Refusion D'Électrodes Consommables Au Sein D'Une Scorie Électroconductrice (Procédé E.S.R.), Revue Métallurgie 62, No 2, 87-114 (1965).

7. N. Robinson and J. A. Grainger, Laboratory Trials On the Remelting of Steels By the Electroslag Process, Metallurgia, 67, No. 4, 161-169, (1963).

8. A. C. Williams, The Electroslag Refining of Steel, Iron and Steel Institute, London, Special Report #77, "Clean Steel", 79-82 (1963).

9. A. C. Williams, Uses of the Electroslag Remelting Process, J.I.S.I., 202, No 7, 581-587, (1964).

10. Anon., Molten Slag Improves ESR Ingot, Iron Age Metalworking International, No 8, p34, (1966).

11. République Francaise Brevet D'Invention, PV no. 874.368: 16 Juillet 1962. Procédé de refusion au sein de la scorie électroconductrice de métaux et alliages dans un cristallisoir métallique réfrigéré, et électrodes et installation pour la réalisation de ce procédé. E. O. Paton Institut de Soudage A L'Electricité, USSR.

12. Anon, Electroslag Remelting of Steel In France, Journal of Metals, 18, No 2, 165-167 (1966).

13. B. I. Medovar et al, Evidence of Running The First Electroslag Furnace Constructed in France Under Soviet License, Stal in English, No 2, 114-118 (1966).

14. W. Martindale, Electroslag Melting Gets Rolling Again, Metalworking News, 8, No 8 (1966).

15. W. A. McKeen et al, Melting Alloys By the Hopkins Process, Metal Progress 82, No 9, 86-89, 116, 118, 120, 123, (1962).

16. Anon, Hopkins Process Finds New Facets, The Iron Age, 193, No 6, 72-73 (1964).

17. Anon, Consumable Electrode Process Licensed, Chemical and Engineering News 43 No 3, 40-41 (Jan. 18, 1965).

18. Anon, The Hopkins Process, 33/ The Magazine of Metals Producing, 3, No 6, 57 - 63 (1965).

19. Anon, Slabs Cast Via Consumable Melting, The Iron Age 197, No 5, p 63 (1966).

20. B. E. Paton and B. I. Medovar, Electroslag Remelting, Engineering Materials and Design 5, No 10, 718-723 (1962).

21. B. E. Paton et al, Achievements In Electroslag Remelting and Further Prospects for the Process, Stal in English, No 11, 862-865 (1962).

22. A. C. Williams, Electroslag Refining and Steel Cleanliness, BISRA Report MG/A/74/64, March/April 1964.

23. B. I. Medovar et al, Possible Sources of Entry By Oxygen, and Methods of Protecting The Metal from Oxidation, During Electroslag Remelting, Automatic Welding, No 11, 36-40 (1961).

24. M. M. Klyuev et al, Study of the Ideal Conditions for Removing Oxygen and Oxide Inclusions When Remelting by Electroslag Process, Automatic Welding, No 3, 66-67 (1962).

25. V. V. Panin et al, X-Ray Investigation of the Electroslag Remelting of Steel, Russian Metallurgy and Mining, No 6, 52-60 (1963).

26. D. A. Dudko et al, Some Features of Droplet Transfer from Heavy Electrodes In Electroslag Welding, Automatic Welding, No 5, 29-37 (1959).

27. M. M. Klyuev et al, Droplet Transfer of Electrode Metal During The Electroslag Remelting of Large Cross-Section Electrodes, Automatic Welding, No 5, 37-41 (1962).

28. B. I. Medovar et al, Dephosphorization of the Metal In Electroslag Welding, Automatic Welding, No 4, 5-6 (1962)

29. V. V. Topilin et al, Electroslag Remelting of Heat-Resistant Stainless Steels, Stal In English, No 9, 700-704 (1963).

30. Yu. A. Shulte et al, Defects In Steel Ingots Produced By The Electroslag Process, Stal in English, No 4, 263-267 (1961).

31. A. F. Tregubenko and V. G. Speranskii, Electroslag Remelting of Steel At the Dneprospetsstal Works, Automatic Welding, No 4, 82-88(1959).

32. A. F. Tregubenko et al, The Electroslag Remelting of Steel, Stal in English, No 3, 190 - 194 (1961).

33. B. I. Maksimovich, Design and Materials For Moulds For Electroslag Remelting, Automatic Welding, No 8, 78 - 79 (1961).

34. Anon., Union Electric Orders Big Flux Melting Furnace, 33/The Magazine of Metals Producing, 4, No 10, P 20 (1966).

35. D. A. Dudko and I. N. Rublevskii, Electromagnetic Stirring of the Slag and Metal Pools In the Electroslag Process, Automatic Welding, No 9, 10-14 (1960).

36. B. E. Paton et al, Electroslag Remelting, Engineering and Materials Design, No 10, 718 - 723 (1962).

37. Anon, Technical Note, Stal in English, No 7, p 546 (1965).

38. Anon, Firth Sterling Moves Full Steam Ahead on Hopkins Remelting, Journal of Metals, 18, No 6, 675 - 677 (1966).

39. B. S. Speranskii et al, Temperature Conditions of the Electroslag Process, Automatic Welding 16 No 1, 9 - 14 (1963).

40. D. A. Dudko et al, Effect of Electroslag Process Conditions On Metal Pool Dimensions When Melting Heavy Section Electrodes, Automatic Welding, No 1, 71 - 79 (1960).

41. R. J. Lott and G. Hoyle, Operating Characteristics of the Electroslag Process, BISRA Restricted Report, MG/A/195/65.

42. R. Laity, Transport Properties, Formalisms and Models for Ionic Transport, Disc. Faraday Soc, 32, 172 - 180 (1961).

43. H. Bloom, A. J. Easteal, Transport Numbers in Pure Fused Electrolytes, Proc., First Australian Conference on Electrochemistry, 1963 Pergamon Press (1965).

44. L. S. Darken, R. W. Gurry, Physical Chemistry of Metals, McGraw Hill (1953).

45. G. Milazzo, Electrochemistry, Theoretical Principles and Practical Applications, Elsevier Publ. Co. (1963).

46. E. A. Daney, G. J. Derge, The Electrical Conductivity of FeOx - CaO slags, Paper presented at the Annual Meeting of the AIME, Chicago, Feb. (1965).

47. M. T. Simnad et al, Ionic Nature of Liquid Iron-Silicate Slags, Trans, AIME, 200, No 12, 1386 - 1390. (1954).

48. R. G. Ward, An Introduction To the Physical Chemistry of Iron and Steelmaking, Edward Arnold, London, Publ. (1962).

49. C. Bodsworth, Physical Chemistry of Iron and Steel Manufacture, Longmans, London, Publ. (1963).

50. R. G. Ward, K. A. Salmon, The Kinetics of Sulfur Transfer From Iron to Slag, Part I, Iron and Steel Institute Journal, 196, No 12 393 - 403 (1960).

51. R. G. Ward, K.A. Salmon, The Kinetics of Sulfur Transfer From Iron to Slag, Part II, Iron and Steel Institute Journal, 201, No 3, 222 - 227 (1963).

52. O. A. Esin, The Electrolysis of Fused Slags, pp 370 - 380 in Contemporary Problems of Metallurgy. A M Samarin, Editor; translated from the Russian and published by Consultants Bureau Enterprises, N. Y. (1960).

53. S. Ramachandran et al, Rate and Mechanism of the Sulfur Transfer Reaction, Trans. AIMME, 206, No 11, 1549 - 1558 (1956).

54. P. B. Crimes, Rates of Mass Transfer in Electroslag Remelting, BISRA Metallurgy Division MG/A/72/64 Aug/Sept 1964.

55. B. I. Medovar et al, A New Method of Refining Fluorospar and Fluoride Welding Fluxes. Automatic Welding, No 4, 9 - 15 (1960).

56. Yu. V. Latash et al, Removal of Non-Metallic Inclusions From the Metal When Remelting By Electroslag Process, Automatic Welding, No 9, 14 - 21 (1960).

57. V. V. Khlynov et al, Mechanism of The Removal of Non-Metallic Inclusions From Drops of Steel During Their Movement In A Slag, Izv. A.N. SSSR, Met Gornoe Delo, No 2, 26-30 (1964). BISI Translation 4160, March 1965.

58. G. Kortüm, J. O'M. Bockris, Textbook of Electrochemistry, Volumes I and II, Elsevier Publishing Company, N. Y., 1951.

59. J. O'M. Bockris, On The Structure of Charged Interfaces, pp 832-863, Proceedings of the First Australian Conference On Electrochemistry, Pergamon Press (1965).

60. J. O'M. Bockris, Electrochemical Aspects of The Deposition of Metals, pp 161-182, ibid.

61. K. J. Vetter, The Determination of Electrode Reaction Mechanisms by the Electrochemical Reaction Orders, pp 47 - 65, Transactions of the Symposium on Electrode Processes, Wiley and Sons Inc (1961).

62. N. E. Richards, B. J. Welch, Anodic Overpotentials and Mechanism of the Anode Process On Carbon in Cryolite - Alumina Electrolytes, pp 901 - 922, Proceedings of the First Australian Conference on Electrochemistry, Pergamon Press (1965).

63. P. Kozakévitch, Surface Tension of Liquid Metals in Oxide Melts, pp 243 - 280 in text T. J. Hughel, Proceedings of the Symposium On Liquids, General Motors Research Laboratories, Warren, Michigan, 1963, Elsevier Publishing Company, N. Y., 1965.

64. M. H. Robinson, Observations on Electrode Melting Rates During Submerged - Arc Welding, Welding Journal, 40, 503_s - 515_s (1961).

65. H. Maecker, Plasmaströmungen in Lichtbögen Infolge Eigenmag, netischer Kompression, Zeitschrift Fur Physik, 141, 198 - 216 (1955)

66. A. A. Wells, A Momentum Principle for Arc Force, British Welding Journal, 9, 227 - 231 (1962).

67. J. M. Sommerville, The Electric Arc, Methuen, London (1959).

68. D. R. Milner et al, Arc Characteristics And Their Significance In Welding, British Welding Journal, 7, 73 - 88 (1960).

69. A. Lesnewich, Control of Melting Rate and Metal Transfer In Gas-Shielded Metal-Arc Welding, Welding Journal, 37, 343_s - 353_s, 418_s - 425_s (1958).

70. J. C. Needham et al, Metal Transfer In Inert-Gas Shield-Arc Welding, British Welding Journal 7, 101 - 114 (1960).

71. L. F. Defize and P. C. vander Willigen, Droplet Transfer During Arc Welding In Various Shielding Gases, British Welding Journal 7, 297 - 305 (1960).

72. W. J. Greene, An Analysis of Transfer In Gas-Shielded Welding Arcs, Applications and Industry, 49, 194 - 202 (1960).

73. S. Glasstone, K. J. Laidler, H. Eyring, The Theory of Rate Processes, McGraw-Hill, 1941.

74. R. J. Lott, Electroslag Refining, Progress Report to August 1964 BISRA Metallurgy Division, Project MG/A/272, Feb/March 1965.

75. J. Lumsden, Thermodynamics of Molten Salt Mixtures, Academic Press, 1966.

76. D. Corson, P. Lorrain, Introduction to Electromagnetic Fields and Waves, W. H. Freeman, Publ. (1962).

77. American Society for Metals, Metals Handbook, 1948 Edition.

78. B. I. Maksimovich, Conditions Under Which A Direct Current Component is Formed When Electroslag Remelting in Water-Cooled Moulds, Automatic Welding, No 4, 42 - 48 (1961).

Element in Metal	General Procedure	ASTM Standard
Carbon	Direct combustion of sample in oxygen atmosphere. Absorb CO_2 in NaOH and determine weight change.	E 30 - 56
Manganese	Dissolve sample in HNO_3, boil with Na BiO_3, filter and titrate with sodium arsenite.	E 30 - 56
Phosphorus	Dissolve sample in HNO_3, oxidize organic matter with $KMNO_4$, boil with H_2SO_3 to expel oxides of nitrogen. Precipitate with ammoniacal ammonium molybdate, add water and NaOH to precipitate and titrate with HNO_3.	E 30 - 56
Sulfur	Direct combustion of sample in oxygen atmosphere. Absorb SO_2 in acidified starch iodide solution, titrating continuously with potassium iodate.	E 30 - 60T
Silicon	Dissolve sample in H_2SO_4 and evaporate, remove iron salts with HCl, ignite in platinum crucible and weigh. Add H_2SO_4 and HF, evaporate, ignite and weigh. Weight difference represents SiO_2.	E 30 - 56
Molybdenum	Dissolve sample in $HClO_4$, fume to remove carbonaceous matter. Mix with NaCNS, $SnCl_2.2H_2O$ and isopropyl ether. Collect ether	E 30 - 56

	layer and measure absorbance or transmittance.	
Aluminum	Spectrographic method	-
Oxygen	Vacuum fusion method	-

Table 1 - Standard methods for ingot and electrode analyses

Element in Slag	General Procedure	ASTM Standard
Manganese	Dissolve slag with perchloric acid, then follow procedure for manganese determination in low alloy steels.	E 30 - 56
Sulfur	Mix slag with iron powder for high temperature fusion, then follow procedure for sulfur determination in low alloy steels.	E 30 - 60T
Iron	Dissolve slag with perchloric acid, reduce iron with stannous chloride and titrate with potassium permanganate.	E 277 (Zimmermann - Reinhar method).

Table II - Standard methods for slag analyses.

WEIGHT PERCENT ELECTRODE ANALYSES

ELECTRODE NUMBER	C	Mn	P	S	Si	O	Al
A-SERIES	.39	1.09	.020	.075	.23	.0078	.028
B-SERIES	.39	1.17	.016	.082	.20	.0033	.027
C-SERIES	.39	1.17	.018	.085	.18	.0030	.027
F-SERIES	.36	1.16	.012	.074	.21	.0031	.025
L-SERIES	.40	1.05	.016	.066	.25	.0021	.022
M-SERIES						.0030	.037
N-SERIES	.39	1.03	.014	.072	.26	.0011	.020
P-SERIES	.39	1.02	.014	.076	.28	.0011	.029

Table III - Chemical analyses for electrode materials.*

* For chemical analyses presented in this thesis the standard errors are expected to be approximately as follows; (Weight percent):
C 0.005; Mn 0.03; P 0.002 ; S 0.005; Si 0.03; O 0.001; Al 0.002.

HEAT NUMBER	ELECTRODE NUMBER	AMPS	VOLTS	WATTS	WEIGHT PERCENT INGOT ANALYSES AT 3 INCHES ABOVE INGOT BASE						WEIGHT PERCENT CAP SLAG ANALYSES			RATE OF ELECTRODE BURNOFF	ELECTRODE DROP SIZE
					C	Mn	P	S	Si	O	Al	Fe	Mn	S	(Gms/Min)	(Gms)
85	L7	300	24	7200		1.04		.042				2.80	3.20	.068	61	2.2
25	A3	365	21	7665		1.11	.012	.035	.08			2.35	2.04	.155	54	2.4
34	B2	385	15	7900		1.22		.024	.06	.0046	.022	2.57	0.68	.235	69	-
76	F2	475	19	9000		1.29		.021				2.23	0.80	.197		
95	M4	520	18	9360						.0046	.027					
24	A2	450	22	9900	.40	1.16	.012	.028	.13	.0016	.010	2.35	1.02	.184	63	1.8
97	M7	450	22	9900											64	1.8
35	B3	525	19	9975		1.13		.025	.13	.0040	.025	2.10	0.52	.299	88	1.0
23	A1	530	23	12200	.39	1.14	.013	.025	.13	.0038	.012	2.20	0.67	.320	93	1.6
47	A10	530	23	12200	.40	1.26	.016	.030	.04	.0030	.012				86	1.6
93	M3	530	23	12200						.0046	.012				109	1.8
82	L10	410	30	12300		1.12		.031				1.80	0.60	.314	115	1.6
36	B4	525	15	13200		1.15		.038	.10	.0029	.011	2.20	0.64	.381	83	1.2
94	M2	520	27½	14300						.0053	.013				119	1.3
33	B1	525	28	14700		1.14		.040		.0039	.013	2.20	0.74	.403	108	1.1
30	A7	630	24	15100	.39	1.16	.008	.040	.13			2.10	0.70	.360	114	1.3

Table IV - Thermal and chemical results for DC positive electrode polarity melts.

HEAT NUMBER	ELECTRODE NUMBER	AMPS	VOLTS	WATTS	WEIGHT PERCENT INGOT ANALYSES AT 3 INCHES ABOVE INGOT BASE							WEIGHT PERCENT CAP SLAG ANALYSES			RATE OF ELECTRODE BURNOFF	ELECTRODE DROP SIZE
					C	Mn	P	S	Si	O	Al	Fe	Mn	S	(Gms/Min)	(Gms)
37	C5	310	21	6500	.38	0.90	.018	.068	.26	.0921	>.30	4.80	1.39	.204	63	5.2
38	C4	370	22	8150	.38	1.00	.022	.074	.07	.0722	.240	1.12	3.02	.109	76	5.8
43	A9	400	23	9200								0.78	3.02	.078	75	5.8
39	C3	440	22	9700	.39	0.89	.019	.065	.16	.0871	>.30	0.78	3.18	.086	79	5.0
77	F5	530	23	12200	.37	0.97	.011	.064	.12	.0440	.130	0.90	1.52	.085		
78	F7	530	23	12200	.38	0.98	.012	.066	.14	.0461	.120	0.90	1.92	.090	66	2.4
100	M8	530	23	12300											70	2.3
41	C2	500	25	12500				.067							86	4.8
42	C1	575	26	15000	.39	0.96	.019	.069	.12	.0514	.125	1.70	.232	.124	90	2.6
160		530	35	18500											80	2.4

Table V - Thermal and chemical results for DC negative electrode polarity melts.

HEAT NUMBER	ELECTRODE NUMBER	AMPS	VOLTS	WATTS	WEIGHT PERCENT INGOT ANALYSES AT 3 INCHES ABOVE INGOT BASE							WEIGHT PERCENT CAP SLAG ANALYSES			RATE OF ELECTRODE BURNOFF	ELECTRODE DROPSIZE
					C	Mn	P	S	Si	O	Al	Fe	Mn	S	(Gms/Min)	(Gms)
109	N5	365	21	7665											86	5.3
112	N7	365	21	7665	.40	1.00	.014	.034	.13	.0035	.011	1.10	1.25	.190	90	6.5
115	N9	530	20	10600	.40	1.04	.011	.021	.19	.0044	.020	1.10	.92	.288	117	3.9
113	N8	450	24	10800	.40	0.99	.010	.027	.16	.0026	.011	1.20	0.74	.444	108	4.7
108	N3	530	23	12200											120	3.4
107	N1	530	23	12200		1.01	.012	.024	.15	.0030	.014	1.10	0.74	.375	128	4.3
118	N2	640	24	15360											148	4.0
119	N6	630	24	15200	.41	1.07	.011	.022	.20	.0031	.017	1.20	0.74	.369	157	4.2
117	N10	530	30	15900	.40	1.00	.012	.034	.13	.0030	.018	1.40	0.93	.365		

Table VI - Thermal and chemical results for AC electrode polarity melts.

MOULD WALL CONTACT	HEAT NO	INGOT ANALYSES 3 INCHES FROM BASE C	Mn	P	S	Si	O	Al	WEIGHT PERCENT CAP SLAG ANALYSES Fe	Mn	S	ELECTRODE BURNOFF RATE (Gms/Min)	ELECTRODE DROPLET SIZE (Gms)
DC POSITIVE ELECTRODE POLARITY HEATS													
ISOLATED	ELECTRODE	.39	1.09	.020	.075	.23	.0078	.028					
	23	.40	1.13	.013	.025	.13	.0046	.012	2.20	.67	.320	89	1.6
	47	.40	1.28	.012	.030	.08	.0030	.012	3.00	.70	.420		
CONDUCTING	ELECTRODE	.38	1.05	.013	.080	.23	.0033	.025	-	-	-	-	-
	49	.39	1.03	.014	.074	.07	.0071	.012	4.20	2.09	.124	113	1.7
	74	.37	.96	.012	.073	.03	.0057	.015	2.56	2.96	.102		
DC NEGATIVE ELECTRODE POLARITY HEATS													
ISOLATED	ELECTRODE	.36	1.16	.012	.074	.21	.0030	.025	-	-	-	-	-
	77	.37	.97	.011	.064	.12	.0440	.130	.90	1.52	.085	65	2.4
	78	.38	.98	.012	.066	.14	.0461	.120	.90	1.92	.090		
CONDUCTING	ELECTRODE	.36	.92	.017	.080	.18	.0033	.020	-	-	-	-	-
	65	.38	.82	.017	.080	.15	.0623	.130	1.34	1.83	.082	54	2.6
	66	.39	.83	.017	.075	.15	.0545	.180	1.34	1.95	.054		
AC ELECTRODE POLARITY HEATS													
ISOLATED	ELECTRODE	.39	1.03	.014	.072	.26	.0011	.020	-	-	-	-	-
	107	.39	1.01	.012	.024	.15	.0030	.014	1.10	.74	.375	124	4.3
	108	.41	1.02	.012	.026	.11	.0016	.013					
CONDUCTING	ELECTRODE	.39	1.03	.014	.072	.26	.0011	.020	-	-	-	-	-
	125	.40	.99	.013	.031	.16	.0016	.016	1.30	.74	.344	125	4.5
	120	.40	1.02	.015	.030	.11	.0017	.015					

Table VII - Thermal and chemical results for electrically isolated and electrically conducting mould wall system

	ANALYSIS AT 3 INCHES ABOVE INGOT BASE	
	WEIGHT % SULFUR	WEIGHT % OXYGEN* (± 0.0004)
ELECTRODE	.072	.0011
SLAG COMPOSITION		
100% CaF_2	.043	.0016
70% CaF_2/30% Al_2O_3	.038	.0027
70% CaF_2/20%Al_2O_3/10% CaO	.025	.0030
60% CaF_2/20% Al_2O_3/20% CaO	.017	.0100

* Average of at least six analyses.

Table VIII - Oxygen and sulfur analyses for ingots remelted with AC current using 4 different slags.

HEAT NO 147

VOLTS 19

AMPS 515

WATTS 7984

Grams sulfur in consumed electrode	1.110	
Grams Sulfur in ingot		0.503
Grams Sulfur in slag		0.642
Grams Sulfur in atmosphere	____	0.005
Totals	1.110	1.150
Error in closure		+ 3.6%

HEAT NO 145

VOLTS 29

AMPS 525

WATTS 15,275

Grams sulfur in consumed electrode	1.171	
Grams sulfur in ingot		0.560
Grams sulfur in slag		0.668
Grams sulfur in atmosphere	____	0.030
Totals	1.171	1.258
Error in closure		+ 7.4%

Table IX - Sulfur balances calculated at two levels of power input (for direct current positive electrode melts).

	WEIGHT PERCENT INGOT ANALYSES AT 3 INCHES ABOVE INGOT BASE							WEIGHT PERCENT CAP SLAG ANALYSES		
	C	Mn	P	S	Si	O	Al	Fe	Mn	S
ELECTRODE	.42	1.07	.013	.062	.26	.0015	.029	-	-	-
AIR ATMOSPHERE IN MOULD	.42	1.10	.016	.029	.16	.0045	.012	2.5	0.66	0.297
ARGON ATMOSPHERE IN MOULD	.42	1.06	.016	.022	.23	.0030	.020	2.2	0.40	0.425

Table X - Chemical analyses for DC positive electrode heats melted under air and argon atmospheres.

INCHES FROM INGOT BASE	ANALYSIS AT INGOT POSITION INDICATED	
	Wt % SULFUR	Wt % OXYGEN
Electrode	.062	.0015
2.0	.023	.0100
2.8	.026	.0045
3.9	.035	.0035
5.4	.040	.0030

Table XI - Sulfur and oxygen analyses as a function of ingot length.
(DC positive electrode polarity).

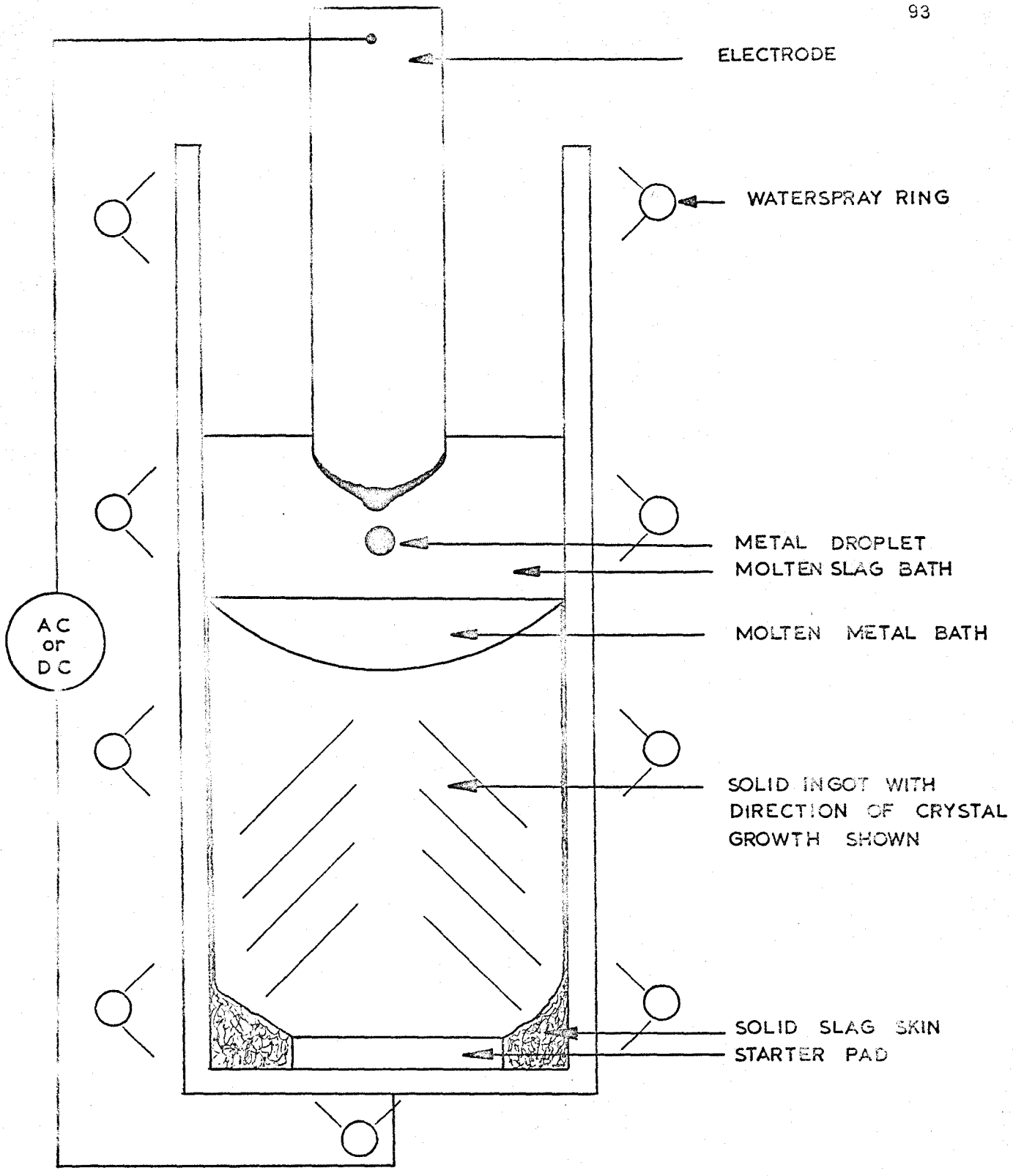

Figure 1 - Schematic drawing for a single-phase alternating or direct current ESR furnace.

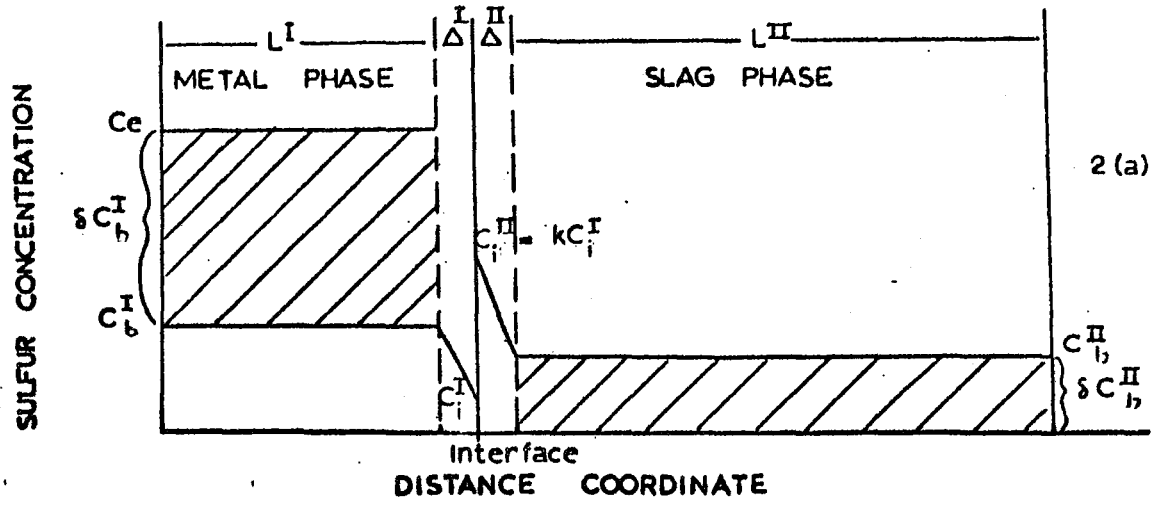

2 (a) INITIAL STAGE

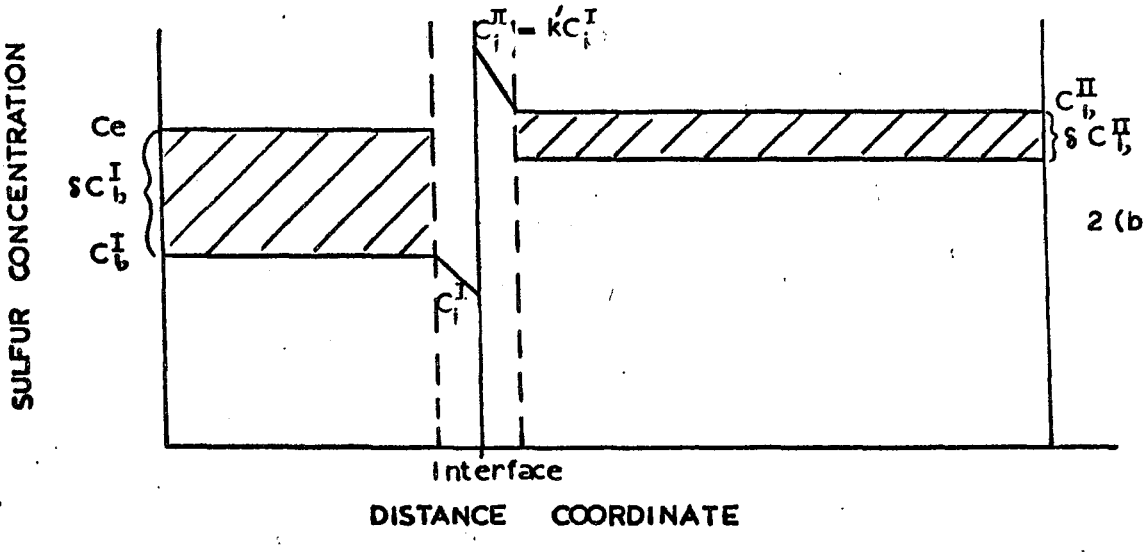

2 (b) INTERMEDIATE STAGE

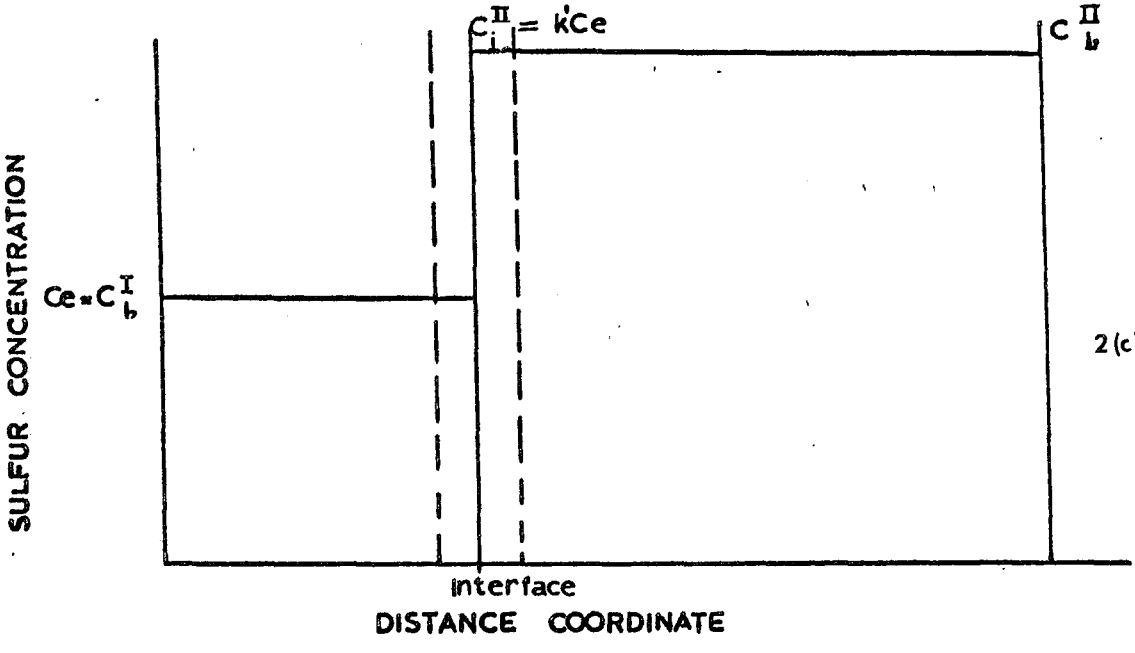

2(c) STEADY STATE

Figure 2 - Diffusion controlled partition of sulfur during an ESR melt.

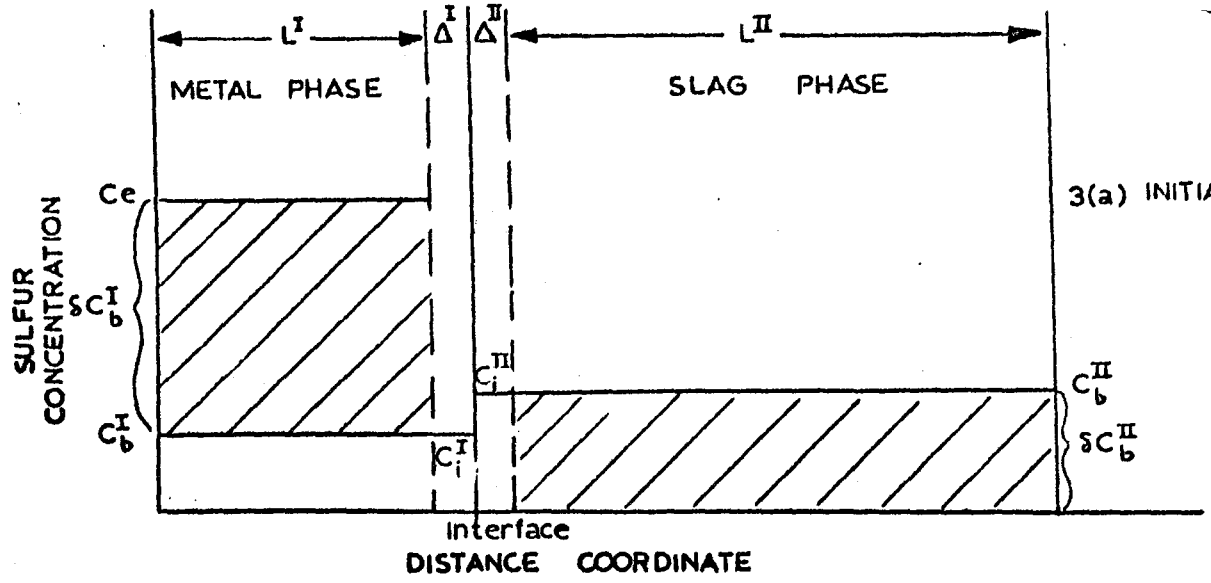

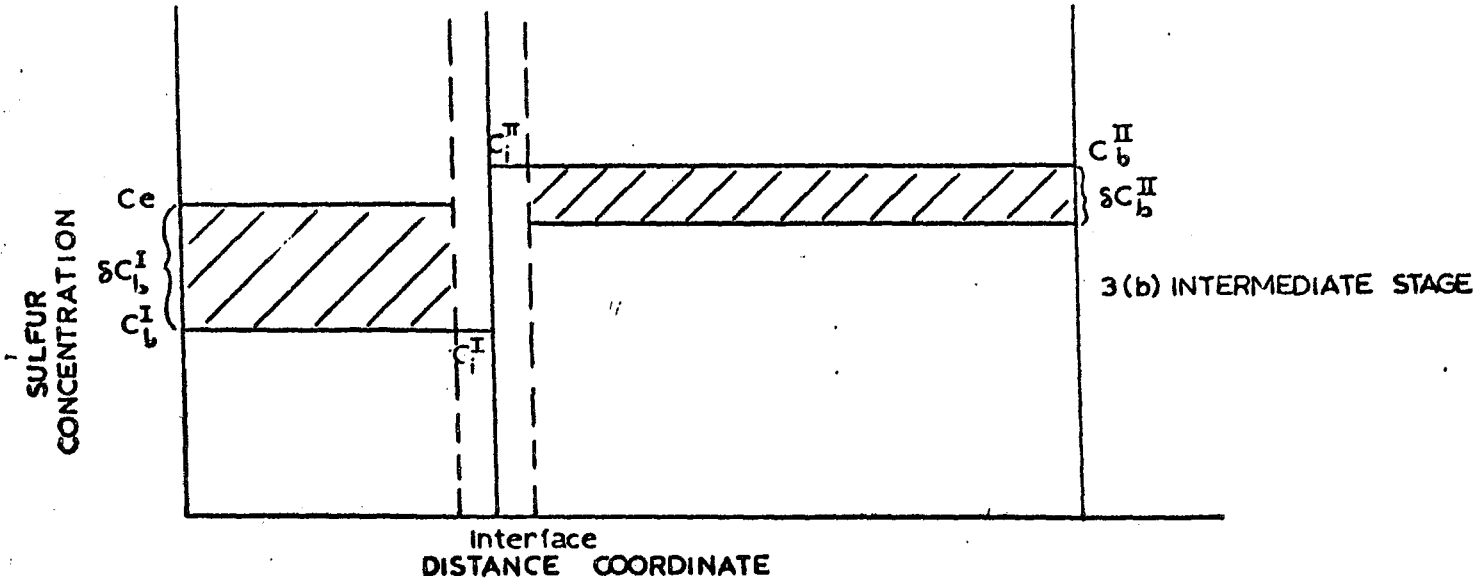

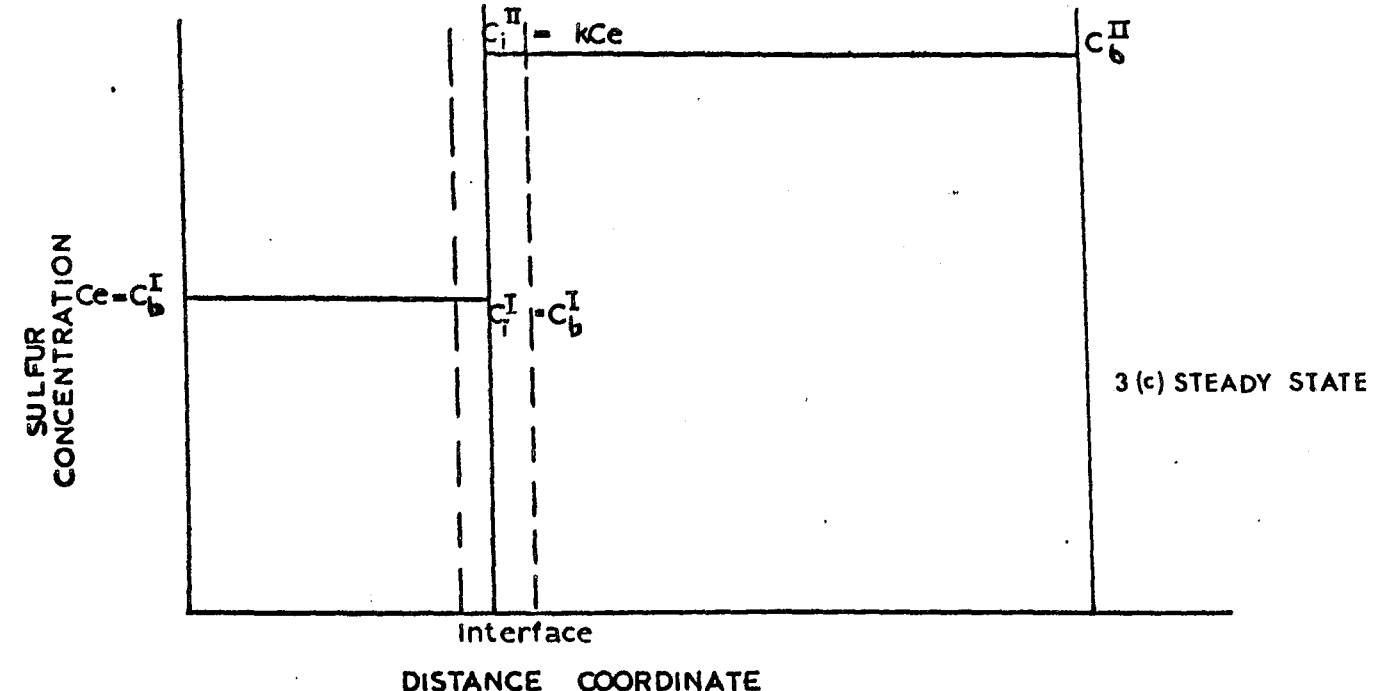

Figure 3 - Charge-transfer controlled partition of sulfur during an ESR melt.

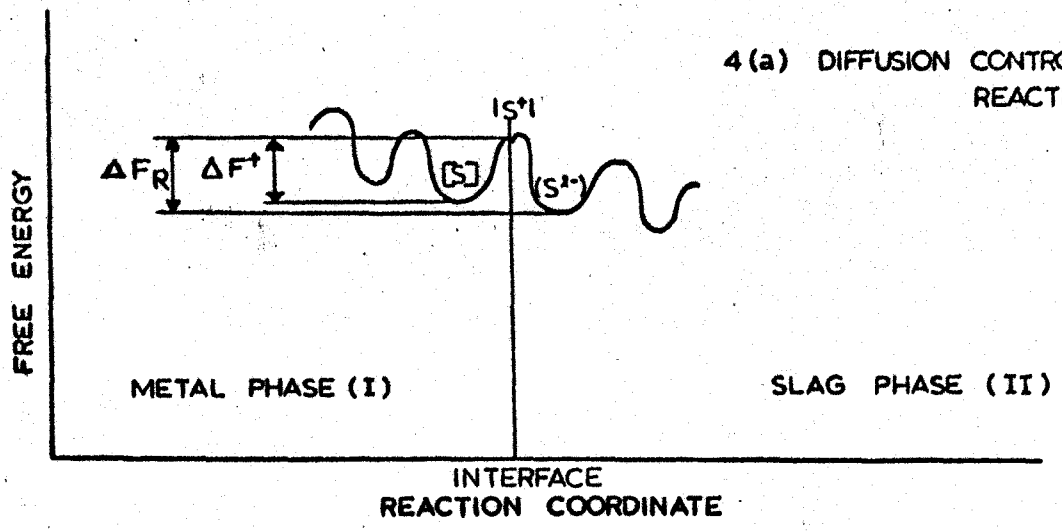

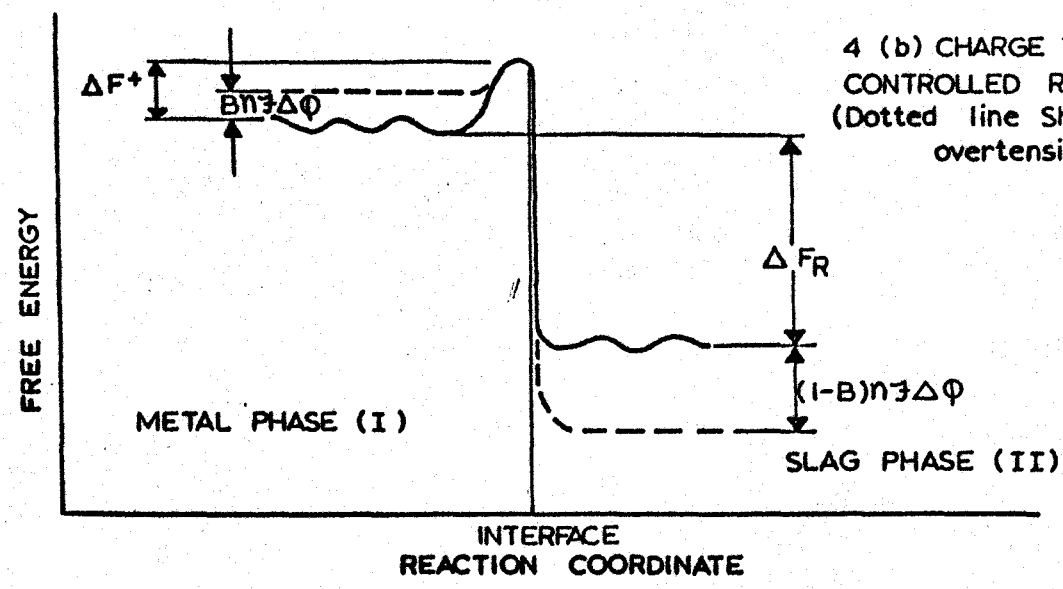

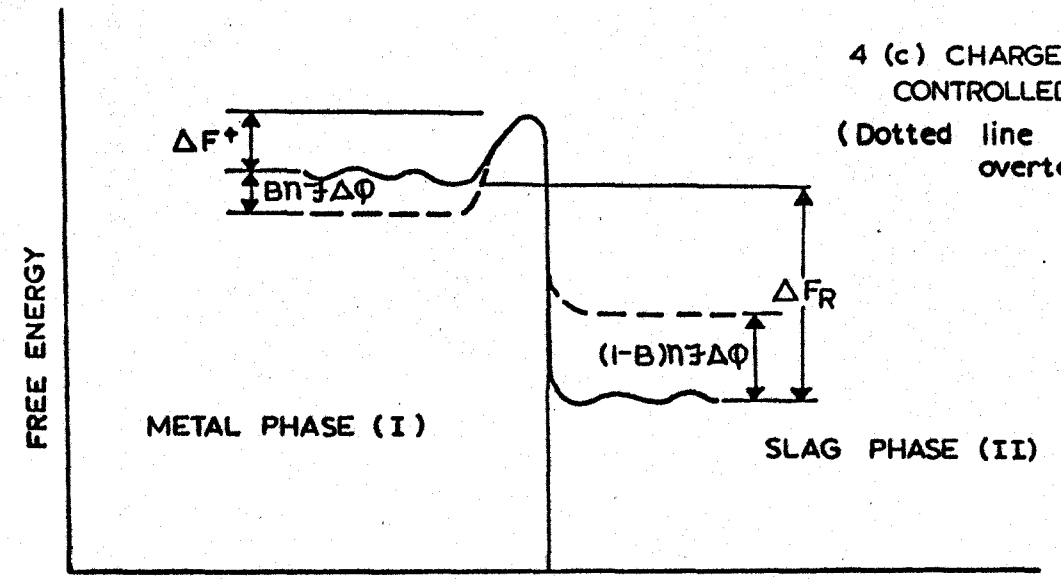

Figure 4 - Energy-reaction coordinate diagrams for diffusion and charge-transfer controlled desulfurization reactions.

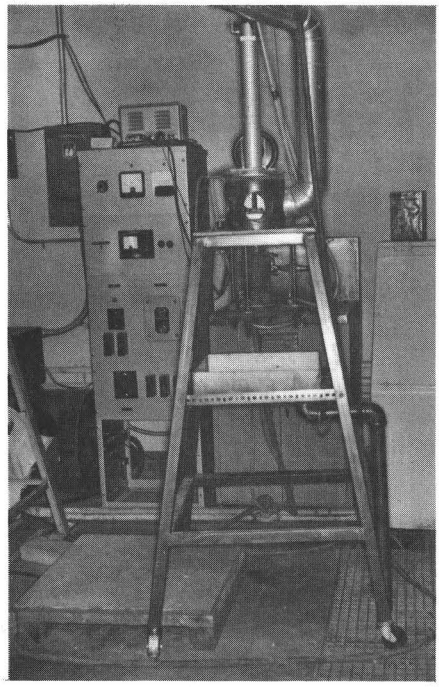

Figure 5 - The Electroslag Furnace

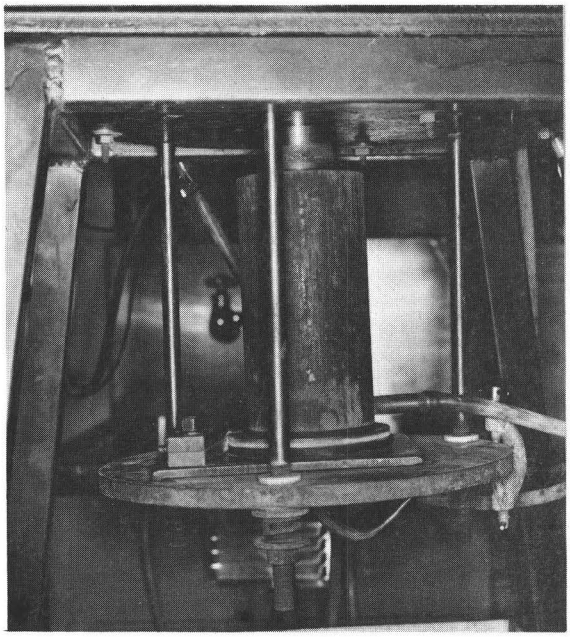

Figure 6 - The mould system clamped in position.

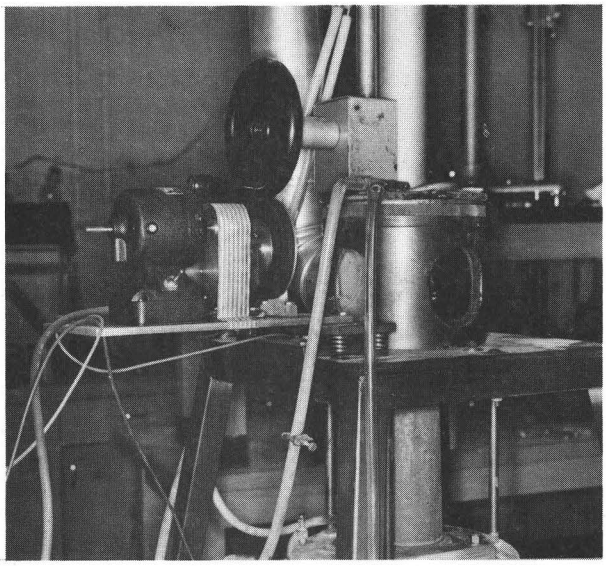

Figure 7 - The mechanical system used to regulate the electrode feed.

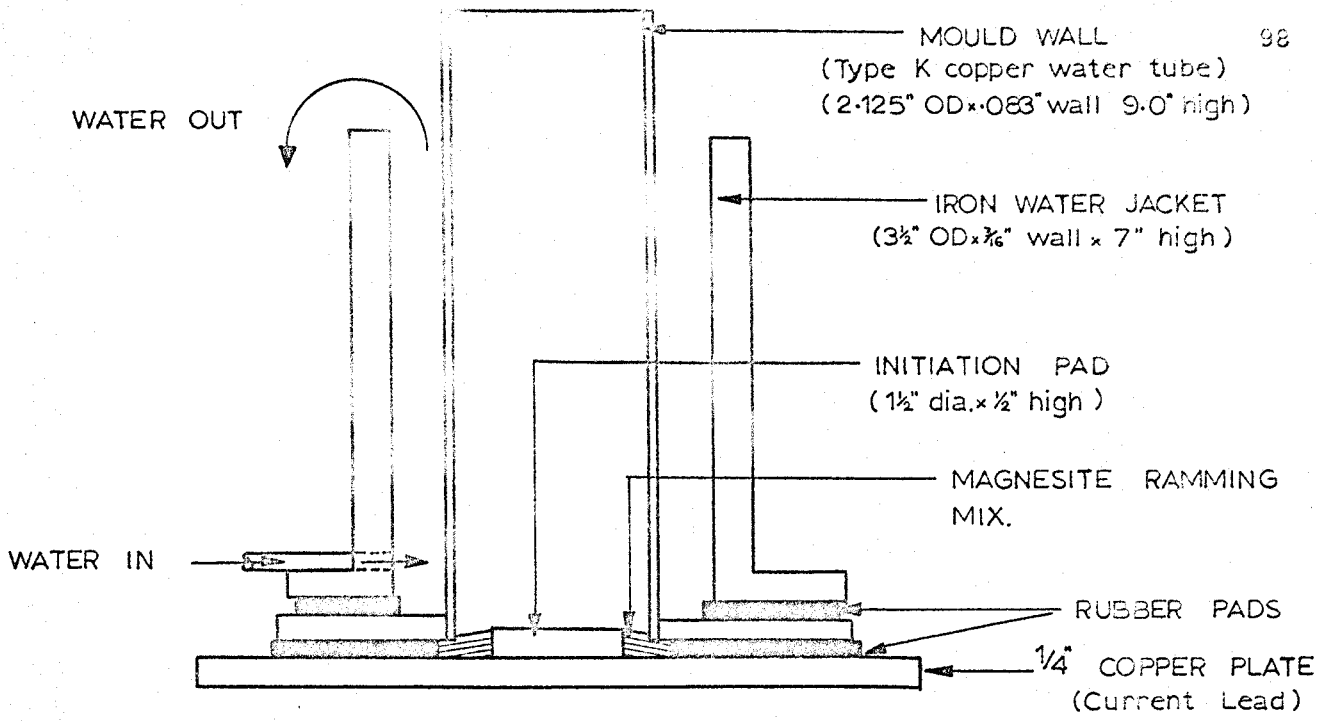

Figure 8 - A longitudinal section through the electrically isolated mould wall system.

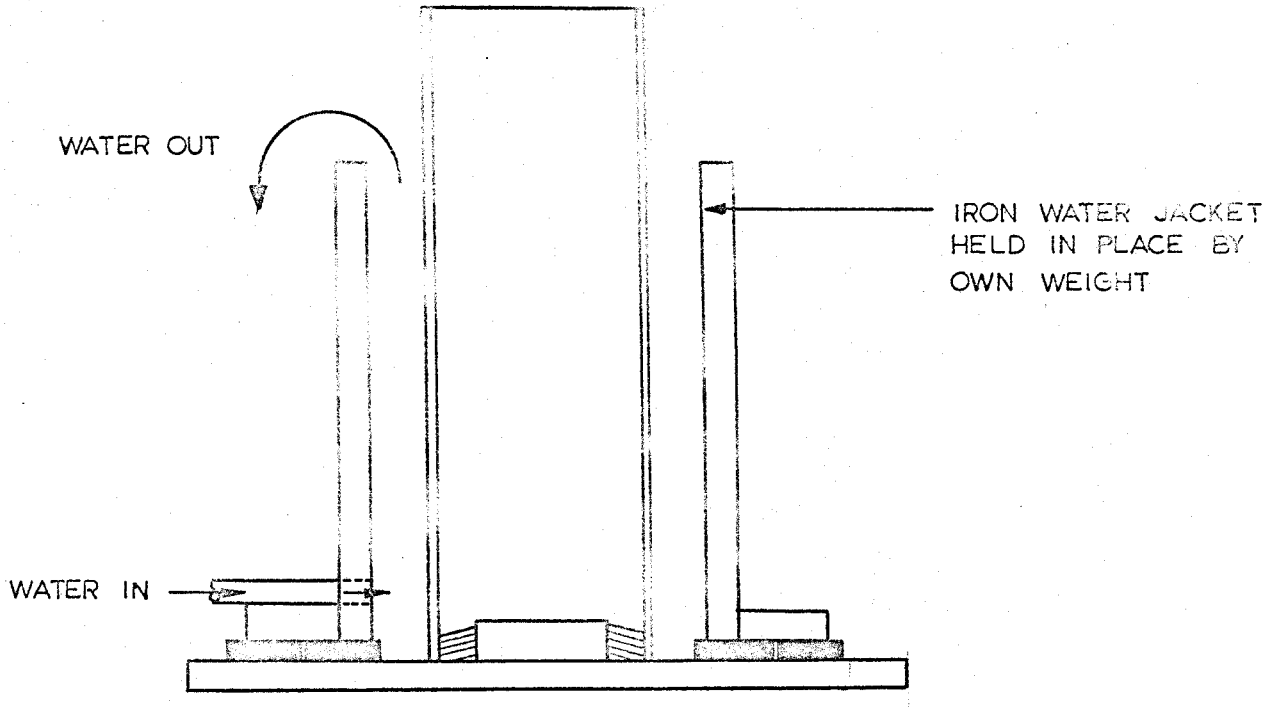

Figure 9 - A longitudinal section through the electrically conducting mould wall system.

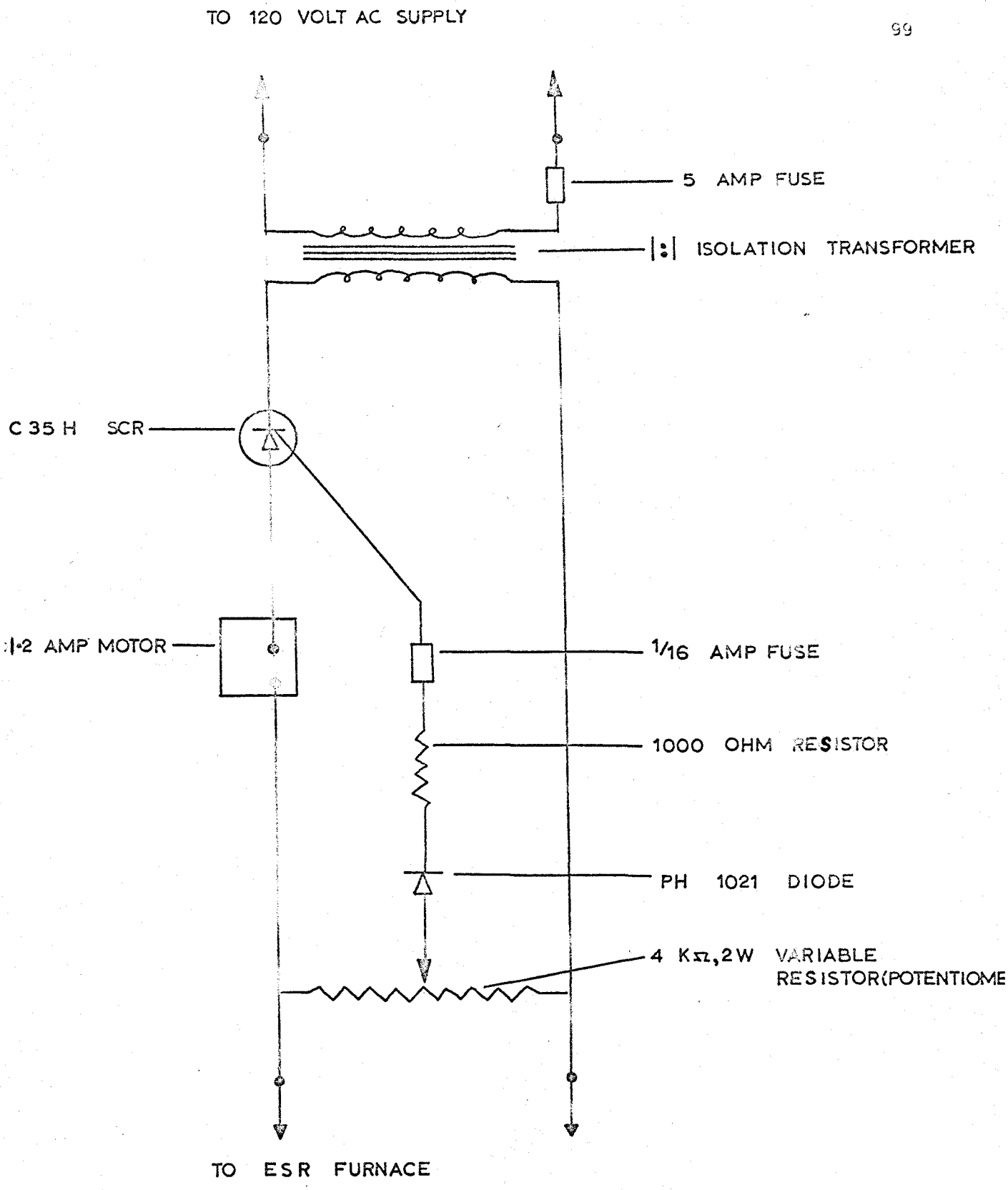

Figure 10 - Electronic control system for the automatic electrode feed.

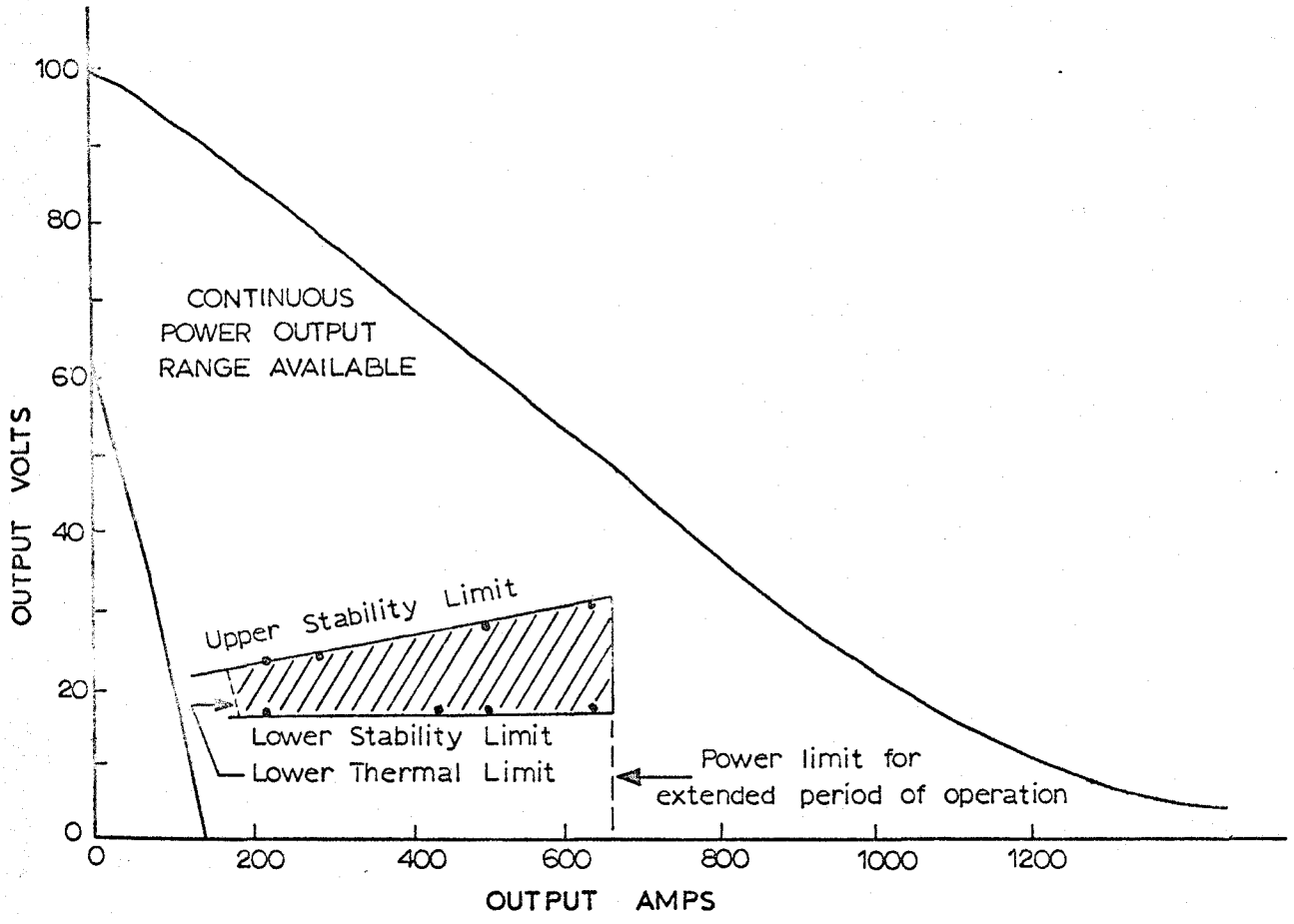

Figure 11 - Stable melt range, as related to the power supply available for the DC positive electrode polarity system.

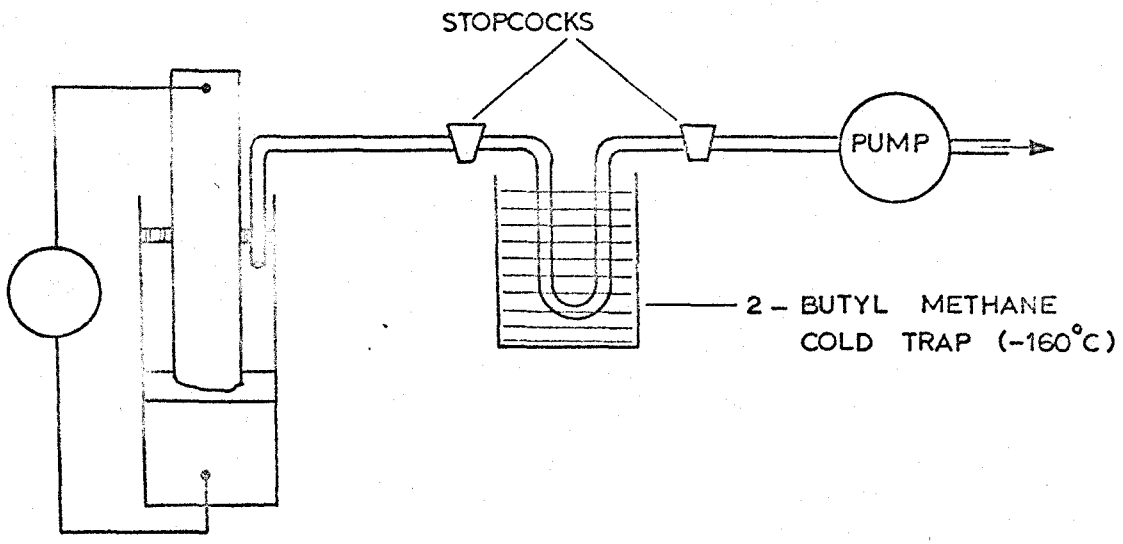

Figure 12 - Apparatus for collecting gaseous sulfur compounds to be subsequently analyzed by mass spectrometry.

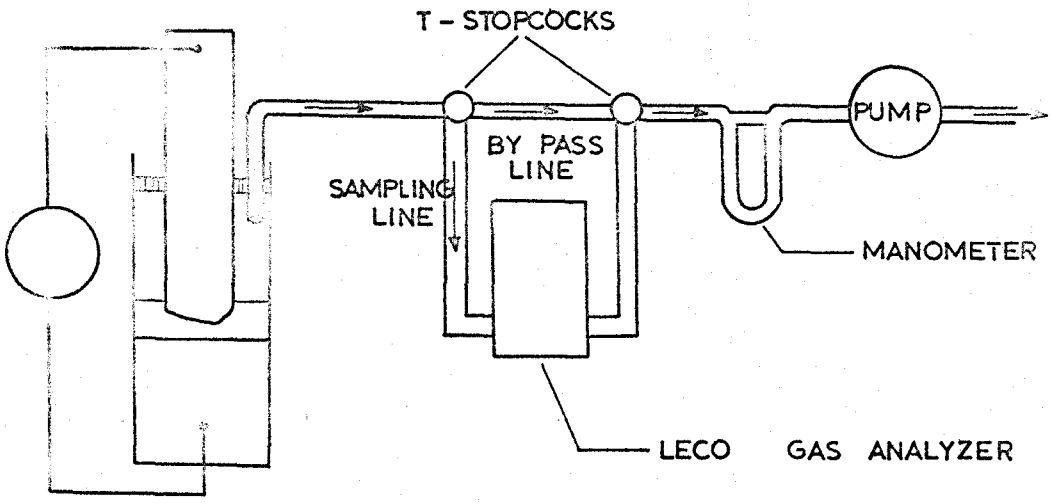

Figure 13 - Apparatus for determining the sulfur content of the mould atmosphere.

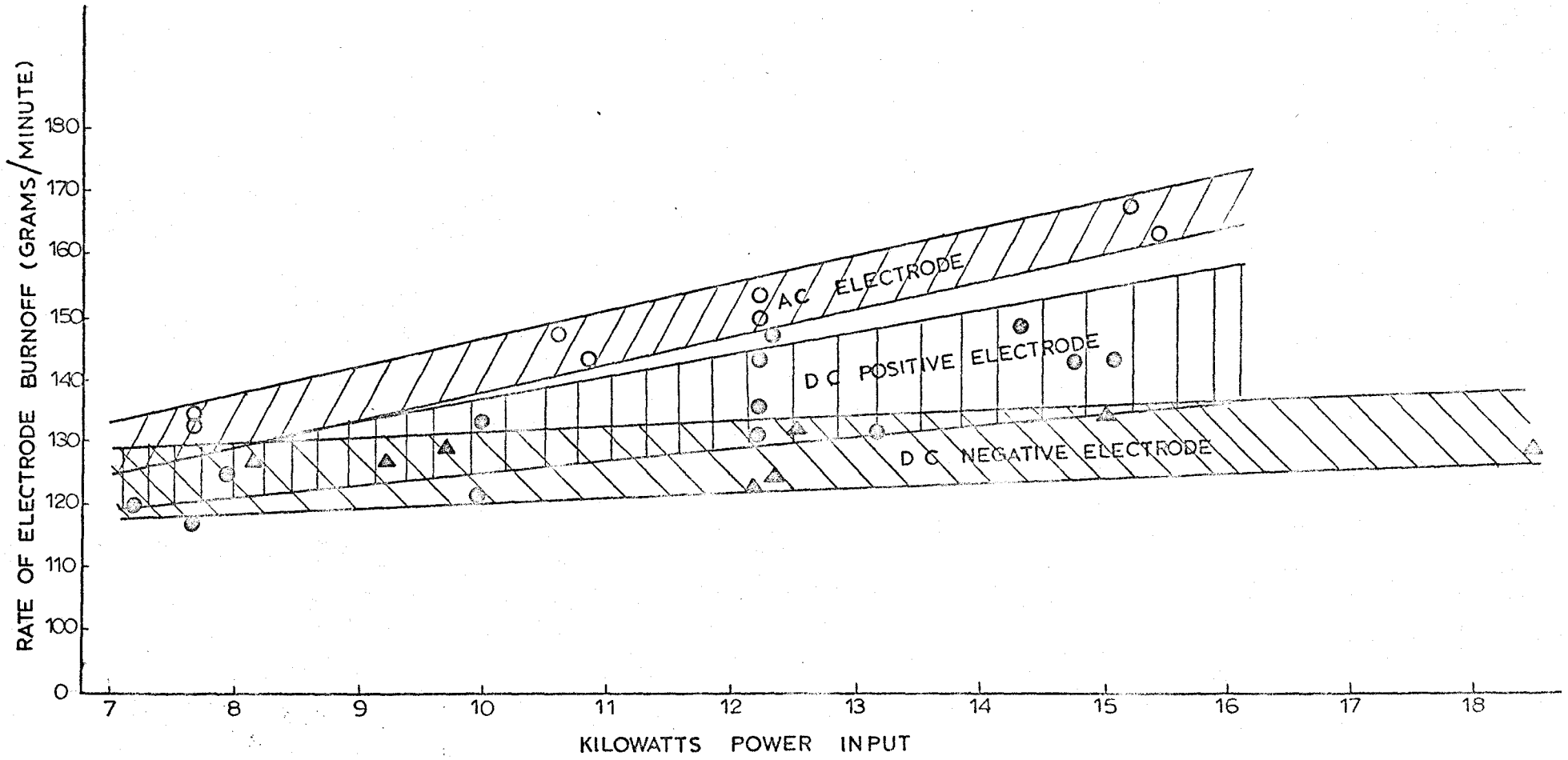

Figure 14 - Change in electrode burnoff rate with increasing power input.

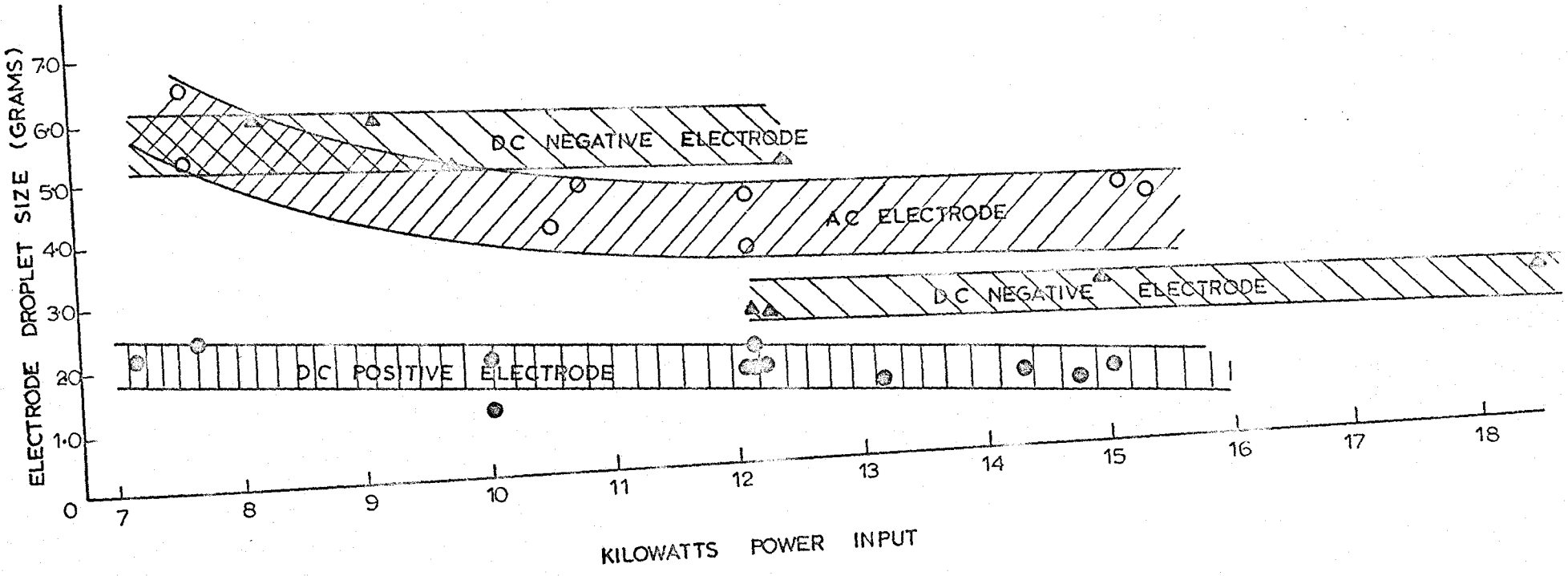

Figure 15 - Change in electrode droplet size with increasing power input.

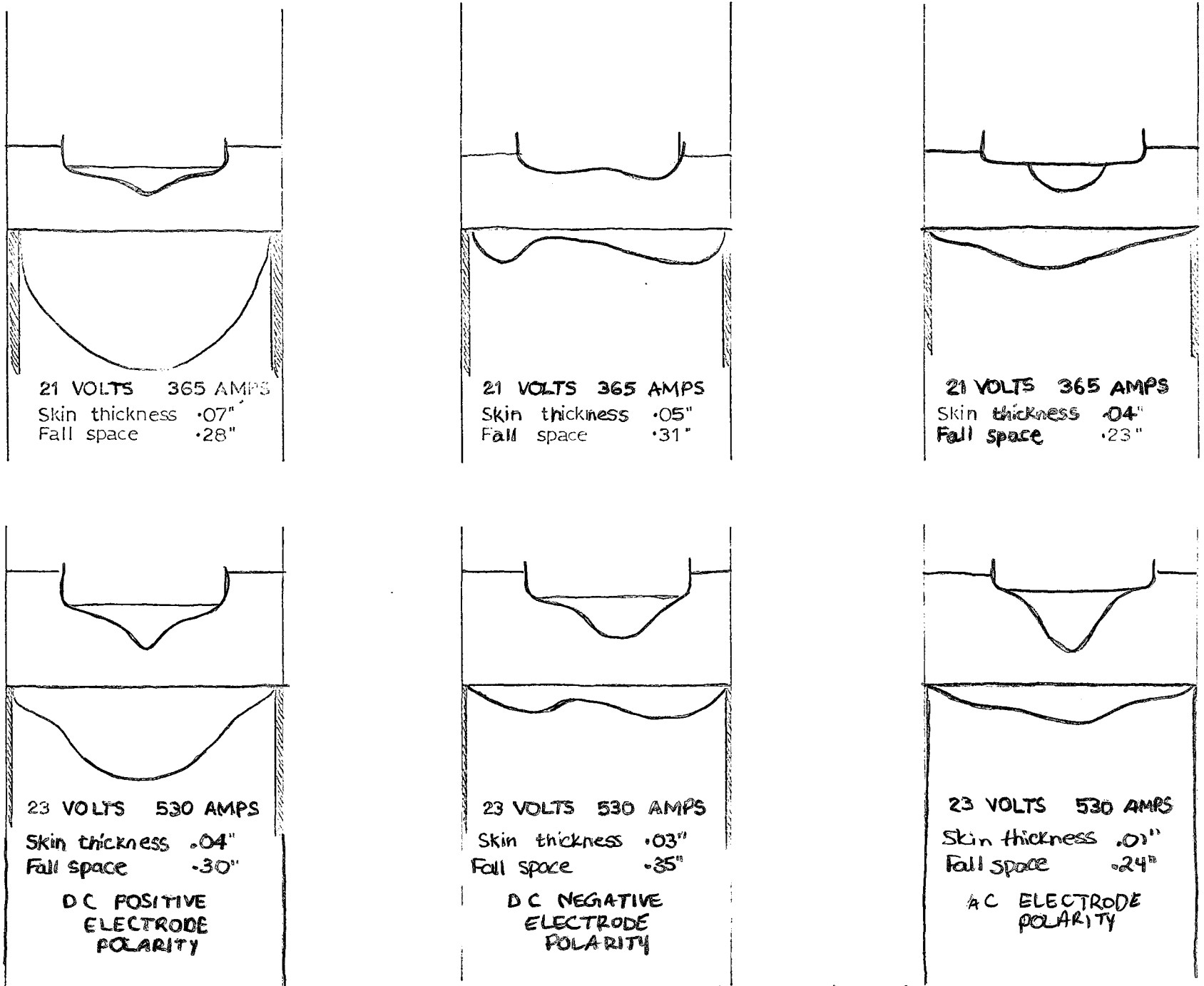

Figure 16 - Changes in thermal characteristics with increasing power input for all three electrode polarity modes

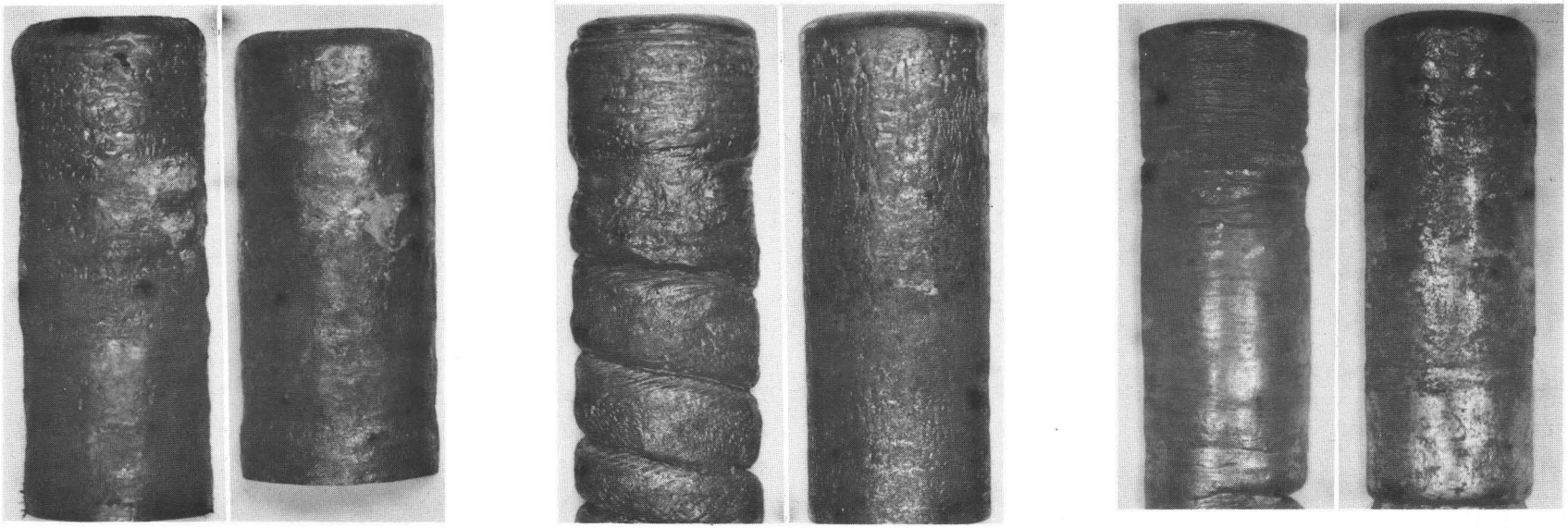

Figure 17 - Photographs showing the improvement in ingot surface finish with increasing power input.

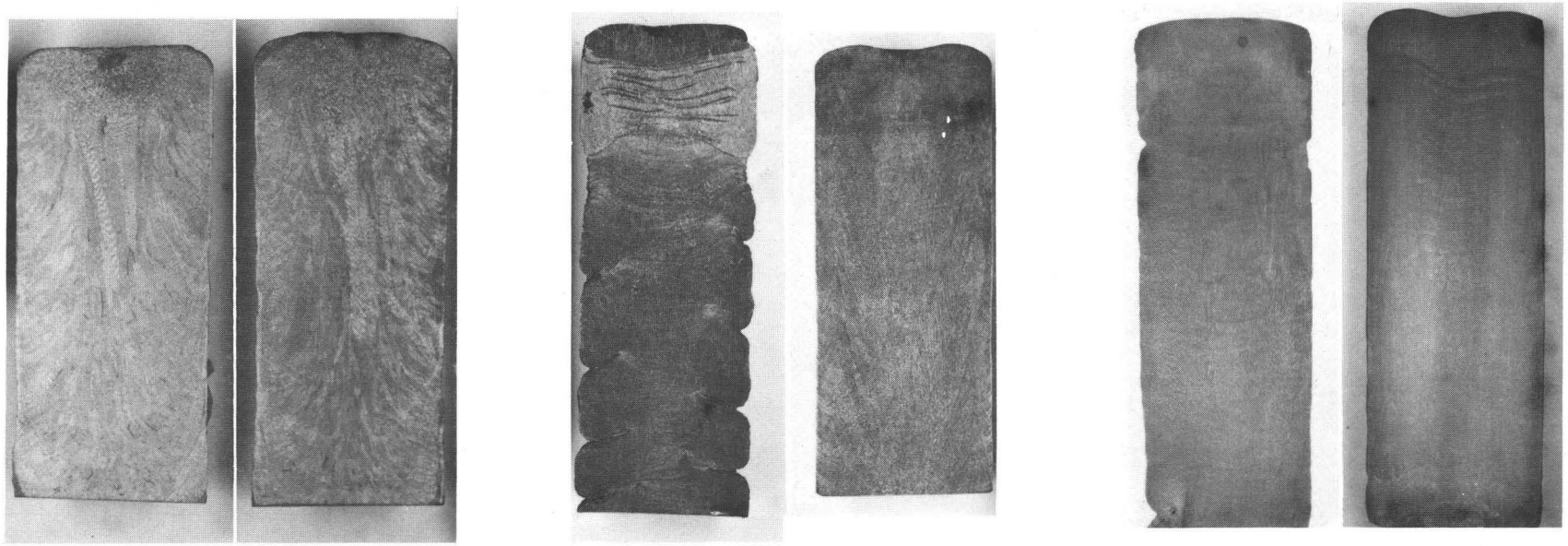

Figure 18 - Photographs showing the improvement in ingot macrostructure with increasing power input.

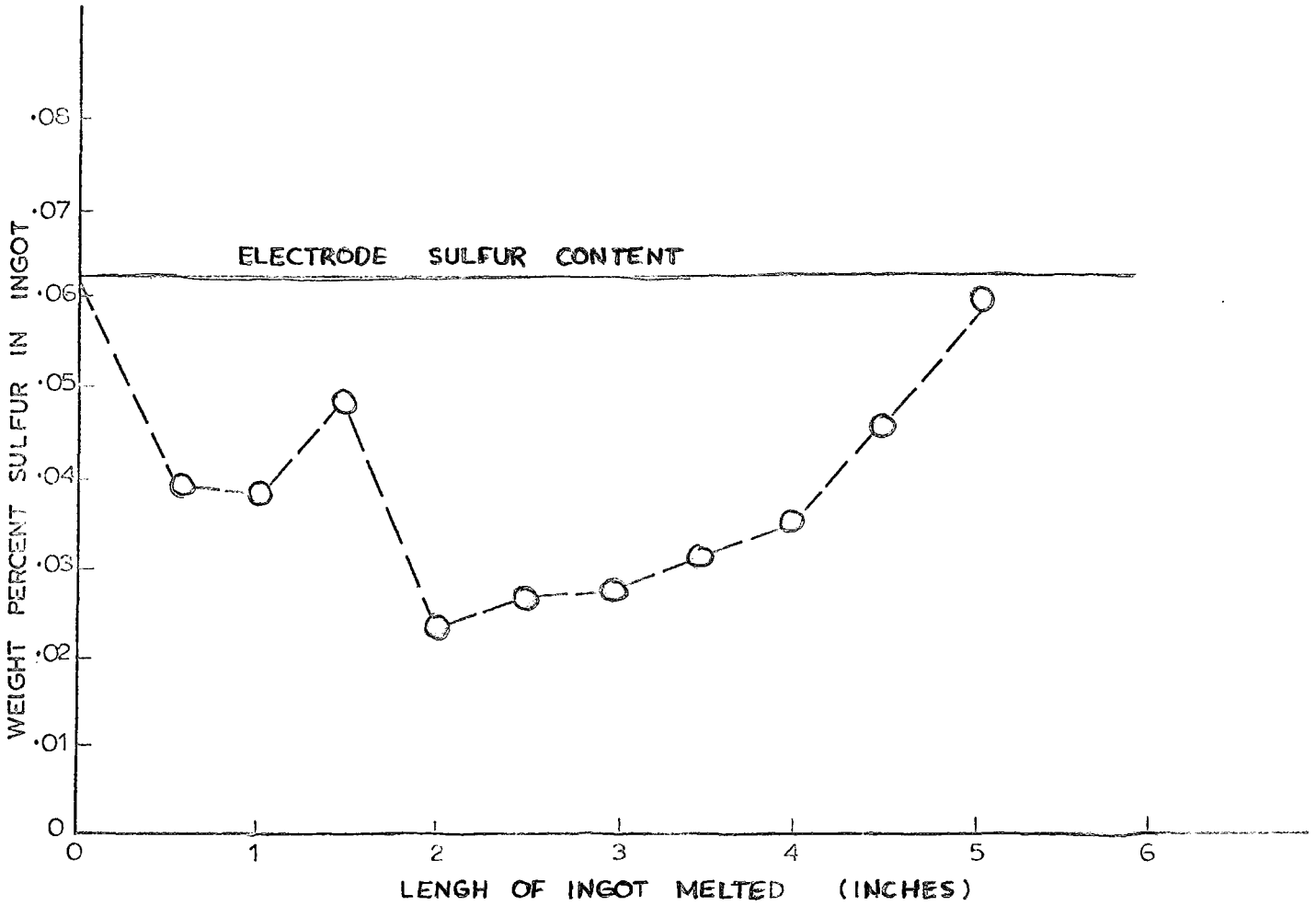

Figure 19 - Variation in sulfur content with length of ingot melted.

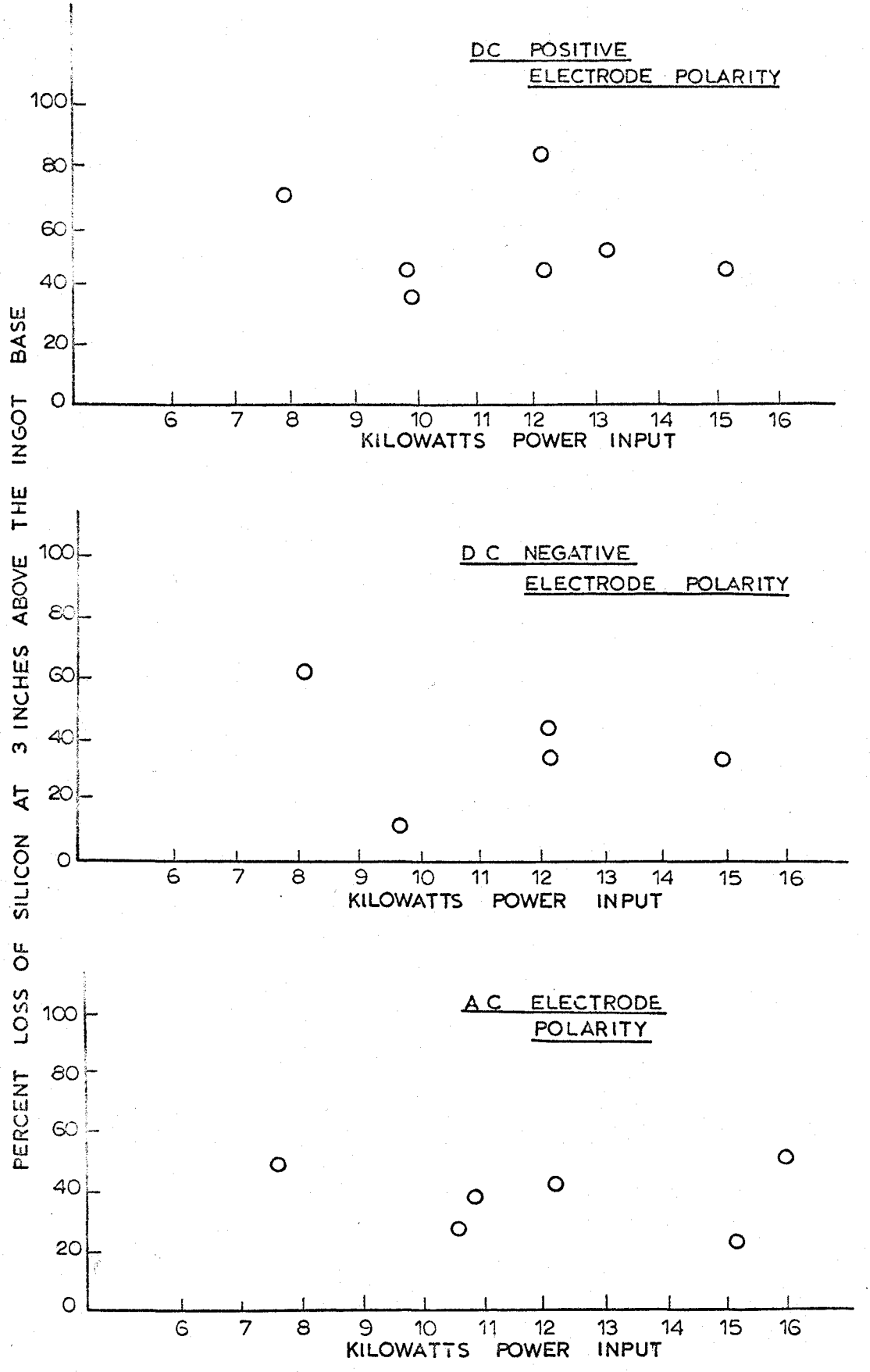

Figure 20 - Effect of power input and electrode polarity on silicon transport.

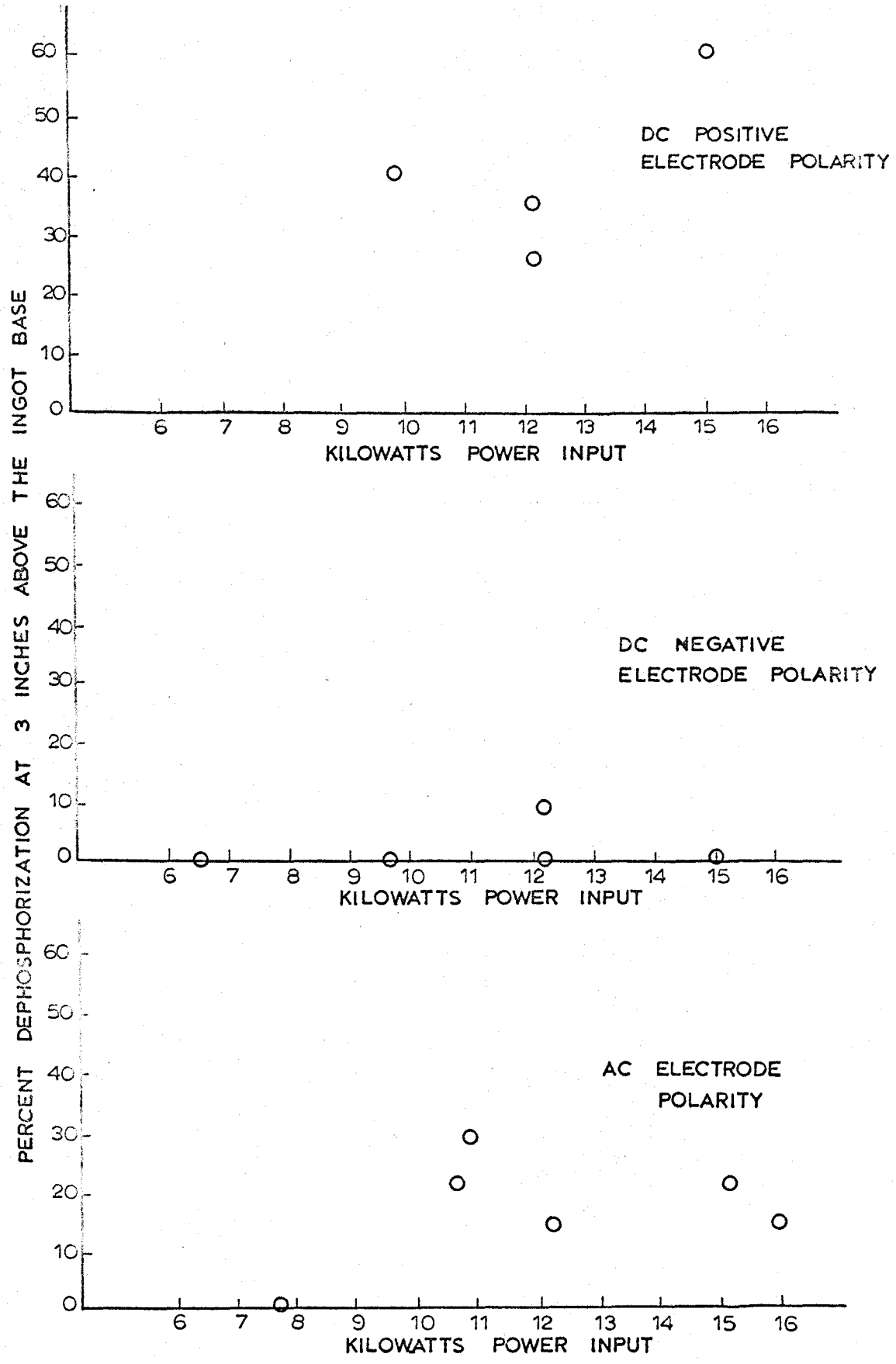

Figure 21 - Effect of power input and electrode polarity on phosphorus transport.

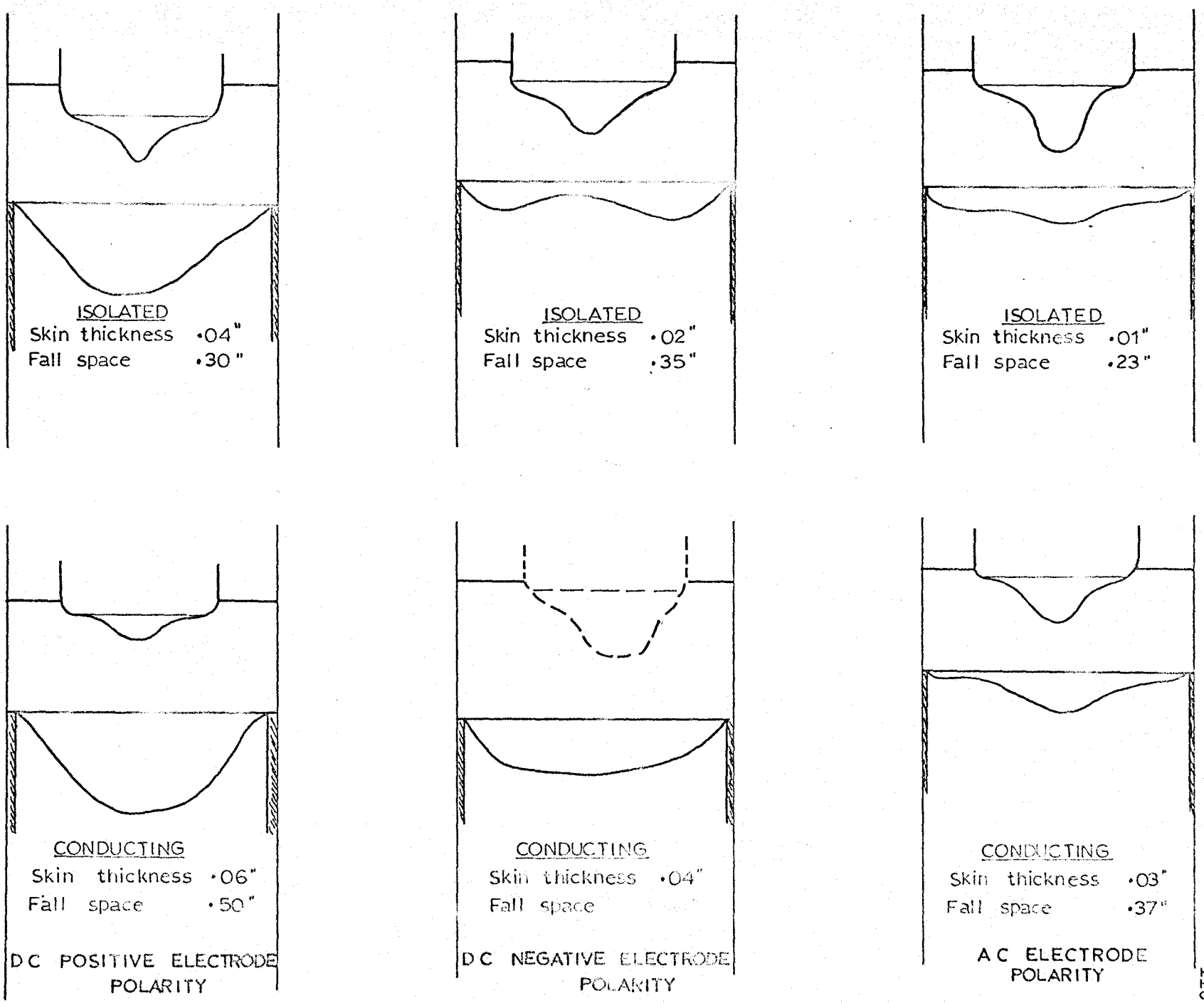

Figure 22 - Variations in thermal characteristics for electrically isolated and conducting mould wall systems.

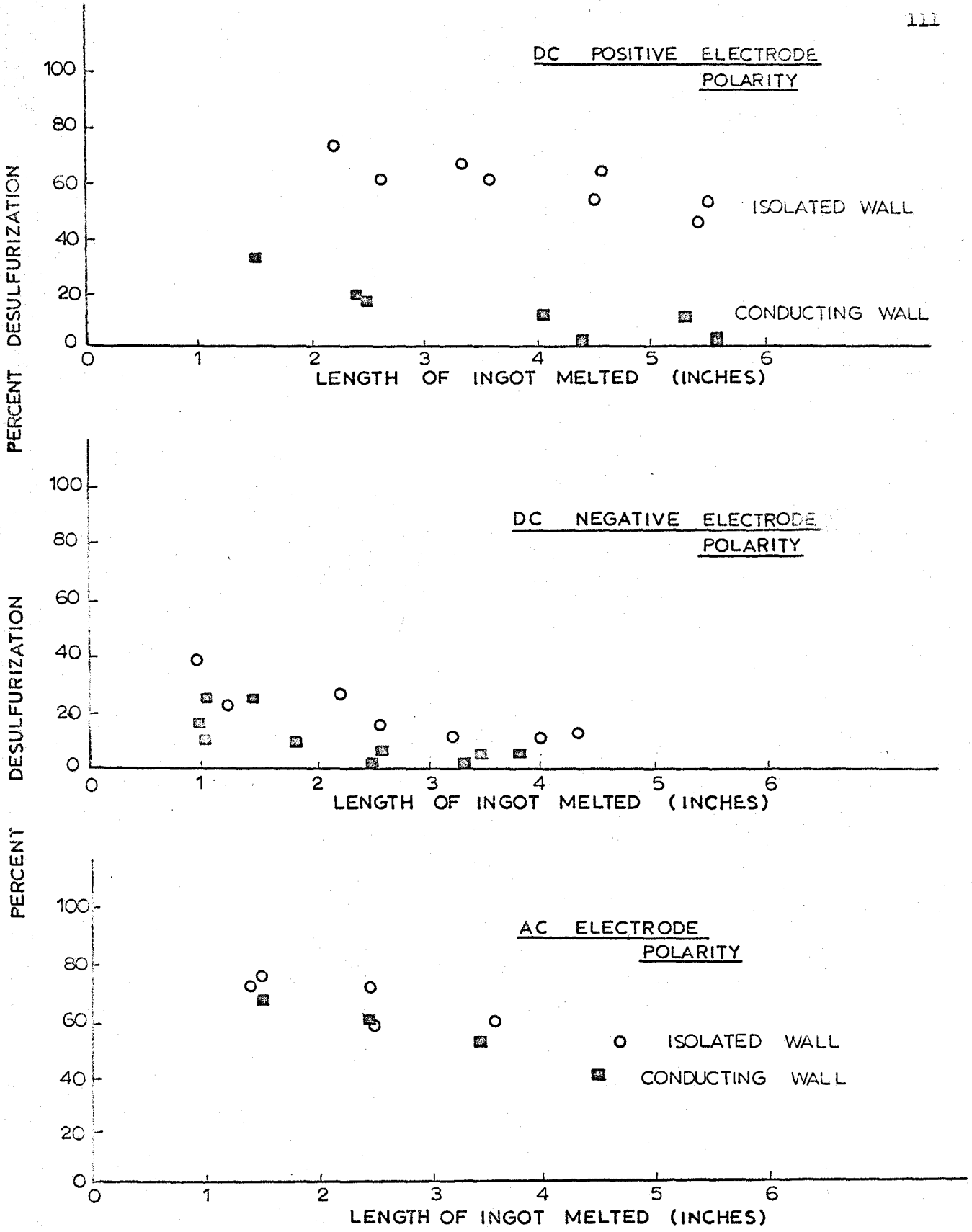

Figure 23 - Effect of electrode polarity and mould wall electrical contact on percent desulfurization.

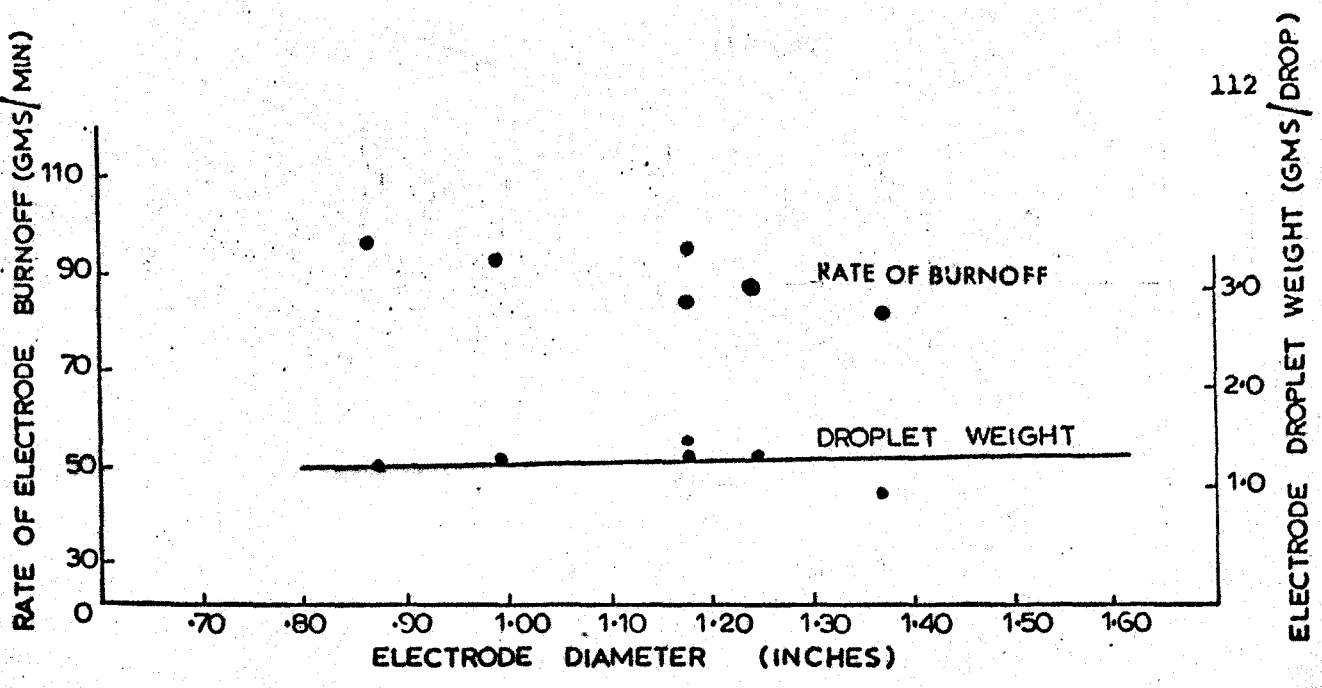

Figure 24 - Change in rate of electrode burnoff and droplet weight with increasing electrode diameter.

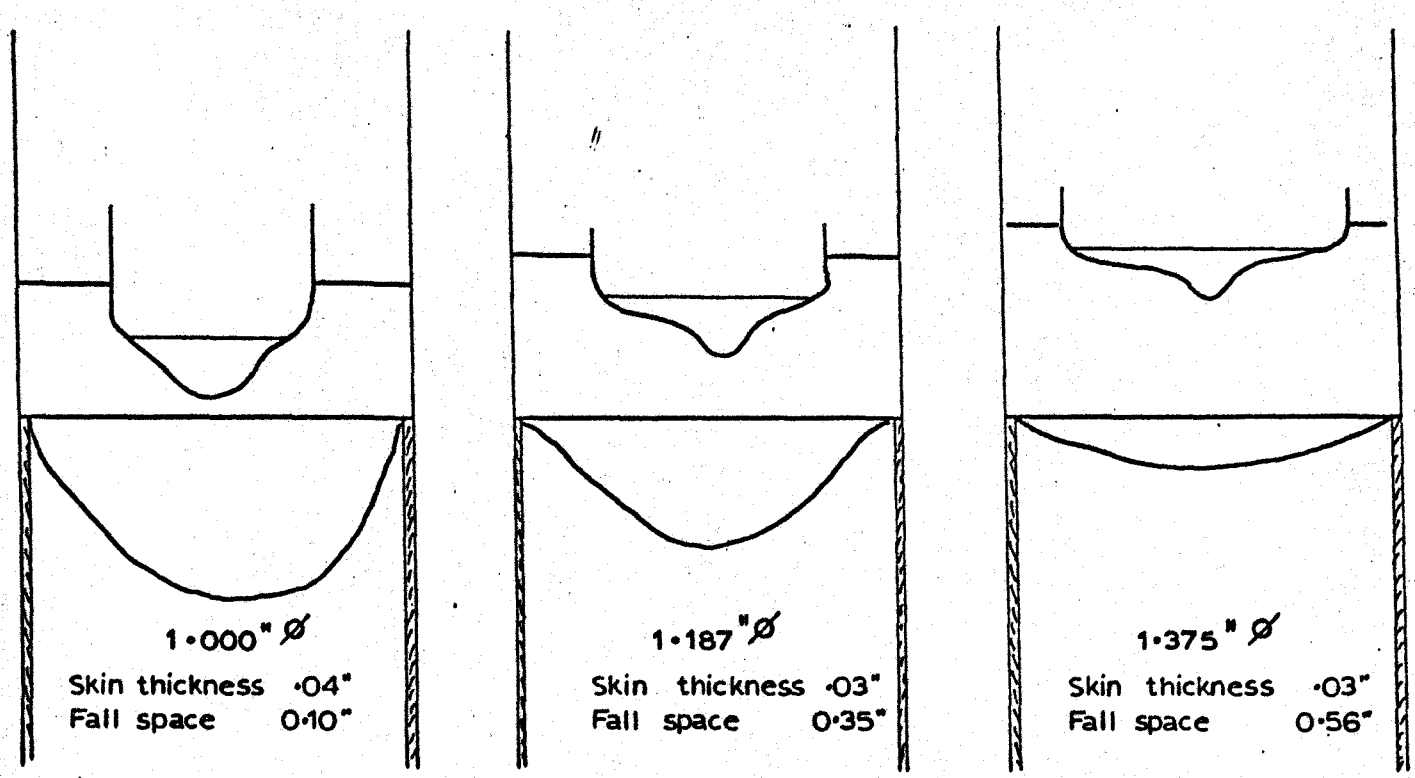

Figure 25 - Changes in furnace thermal characteristics with increasing electrode diameter.

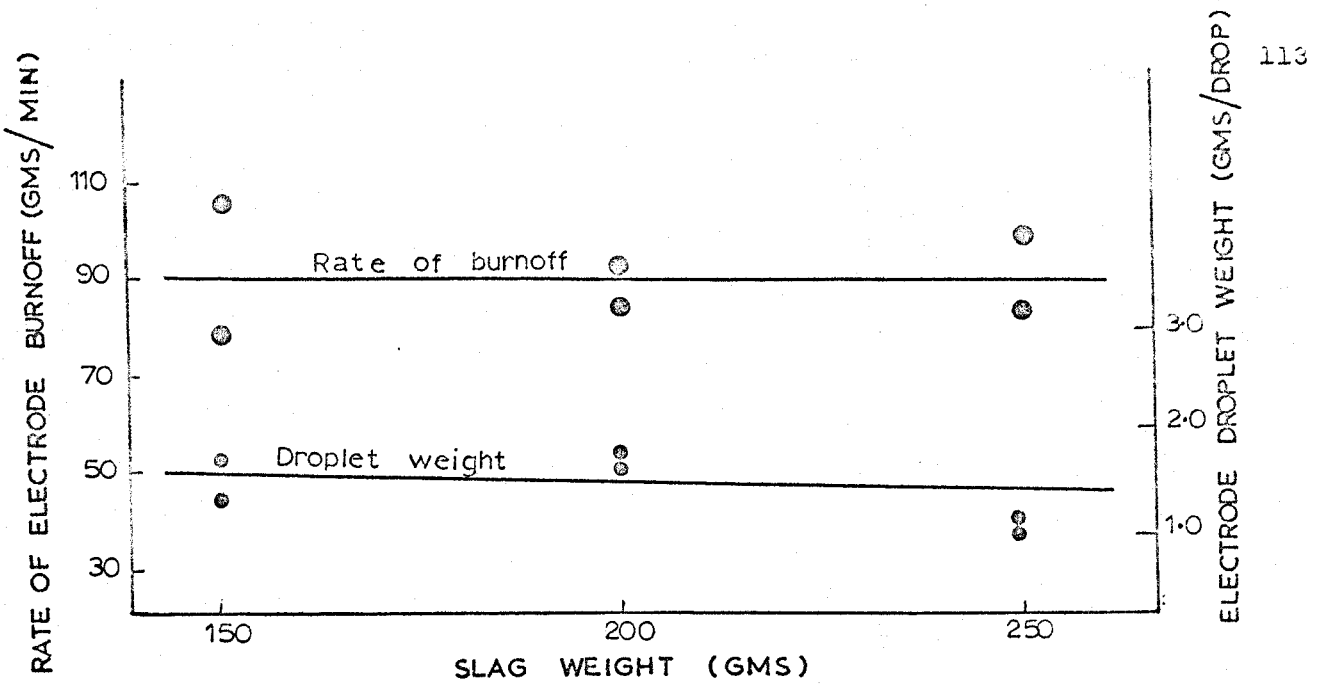

Figure 26 - Change in rate of electrode burnoff and droplet weight with increasing slag volume.

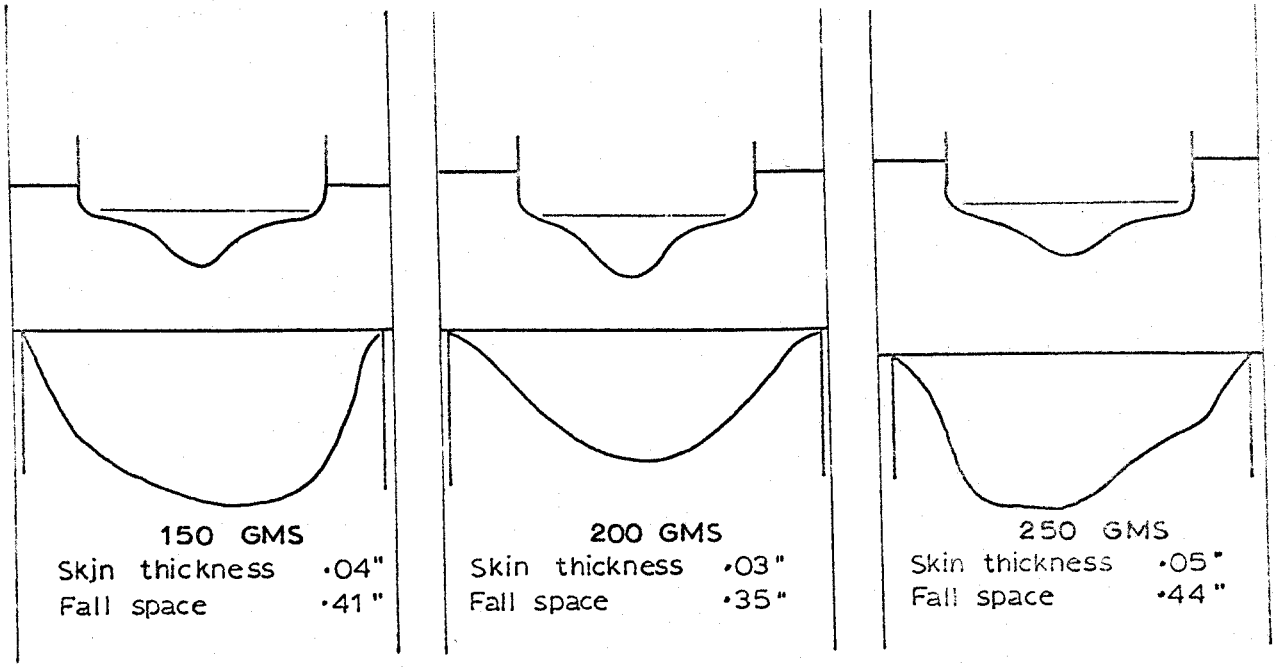

Figure 27 - Changes in furnace thermal characteristics with increasing slag volume.

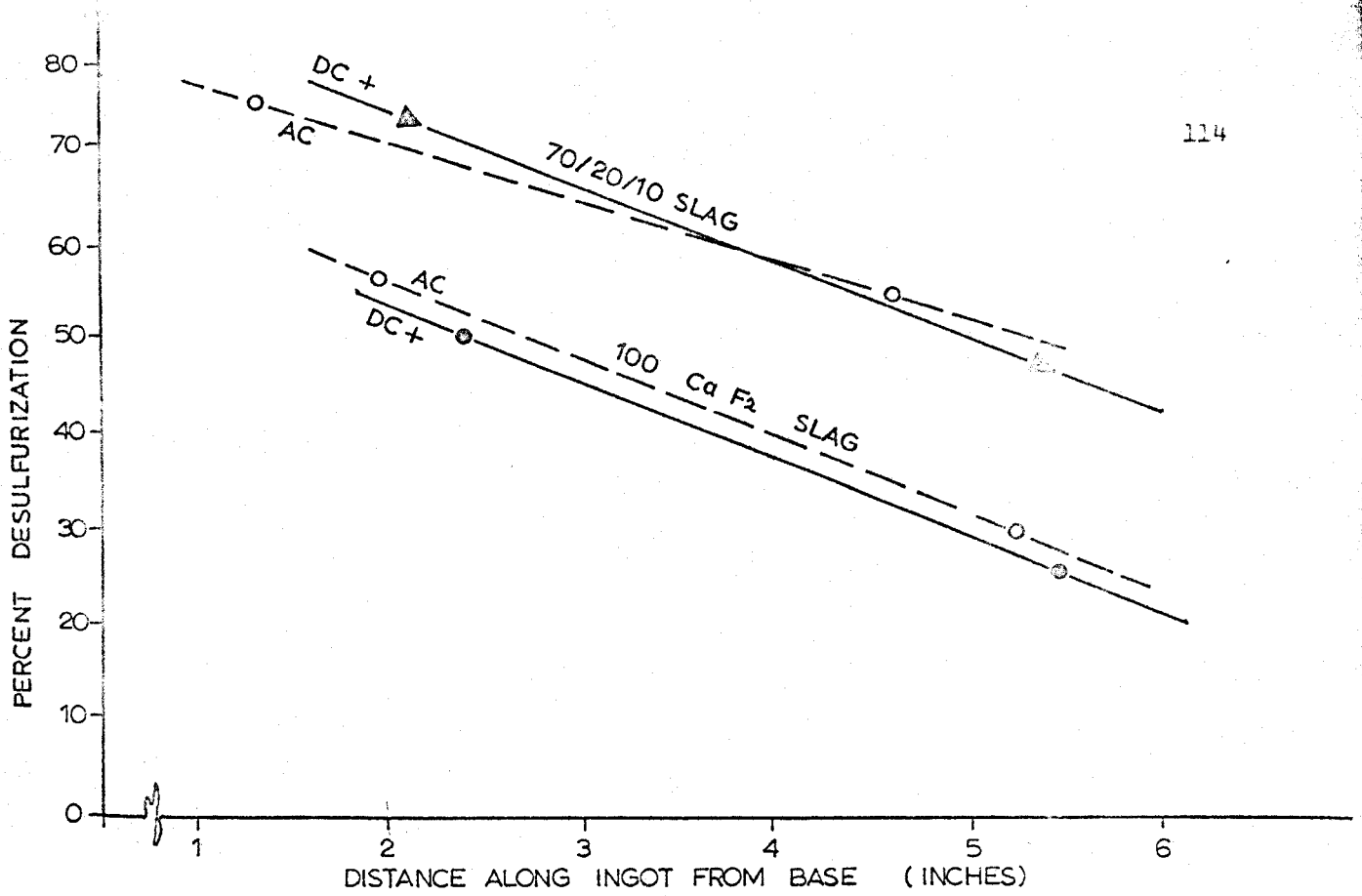

Figure 28 - Percent desulfurization versus length of ingot melted using two different slags.

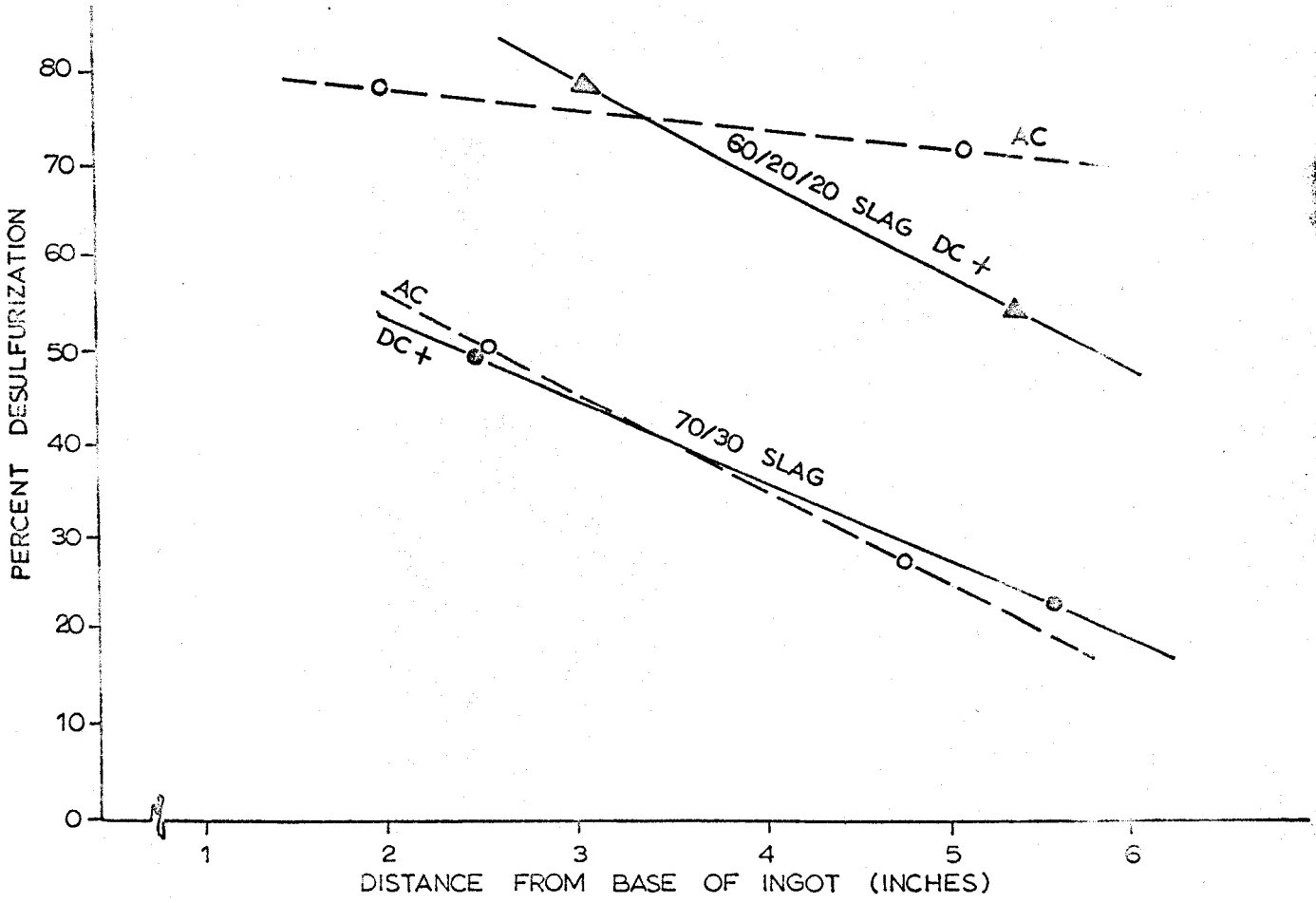

Figure 29 - Percent desulfurization versus length of ingotmelted using two different slags.